Sequence specific visualization of DNA

in live mammalian cells

A Dissertation

Submitted for the Doctoral Degree

Department of Biology

University of Hamburg

by

Giulia Mearini

from Italy

Hamburg, 2005

The present dissertation was prepared in the time from March 2001 until October 2004 at the department of Molecular Cell Biology of the Heinrich-Pette-Institute for Experimental Virology and Immunology at the University of Hamburg.

Genehmigt vom
Fachbereich Biologie der
Universität Hamburg
auf Antrag von Herrn Professor Dr. W. DEPPERT
Weitere Gutachter der Dissertation:
Herr Professor Dr. E. MANDELKOW

Tag der Disputation: 10. Dezember 2004
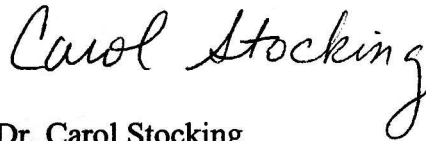
Hamburg, den 26. November 2004
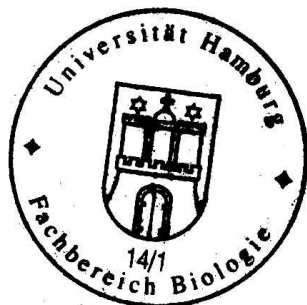
Professor Dr. Arno Frühwald
Dekan

Fachbereich Biologie
Universität Hamburg
Martin Luther King-Platz 2
D-20146 Hamburg

Sehr geehrte Damen und Herrn,

hiermit bestätige ich, dass die von Frau Giulia Mearini mit dem Titel "Sequence specific visualization of DNA in live mammalian cells" vorgelegte Doktorarbeit in korrektem Englisch geschrieben ist.

Mit freundlichen Grüssen,

Dr. Carol Stocking

Arbeitsgruppe Molekulare Pathologie
Heinrich-Pette-Institut
Martinistraße 52
20251 Hamburg

Acknowledgements

Contents

List of Figures

List of Tables

Abbreviations

bp	base pair
CFP	Cyan Fluroscence Protein
CHO	Chinese Hamster Ovary
DABCO	1,4-diazabizyclo[2.2.2]-octane
dhfr	dihydrofolate reductase
DMEM	Dulbecco's modified Eagle's medium
DMSO	Dimethyl sulfoxide
DNA	Deoxyribonucleic Acid
DRB	5,6-dichloro-D-ribofuranosylbenzimidazole
dsDNA	double strand DNA
FACS	Fluorescence Activated Cell Sorting
FCS	Fetal Calf Serum
FISH	Fluorescence *in situ* hybridization
FITC	Fluorescein Isothiocyanate
FRAP	Fluorescence Recovery After Photobleaching
g	gravity force
GFP	Green Fluorescence Protein
hnRNA	heterogeneous nuclear ribonucleic acid
IDMEM	Iscove's modified Dulbecco's medium
J	pseudoisocytosine
K	lysine
kDa	kilodalton
M	Molar
Mbp	Mega base pair
NLS	Nuclear Localisation Signal
O	Ethylene glycol
PBS	Phosphate Buffer Saline
PCR	Polymerase Chain Reaction
PEI	Polyethylenimine
PIPES	Piperazine-1,4-bis-2-ethanesulfonic acid
PML	Promyelocytic leukaemia
PNA	Peptide Nucleic Acids
PPD	p-Phenylenediamine
RNA	Ribonucleic Acid
ROI	Region of Interest
SAF-A	Scaffold Attachment Factor-A
SDS	Sodium Dodecil Sulfat
S/MAR	Scaffold/Matrix Attachment Regions
SV40	Simian Virus 40
YFP	Yellow Fluorescence Protein
4D	four dimensional
3D	three dimensional

1 Introduction

1.1 The cell nucleus

The defining characteristic of eukaryotic cells is the nucleus. It is the most prominent structure within a cell and has a diameter of approximately 10 μm. The nucleus was first seen in 1802 by Franz Bauer and its dimensions make it the biggest cellular organelle visible by light microscopy. The nucleus stores the hereditary material (DNA) as a complex with proteins, the chromatin, and is highly organized. Many fundamental processes like replication, transcription, recombination and DNA repair take place in this organelle. However, even though a lot is known about the biochemistry of these processes, the nuclear organization that supports them is not yet clear. The next sections will give a brief review on the nuclear organization, nuclear dynamics and how to visualize sequence specific DNA.

1.1.1 Nuclear architecture

The nucleus is separated from the cytoplasm by a double membrane which separates chemical reactions taking place in the cytoplasm from reactions happening within the nucleus. The inner and outer membranes are fused at many thousand points to form the nuclear pores. Active and passive transport of macromolecules takes place through the pores, providing a nuclear chemical composition which differs from the cytoplasmic one. The nuclear membrane is stabilized on the outside by intermediate filaments of the cytoskeleton, and on the inside by the nuclear lamina, a complex meshwork of lamin proteins. This lamina is involved in the maintenance of nuclear shape and provides mechanical strength. In addition, the lamina determines the spatial organization of nuclear pores within the nuclear membrane, acts as an anchor for heterochromatin and regulates transcription (Foisner, 2001). Interestingly, lamins have also been reported within the nucleoplasm (Bridger *et al.*, 1993), and are often associated with sites of DNA replication (Moir *et al.*, 2000). Figure 1.1 shows a schematic representation of a cell nucleus.
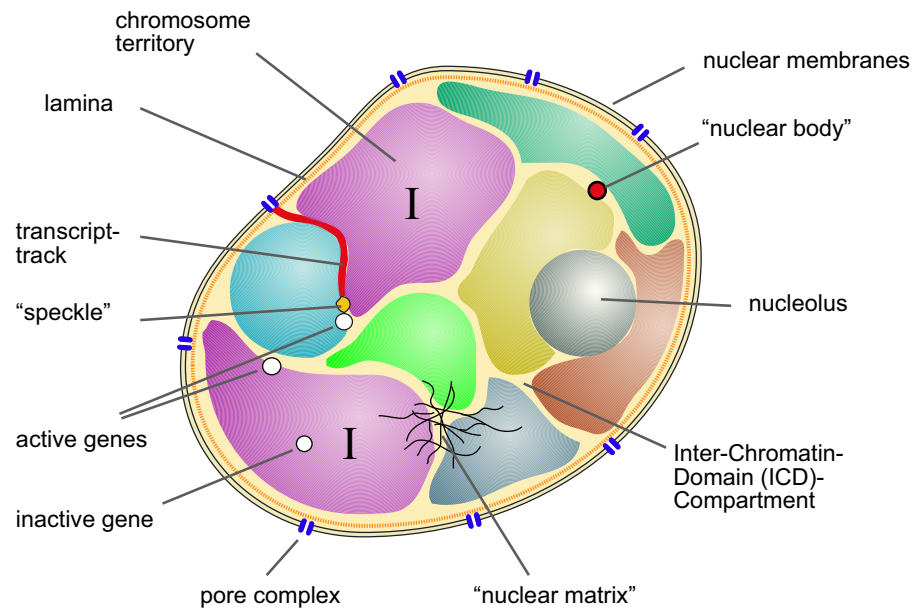
Figure 1.1: Nuclear architecture. The nucleus is a highly complex organelle which is separated from the cytoplasm by the nuclear membrane. The nuclear interior is divided in numerous functional and structural regions, called subcompartments. The largest structures are the chromosome territories (shown as islands in different colors) which are separated by non-chromatin areas. Numerous nuclear bodies reside in this so-called interchromatin domain (ICD) compartment, which are involved in gene expression, RNA processing and genome replication. From Fackelmayer (2000).

1.1.1.1 Nuclear compartments

The nucleus contains many discrete subcompartments that, in contrast to cytoplasmatic compartments, are not surrounded by a membrane. However they can be considered as 'compartments' because they contain defining subsets of resident proteins, they can be morphologically identified by light and electron microscopy, and some of them can be biochemically isolated (Dundr and Misteli, 2001). Even though only the nucleolus and PML bodies are described here, because they are of significant relevance in this work, other subcompartments such as speckles and Cajal bodies are also highly important for nuclear functions and architecture (Dundr and Misteli, 2001).

The nucleolus

The nucleolus is the most prominent substructure in the nucleus of eukaryotic cells. It forms around clusters of tandem repeats of rRNA genes, so-called nucleolar organizing regions (NORs), and is the site of rRNA synthesis, processing and assembly of ribosomal subunits. It disassembles at the onset of mitosis and

reappears in daughter cells as soon as rRNA genes are transcribed again. At the electron microscope, three morphologically distinct regions can be seen: the fibrillar centres (FCs) surrounded by the dense fibrillar component (DFC) and the granular component (GC) (Scheer and Hock, 1999). These three components reflect the vectorial process of ribosome biogenesis which starts with rRNA genes transcription in the FCs and ends at the GC with the assembly of mature rRNA and proteins to form ribosomal subunits (Carmo-Fonseca *et al.*, 2000).

The protein markers of the nucleolus are nucleolin, fibrillarin and nucleophosmin/B23, all of them involved in pre-rRNA processing and ribosome assembly (Scheer and Hock, 1999). Beyond ribosome biogenesis, the nucleolus is also involved in other processes like maturation of several small RNA, regulation of the tumor-suppressor p53, and is the site of interaction for some viruses and viral proteins (Pederson, 1998; Carmo-Fonseca *et al.*, 2000; Hiscox, 2002).

PML nuclear bodies

Promyelocytic leukaemia (PML) nuclear bodies (NBs) are small doughnut-like shaped nuclear subdomains scattered throughout the nucleoplasm. These dynamic domains localize in the interchromatin domain (ICD) compartment and associate with the nuclear matrix. Mammalian cells contain typically 10-30 NBs with a diameter ranging in size between 0.2-1 μm, although number and size vary through the cell cycle (Lamond and Earnshaw, 1998). PML was originally identified in patients suffering from acute promyelocytic leukaemia (APL), where it is fused with RARα (retinoic acid receptor-α) by a chromosomal translocation (t15;17) forming the oncoprotein PML-RARα.

The major component of these bodies is PML, but more than 30 other proteins are found to colocalize with PML in the NB either transiently or constitutively. The function of PML nuclear bodies is not yet clear, but there is much evidence for its involvement in transcriptional control, apoptosis, tumor suppression and nuclear storage (Zhong *et al.*, 2000; Dundr and Misteli, 2001; Hofmann and Will, 2003). In addition, several viral genome and viral proteins were found associated with these bodies (Everett, 2001).

1.1.1.2 DNA organization

Human cells contain around 2 m of DNA, but the diameter of a nucleus is just around 10 μm. To fit into this small volume, DNA must be highly condensed. Histone and non-histone proteins help in the condensation process, forming a complex called chromatin. The first level of organization is the nucleosome, which consists in ∼165 bp of DNA wrapped around an octamer of core histones (two copies of each H2A, H2B, H3, H4), forming a fiber with a diameter of 10 nm. The second level of organization is achieved with help of a fifth histone protein, H1, which stabilizes the condensed nucleosomal string in a fiber of about 30 nm, known as the solenoid. The 30 nm fibers are further organized in loops ranging in size from 5 to 300 kb and are anchored at the nuclear matrix via specific DNA sequences (see below sections 1.1.1.4 and 1.2). In the last decade, the existence of an additional level of chromatin organization was demonstrated, the 100-130 nm chromonema fibers, as an intermediate in the pathway of chromosome condensation or decondensation (Belmont and Bruce, 1994; Robinett *et al.*, 1996; Belmont *et al.*, 1999b).

1.1.1.3 Chromosome territories

Staining the interphase nucleus with DNA dyes, such as DAPI or Hoechst 33258, or with the histone H2B fused to GFP shows that the nuclear distribution of DNA is not homogeneous (Zink *et al.*, 2003). In fact, there are brighter regions (heterochromatin) at the nuclear periphery and darker regions (euchromatin) in a more central position. These regions correspond to a different packaging density of the DNA, correlating with the activity of genes present in these regions. Chromosomal DNA occupies distinct, non-overlapping domains in the interphase nucleus, called 'chromosome territories' (Cremer and Cremer, 2001). These territories are visualized in fixed cells by FISH (fluorescence *in situ* hybridization) technique (Lichter *et al.*, 1988), and also in living cells by labeling of DNA with fluorescent nucleotide analogs followed by segregation over several cell cycles (Zink *et al.*, 1998b). In each territory, the long and short chromosome arms are spatially separated and chromatin is arranged in globular entities called subchromosomal domains or foci, probably related to gene expression and DNA replication (Fackelmayer, 2004). The volume occupied by a single territory

depends on the amount of the DNA constituting the chromosome, so that bigger chromosomes occupy bigger volumes. Even though the positions of the territories are quite variable in different cell types, their relative position depends on gene contents and activity. Thus, gene-rich chromosomes can be found in the nuclear interior, whereas gene-poor chromosomes are at the nuclear periphery (Croft *et al.*, 1999). Interestingly, within a chromosome territory, active genes localize at the periphery while inactive gene are often found in their interior (Verschure *et al.*, 1999). However, the chromatin organization in subchromosomal foci allows the presence of active genes also in more internal regions (Mahy *et al.*, 2002a).

The space between chromosome territories is sometimes referred to as the interchromatin domain (ICD) compartment, and consists of highly convoluted channels running also inside the territories (Visser *et al.*, 2000). Since the transcriptional activity takes place at the boundary of the chromosome territories and at subchromosomal foci, it is likely that the newly synthesized RNA is deposited directly into the interchromatin space. In fact, this domain is rich in proteins involved in transcription and RNA processing (Verschure *et al.*, 2002). In some cases chromatin loops extend from the territory to the interchromatin domain, likely due to the high gene density and high level of transcription of these regions (Mahy *et al.*, 2002b). Many nuclear subdomains, such as speckles, Cajal bodies and PML bodies do not contain chromatin, and are found in expanded areas of the interchromatin compartment.

1.1.1.4 The nuclear matrix

The presence of a cytoskeleton in the cytoplasm of eukaryotic cells, composed of several different filaments and providing support for many processes, lead to the hypothesis of the existence of a similar structure also in the nucleus. The first evidence of such a proteinaceous network can be dated back to the end of the 1940s (Zbarskii and Debov, 1948). The definition of the 'nuclear matrix' for a proteinaceous network remaining after extraction of soluble proteins and enzymatic removal of the chromatin, was introduced by Berezney and Coffey (Berezney and Coffey, 1974). A current hypothesis suggests that this 'matrix' gives shape to the nucleus and can be seen as a platform (with structural and

functional roles) upon which the chromatin is organized and processes like DNA replication and transcription take place.

In the classical extraction procedures, nuclei are incubated with DNaseI, to remove chromatin, followed by 2 M NaCl extraction, to release all soluble proteins. The obtained nuclear matrix consists of the nuclear lamina, remnants of nucleoli and a fibrogranular network of proteins and RNA. When the matrix is prepared without the final high salt extraction it appears at the electron microscope as a network of fibers with diameter of 20-50 nm and many complexes bound to it. With high salt extraction, these complexes can be removed to reveal a network of highly branched fibers with a diameter of 2-3 nm, constituted by proteins and hnRNA (He *et al.*, 1990). When the preparations are treated for a short time with RNase, the structure collapses, indicating a fundamental role for hnRNA in the matrix (Nickerson *et al.*, 1989; Ma *et al.*, 1999).

The protein composition of the nuclear matrix was determined by 2D electrophoresis analysis, demonstrating that it is composed by a multitude of proteins, some of them being cell-type specific. The majority of nuclear matrix proteins are hnRNP (Fey *et al.*, 1986).

The *in vivo* existence of a nuclear matrix is often debated (Pederson, 2000b; Hancock, 2000). The skeptic scientists mainly criticize the harsh procedure for *in vitro* preparation which could lead to the formation of artifacts. Moreover, they underline that this structure is always seen in *in vitro* preparation, but not in living cells. Recent results obtained in my laboratory show for C280-GFP, the carboxyterminal part of the nuclear matrix associated and S/MAR binding protein SAF-A fused to GFP, a three dimensional sponge-like localization in live, unextracted nuclei (Herrmann, 2002). Another criticized aspect is the contradiction between the concept of a nuclear matrix and the *in vivo* demonstrated mobility of many matrix-associated proteins (Pederson, 2000b; Hancock, 2000). However this is only an apparent contradiction since it was shown that macromolecules diffuse within the nucleus 3-5 fold slower than in aqueous solution (Seksek *et al.*, 1997). Thus, the matrix should not be seen as a rigid, immobile structure, but as a dynamic entity.

1.2 Scaffold/Matrix Attachment Regions (S/MAR)

Higher order chromatin organization is achieved by anchoring the DNA to the nuclear matrix. In this way, the chromatin fibers are segregated into discrete and topologically independent loop domains constrained at their base by interaction with the nuclear matrix. The specific DNA sequences making contacts with this structure are called, depending on the isolation method, scaffold or matrix attachment regions (S/MAR). S/MAR elements, with a size between 0.2 and 3 Kb, are normally found outside coding regions and close to *cis*-regulatory sequences such as promoters or enhancers, where they have been shown to affect chromatin accessibility (Jenuwein *et al.*, 1997) and specific histone modifications associated with trancriptionally active genes (Martens *et al.*, 2002). They are evolutionary conserved in function, and even though it was not possible to deduce a consensus sequence, S/MAR elements show some common features. They are composed of AT-rich sequences with homopolymeric runs of A or T bases ('A-tracts'). A comparison between S/MAR elements from a variety of eukaryotic organisms showed the existence of a bipartite matrix recognition signature (MRS). Although all MRS are associated with S/MAR, not all known S/MAR contain a MRS suggesting the existence of two classes of S/MAR, one with and one without MRS (van Drunen *et al.*, 1999). Recently it has been shown that the introduction in transgenic mice or transfected cell lines of multiple-copy S/MAR constructs lead to a selection of S/MAR for the binding to the matrix, although they all have the same primary sequence. These observations suggest the presence within the cell of a regulatory system that manage the use of S/MAR elements (Heng *et al.*, 2004).

Beside structural functions and contribution to chromosome condensation during cell division (Hart and Laemmli, 1998), S/MAR elements are also affecting transcriptional level in a context-dependent manner, providing a significant enhancement of transcription after stable integration of the transfected construct (Schubeler *et al.*, 1996). Interestingly, S/MAR have been shown to be necessary for replication and episomal maintenance of a non-viral vector designed for gene therapy (Piechaczek *et al.*, 1999; Jenke *et al.*, 2002; Jenke *et al.*, 2004).

1.2.1 S/MAR binding proteins

The binding of S/MAR elements to the matrix is mediated by S/MAR binding proteins, many of which are now identified and well characterized. Among them are ubiquitous, abundant proteins such as topoisomerase II (Adachi *et al.*, 1989), histone H1 (Izaurralde *et al.*, 1989), LaminB1 (Luderus *et al.*, 1992), HMGI/Y (Zhao *et al.*, 1993) and nucleolin (Dickinson *et al.*, 1995), but also proteins that are expressed in a more cell-type-specific way, such as SATB1 (Dickinson *et al.*, 1992). In previous work of my laboratory, two other S/MAR binding proteins, SAF-A and B (scaffold attachment factor-A and B), were identified (Renz and Fackelmayer, 1996; Romig *et al.*, 1992). These two proteins, which share the same DNA binding domain, are not further related, although both are involved in nuclear architecture and processing of RNA.

SAF-A is a very abundant protein (2×10^6 molecules/nucleus), and is a major component of the nuclear matrix. It is a big (120 kDa) multifunctional protein which interacts both with DNA and RNA. The DNA binding domain (SAF-box) is localized at the amino-terminal end of the protein. The specific binding to S/MAR elements requires a cooperative interaction of many SAF-A molecules (Kipp *et al.*, 2000). SAF-A also interacts with RNA via an RGG-box located at the carboxy-terminus (Kiledjian and Dreyfuss, 1992). The binding to the nuclear matrix involves the C-terminus of the protein (Herrmann, 2002). The importance of SAF-A in the nucleus is underlined by the fact that it is not possible to generate knock-out mice.

1.3 The nucleus is a dynamic organelle

The nucleus is a highly dynamic organelle. With the introduction in the 1990s of the green fluorescent protein (GFP) from the jellyfish *Aequorea victoria* and its spectral variants, studying nuclear dynamics in living cells became possible. GFP is a small protein (27 kDa) which can be used to tag other proteins without interfering with their localization or functions. Mutagenesis of the original green protein has produced a variant (enhanced GFP), which is faster in folding the fluorophore, brighter and more stable, and folds correctly at 37°C. Moreover it was possible to obtain variants with differing absorbance and emission spectra,

such as CFP (cyan fluorescent protein) and YFP (yellow fluorescence protein), allowing simultaneous visualization of distinct GFP variants in living cells (Lippincott-Schwartz and Patterson, 2003).

1.3.1 Fluorescence imaging methods

The combination of fluorescent technology with developments in fluorescent microscopy and digital data analysis, gave new input to imaging methods such as FRAP (fluorescence recovery after photobleaching), FLIP (fluorescence loss in photobleaching), FRET (fluorescence resonance energy transfer) and FCS (fluorescence correlation spectroscopy), to study localization, dynamics and interactions of proteins in living cells.

In FRAP experiments, fluorescent molecules are irreversibly photobleached with a high-intensity laser beam in a small region of the cell, and the subsequent movement of non bleached fluorescent molecules into the photobleached area is recorded at low laser power at regular time intervals. In this way it is possible to determine the mobile fraction and the diffusion coefficient of the analyzed molecule (Houtsmuller and Vermeulen, 2001).

FLIP is performed by repeatedly photobleaching an area of the cell while images of the entire cell are collected. The loss of fluorescence from outside the bleached area provides information about the connection of the two regions (Lippincott-Schwartz *et al.*, 2001).

FRET imaging relies on distance-dependent transfer of energy from an excited donor fluorophore to an acceptor fluorophore. Transfer of energy will happen only if the two labeled elements are physically interacting (van Roessel and Brand, 2002).

In FCS, fluctuations of fluorescent molecules are measured in a microvolume, typically in the femtoliter range, over a short period of time. This technique can be used to measure diffusion coefficients and binding constants (Phair and Misteli, 2001).

1.3.2 Protein dynamics

Even though there is a huge amount of nucleic acids and proteins in the nucleus, which could provide a viscous environment, photobleaching experiments for several fluorescent nuclear proteins underlined that many of them are highly

mobile within the nucleus (Misteli, 2001). Their mobility seems to be consistent with passive diffusion, since ATP depletion, or reduction of temperature, does not effect recovery rates (Phair and Misteli, 2000). Moreover, the proteins diffuse in the nucleus 3-5 fold slower than in aqueous solution, independently of their size (up to 500 kDa), as demonstrated with microinjected FITC-dextrans and Ficoll (Seksek *et al.*, 1997). Among the proteins with fast recovery are transcription factors such as steroid receptors (McNally *et al.*, 2000; Stenoien *et al.*, 2001), chromatin binding proteins such as HMGA1, HMG-17 and histone H1 (Phair and Misteli, 2000; Lever *et al.*, 2000; Misteli, 2000; Harrer *et al.*, 2004), splicing factors such as SF2/ASF (Phair and Misteli, 2000; Kruhlak *et al.*, 2000), rRNA processing enzymes such as fibrillarin (Phair and Misteli, 2000) and DNA repair enzymes such as the endonuclease ERCC1/XPF (Houtsmuller *et al.*, 1999). However, there are also proteins with a very slow recovery rate, such as lamin A and B (Broers *et al.*, 1999; Moir *et al.*, 2000), or core histone protein H2B (Lever *et al.*, 2000). Interestingly, FRAP experiments showed that most proteins move slower than expected considering only their molecular weight (Phair and Misteli, 2000; Pederson, 2000a). Moreover, biologically inactive proteins move 10 to 200 times faster than the active counterparts excluding collisions with nuclear components as a reason for the slow movement (Houtsmuller *et al.*, 1999; Phair and Misteli, 2000; Kruhlak *et al.*, 2000). The effective mobility of a protein is rather greatly determined by its interactions with other nuclear components such as the chromatin or the nuclear matrix (Kruhlak *et al.*, 2000; Shopland and Lawrence, 2000).

The histone H1, a chromatin binding protein, showed in FRAP experiments a continuous exchange from chromatin and a complete recovery in the photobleached area after 4 min (Lever *et al.*, 2000; Phair and Misteli, 2000). The behavior of histone H1 is explained with a 'stop-and-go' model were the protein binds the chromatin a few minutes and then falls off, diffusing freely in the nucleus until it finds a free binding site again. The same model applies also for other chromatin binding proteins, such as HMG proteins (Misteli, 2001). Transcriptional factors such as glucocorticoid receptor (GR) and estrogen receptor (ER) are even faster than histone H1. As long as ligands are present, the receptors bind to their response elements, but this binding is highly

dynamic allowing rapid exchange of receptor molecules on the DNA. For this mechanism of interaction, an 'hit-and-run' model is proposed, with a residence time of the receptors on the response elements of only few seconds (McNally *et al.*, 2000; Stenoien *et al.*, 2001).

1.3.3 Nucleic acids dynamics

High mobility is not a feature unique to proteins. Poly(A)-RNA was visualized by hybridization with fluorescent oligonucleotides and it was found to move fast within the nucleus by energy independent diffusion (Politz *et al.*, 1999). Even though in the past the mobility of mRNP (messenger ribonucleoprotein particles) was thought to combine passive diffusion and ATP-dependent processes (Calapez *et al.*, 2002), it is now clear that mRNPs dynamics is due exclusively to energy-independent processes (Shav-Tal *et al.*, 2004).

Mobility of DNA in the nucleus and cytoplasm was measured by microinjection of fluorescein labeled dsDNA fragments of variable size. In the cytoplasm, DNA diffusion is size-dependent (almost free diffusion for fragments up to 1 000 bp). In contrast, DNA fragments of all sizes diffused very slow in the nucleus (Lukacs *et al.*, 2000). In this work particular attention is given to the dynamics of plasmid DNA and of specific chromatin loci. Methods to visualize chromatin in living cells for studies on its dynamics are described in section 1.4.

1.3.4 Subcompartment dynamics

It is possible to observe nuclear subcompartments such as nucleoli, PML nuclear bodies, Cajal bodies and speckles, which are not delineated by a membrane, but nevertheless maintain their shape for hours. However, FRAP analysis reveals that the protein components of these compartments are in continuous rapid flux between the compartment and the nucleoplasm (Misteli, 2001; Dundr and Misteli, 2001). Interestingly, in addition to protein trafficking in and out a nuclear compartment, the compartments themselves can move *in toto* within the nucleus (Belmont, 2003). A significant example are Cajal bodies (CBs) which move with anomalous diffusion, alternating association with chromatin and diffusion within the interchromatin space. The mobility of CBs suggests that their interaction with chromatin requires ATP and active transcription (Platani *et al.*, 2002).

1.3.5 Dynamics and transcription

Natural or synthetic transcriptional inhibitors are useful tools to study mechanisms of complex biomolecular processes in living cells, like transcription. The synthetic adenosine analog 5,6-dichloro-1-β-D-ribofuranosylbenzimidazole (DRB) was first described in the 1950s as a synthetic inhibitor of the multiplication of several RNA and DNA viruses, and later shown to selectively inhibit transcription of hnRNA and mRNA by RNA polymerase II (pol II) (Yamaguchi *et al.*, 1998). Several *in vivo* and *in vitro* experiments have identified the elongation step of pol II as the target for DRB so that long transcripts are almost completely absent, while there is an accumulation of short promoter-proximal transcripts (Chodosh *et al.*, 1989). Nickerson and coworkers demonstrated the connection between chromatin organization and proper synthesis of RNA. In fact, the disruption of nuclear RNA induced collapse of the nuclear matrix, RNA being one of its major component, and simultaneously collapse of chromatin organization (Nickerson *et al.*, 1989). Moreover, the treatment of cells with DRB induces a reversible dissociation of nucleoli so that the fibrillar component (FC) disperses throughout the nucleus and forms the so-called nucleolar 'necklaces' (Scheer *et al.*, 1984).

1.4 *In vivo* visualization of DNA

As described in the previous sections, the nucleus is highly organized and compartmentalized. In interphase nuclei, genomic DNA is organized in discrete chromosome territories as demonstrated in FISH experiments (Croft *et al.*, 1999; Cremer and Cremer, 2001). However, experimental artifacts arising during permeabilization of the nuclei and denaturation of DNA for hybridization could affect the obtained conclusions on territory dimension, shape and surface structure (Zink *et al.*, 1998b). Therefore it was necessary to develop new methods to investigate chromosome organization and dynamics in interphase nuclei of living cells (Zink and Cremer, 1998a).

In a first approach, chromatin was fluorescently labeled using dihydroethidium, a membrane-permeant derivative of ethidium bromide, and in interphase nuclei the chromatin was very immobile (Abney *et al.*, 1997). In another

approach, the histone H2B gene was fused with the gene coding for the green fluorescence protein. The resulting H2B-GFP fusion proteins were properly incorporated into nucleosomes allowing high resolution imaging of bulk chromatin in interphase as well as during mitosis (Kanda *et al.*, 1998). In another study, GFP was fused to CENP-B, a protein that binds specifically to the centromeric α-satellite sequences, showing that centromeres were primarily stationary, although motility of individual, or small groups of centromeres, was occasionally observed at low rate (7-10 µm/h) (Shelby *et al.*, 1996). *In vivo* visualization of individual chromosome territories in nuclei of human living cells is possible by labeling the DNA with fluorescent nucleotide analogs. Semiconservative replication results in labeling of the two chromatids derived from each replicated chromosome. After several further cell cycles, there are cells in which just few or one chromosome territory are labeled (Zink and Cremer, 1998a; Manders *et al.*, 1999).

Independently from the experimental approach, it was shown that the chromatin is characterized by both highly dynamic short-range mobility and constrained long-range movements (Gasser, 2002).

Two different labeling methods were used in this work to investigate the localization and mobility of sequence specific DNA in live mammalian cells. Exogenous small circular DNA was labeled using synthetic DNA analogs (PNA) tagged with rhodamine. PNA were designed to recognize a short purine rich sequence inserted in several different plasmids and the presence of the fluorochrome allowed, after microinjection, following the fate of these molecules in nuclei of living cells.

In a second approach, chromosomal loci were labeled with the bacterial *lac* operator/repressor system. The *lac* repressor, a strong DNA binding protein, is fused to GFP thus allowing direct visualization of the interaction with the operator sequences by fluorescence microscopy. The next sections describe these two methods in more details.

1.5 Peptide nucleic acids (PNA)

Peptide nucleic acids (PNA) are synthetic oligonucleotides with a modified backbone. In these DNA analogs, the sugar-phosphate of DNA backbone is replaced by a pseudopeptide backbone composed of N-(2-aminoethyl)glycine units, to which the purine and pyrimidine bases are attached via a methyl carbonyl linker. These molecules were invented in 1991 by Peter E. Nielsen (Nielsen *et al.*, 1991). The uncharged backbone confers peculiar chemical properties to PNA which make them a powerful tool in a variety of research applications such as gene therapy and molecular genetics (Nielsen, 2001; Wang and Xu, 2004; Pellestor and Paulasova, 2004).

1.5.1 Structure and properties

Peptide nucleic acids are synthesized on a solid phase with a similar protocol as used for the synthesis of peptides (Christensen *et al.*, 1995). Unlike DNA and RNA, the PNA backbone is uncharged. Consequently the electrostatic repulsion with negative charged DNA or RNA is not present during hybridization, leading to a higher stability of the PNA-DNA or PNA-RNA complex in comparison to DNA-DNA or RNA-RNA duplexes. The extremely high stability of PNA-DNA and PNA-RNA complexes is also confirmed by higher melting temperature (T_m) values compared to DNA duplex or RNA. PNA binding to dsDNA targets can be influenced by the presence of salts. PNA can be modified to render their binding independent from ionic strength, for example by introduction of
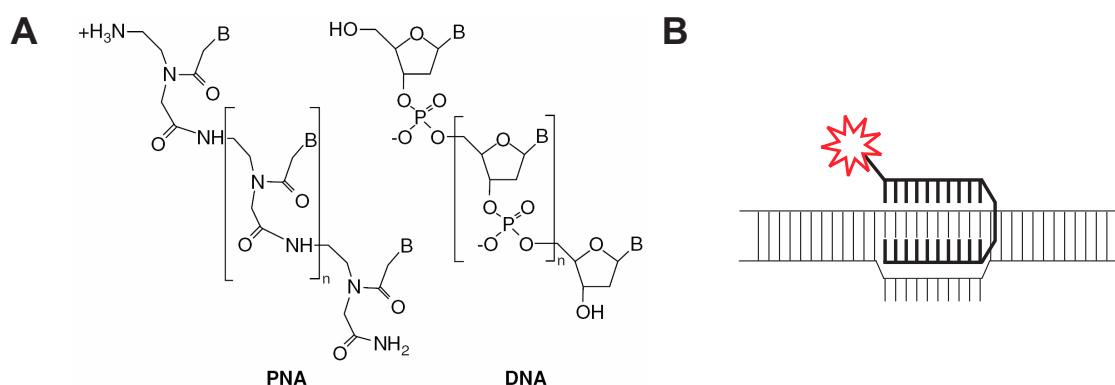
Figure 1.2: Chemical structure of PNA and triplex formation. (A) Comparison of the chemical structure of PNA and DNA. B: nucleobases (from Svahn *et al.*, 2004). (B) Schematic representation of (PNA)$_2$/DNA triplex and noncomplementary DNA displaced strand. The ladder represents the DNA, in bold the PNA labeled with a flurochrome (red star).

positively charged group such as lysines or arginines (Bentin *et al.*, 2003). In addition, the substitution of cytosines with pseudoisocytosines (J) results in an independence from pH (Egholm *et al.*, 1995). The modified backbone of the PNA is also responsible for the resistance to nucleases and peptidases inside the cells (Demidov *et al.*, 1994). BisPNA, as used in this work, are two PNA oligomers linked together via a flexible ethylene-glycol linker. These molecules bind to dsDNA by strand invasion: the first strand of the PNA recognizes the target sequence on the dsDNA and interacts via Watson-Crick base pairing rules. The flexible polylinker allows the molecule to fold back, so that the second strand can interact with the PNA-DNA duplex via Hoogsteen hydrogen bonds resulting in a highly stable triplex.

1.5.2 Applications

The specificity and stability of PNA binding to DNA can be exploited in many research fields.

A first application of these molecules was as an antisense agent in gene therapy. This application takes advantage of the high stability of PNA *in vivo*, which is many hours compared to maximum 15 min of DNA or RNA oligonucleotides (Wang and Xu, 2004). On the other side, one of the major obstacle using PNA as an antisense agent is their slow cellular uptake into living cells. More recent results show that coupling to small peptides containing a nuclear localization signal (NLS) (Branden *et al.*, 1999; Cutrona *et al.*, 2000; Braun *et al.*, 2002) or conjugation to the DNA intercalator 9-aminoacridine combined with lipofectamine cellular delivery (Shiraishi and Nielsen, 2004), are sufficient to speed up the delivery into the cells. Inside the nucleus PNA are targeted to a specific DNA sequence in the promoter, impeding access of RNA polymerase to DNA, or blocking polymerase progression (Nielsen *et al.*, 1994). On the other hand the D-loop generated from the binding of PNA can induce gene expression in some cases (Wang *et al.*, 1999). As an antisense agent PNA recognizes specific sequence on messenger RNA independently of the RNA secondary structure, but, in contrast to oligonucleotides which activate the RNaseH, they act through steric interference of RNA processing, transport to cytoplasm, and translation (Knudsen and Nielsen, 1996). Antisense PNA were

designed against various mRNA to down-regulate their expression, such as the oncoprotein MDM2 (Shiraishi and Nielsen, 2004) or the human caveolin-1, a small protein involved in the formation of invaginations at the plasma membrane (Liu *et al.*, 2004).

Another field of application takes advantage from the possibility to conjugate PNA with fluorophore such as fluorescein or rhodamine. These labeled PNA can be used as probes for FISH to explore chromosome structure on metaphase or interphase chromosomes, as well as for molecular diagnostic (Molenaar *et al.*, 2003; Paulasova *et al.*, 2004). The power of PNA probes lies in very specific and discriminant interactions with nucleic acid targets, which allow a single base discrimination, and a very low background.

PNA are also used as probes for nucleic acid biosensors, a technology which holds promises for rapid detection of specific DNA sequences. In this method PNA are immobilized onto optical, electrochemical or mass-sensitive transducers to detect complementary or mismatched strands in the analyzed solution. The hybridization is then transformed into an electric signal by the transducer (Ray and Norden, 2000).

In PCR analysis, PNA can be used as direct competitors for one of the site recognized by the primer on the template, thus inhibiting the amplification. In Q-PNA PCR, a variation of real-time PCR, the quencher-labeled PNA hybridizes with one of the primer which carries a fluorescent dye, quenching its fluorescence. Incorporation of the primer in a double strand amplicon displaces the Q-PNA and liberates the fluorescence of the dye tagged to the primer (Fiandaca *et al.*, 2001).

1.6 *Lac* operator/repressor system

For direct visualization of chromatin loci and their dynamics in living mammalian cells, Belmont and coworkers developed an approach based on the use of the *lac* operator/repressor system (Robinett *et al.*, 1996; Belmont *et al.*, 1999a; Belmont, 2001). The advantage of this system is that protein-DNA interactions are less perturbing than *in situ* hybridization techniques with oligonucleotides requiring denaturation of DNA. Moreover the fusion of the *lac*

repressor to GFP allows a direct visualization in living cells.

There were several reasons for choosing this system. First, it was demonstrated *in vitro* that the *lac* repressor is still able to bind to its target sequence packaged within nucleosomes (Chao *et al.*, 1980), and the binding was confirmed in living eukaryotic cells (Hu and Davidson, 1987). Additionally, both the protein and the DNA sequence are very well characterized and mutants exist which could be used to improve the system (Belmont and Straight, 1998).

In the system used in this work, the 8-mer operator sequence is amplified to 256-copies of direct repeats with a directional cloning approach (Robinett *et al.*, 1996) and the repressor is mutated at the carboxy-terminus to prevent the formation of tetramers (Chen and Matthews, 1992). The inserted *lac* operator array can be identified in three ways: (1) staining of fixed cells with purified *lac* repressor followed by immonofluorescence or immunogold, (2) transformation with *lac* repressor fused with NLS for nuclear localization followed by immunostaining, (3) *in vivo* expression of GFP-*lac* repressor-NLS fusion protein and direct detection. Broader applications are possible due to the several spectral variants of GFP, such as YFP and CFP, and also the possibility to put the system under transcriptional control (Tsukamoto *et al.*, 2000).

The high detection sensitivity and stability in several different organisms make the *lac* operator/repressor system suitable for many applications. One of the first applications was to elucidate the dynamics of chromosome segregation in organisms, such as bacteria, in which condensed chromosomes are not visible and are highly sensitive to sample-preparation. In *Bacillus subtilis* it was possible to demonstrate the bipolar segregation of origins in sporulating cells, with integration of the *lac* operator near the origin (Webb *et al.*, 1997). The same system was used to visualize chromosomes in *Caenorabditis elegans* and to easily identify polyploid cells (Belmont and Straight, 1998). In living *Arabidopsis taliana* plants it was used to observe specific tagged chromosome loci in different cell types (Kato and Lam, 2001). The *lac* operator/repressor system was also used in other organisms such as *Saccharomyces cerevisiae*, *Drosophila melanogaster* and mammalian cells to study chromosome mobility in different stages of the cell cycle (Straight *et al.*, 1996; Marshall *et al.*, 1997; Vazquez *et al.*, 2001; Heun *et al.*, 2001; Thomson *et al.*, 2004). Recently, to observe the

spatial and temporal organization of AAV (adeno-associated virus 2) replication in living cells, 40 *lac* repressor binding sites were cloned into the AAV genome and the recombinant genome visualized by binding to *lac* repressor fused to EYFP (enhanced yellow fluorescence protein) (Fraefel *et al.*, 2004).

In another interesting application the *lac* operator/repressor system was combined with gene amplification. In this way, it was possible to selectively visualize the cell cycle dynamics of a ~ 90 Mbp, late replicating, heterochromatic homogeneously staining region (HSR) which behaves as an endogenous band (Li *et al.*, 1998).

2 Aims of the work

What happens to foreign DNA once it has reached the nucleus during viral infection, application of gene therapy or simple transfection? In this work we try to address the question by investigating the localization and dynamics of plasmid DNA. To this end we will need to fluorescently label the plasmids to allow direct visualization in living cells and a delivery method which does not interfere with cellular vitality.

In the second part of this work, we will study the dynamics of endogenous DNA which is known to be locally constrained, focusing on the association of this limited movement with the transcriptional status of the cell and the nuclear localization of the analyzed chromatin locus.

3 Materials and methods

3.1 Materials

3.1.1 Devices, chemicals and equipment

Devices

PCR machine	Light Cycler, Roche
	Mastercycler Gradient, Eppendorf
Light microscope	Axiovert 25, Zeiss
	Axiovert 35, Zeiss
Confocal microscope	LSM 510 Meta, Confocor 2, Zeiss
Microinjection System	Micromanipulator 5170, Eppendorf
	Microinjector 5242, Eppendorf
	Jun Air compressor
Electroporation System	GenePulserII, Bio-Rad
Spectrophotometer	SmartSpec 3000, Bio-Rad
Centrifuges	SuperT21, Sorvall
	Micro Centrifuge 5415D, Eppendorf
	L70 Ultracentrifuge Beckmann
Sterile work bench	HeraSafe, Heraeus
pHmeter	Model CG842, Schott
Gel documentation	BioDocAnalyze, Biometra

Chemicals

Acetic acid (glacial)	Merck
Agar	Difco
Agarose	Sigma
Alcian blue	Fluka
Bromophenolblue	Roth
Cesiumchloride	Roth
DABCO	Sigma
EDTA	Merck
Ethanol p.a.	Merck
Ethidium bromide	Roth

FITC-dextran (250KDa)	Sigma
Glycerin	Merck
Hypoxanthine	Sigma
Isopropanol	Merck
Nocodazole	Sigma
Polyethylenimine (PEI)	Sigma
p-Phenylenediamine (PPD)	Sigma
SDS	Roth
Thymidine	Sigma
Tris	Merck
Triton X-100	Sigma
Trypton	Merck
Yeast extracts	Difco

Antibiotics

Ampicillin	Roche
Kanamycin	Sigma
Hygromycin B	Roche
Penicillin	PAA
Streptomycin	PAA

Enzymes

Restriction enzymes	NEB Biolabs
RNase, DNase free	Roche
T4 ligase	Roche

Inhibitor of transcription

DRB	Sigma

Cell culture

DMEM High Glucose medium	PAA
CO_2-Independent medium	Gibco
IDMEM	Sigma
L-Glutamine	Life Technologies
DMSO	Merck

FCS gold	PAA
FCS dialyzed	PAA
Trypsin-EDTA solution	PAA
Petri dishes ($\varnothing$ 100 mm)	Greiner
Petri dishes ($\varnothing$ 60 mm)	Nunc
Glass bottom dishes ($\varnothing$ 35 mm)	MatTek Corporation
96, 24, 6 wells plates	Greiner

Microinjection-associated equipment

CELLocate, gridded coverslips (175 μm)	Eppendorf
Femtotips II	Eppendorf
Microloader	Eppendorf
Centricon 30 kDa cut-off	Millipore
Ultra free 100 kDa cut-off	Millipore
Filter ($\varnothing$ 0.2 μm)	Schleicher und Schuell

DNA molecular weights

Gene Ruler 100bp	MBI Fermentas
λDNA Eco130I (StyI)/MluI	MBI Fermentas

DNA dyes

Hoechst 33258	Sigma
TO-PRO-3 Iodide	Molecular Probes

Kits

GFX-PCR purification Kit	Pharmacia
Light Cycler FastStart DNA Master SYBR Green I	Roche

3.1.2 Buffers and solutions

1x PBS (1l)	8 g NaCl
	0.2 g KCl
	1.44 g Na_2HPO_4
	0.24 g KH_2PO_4
	pH 7.4

LB medium (1l)	10 g NaCl
	10 g Trypton
	5 g Yeast extract
	(+ 1.5 % agar for plates)

SOC medium (1l)	20 g Trypton
	5 g Yeast
	0.5 g NaCl
	20 ml Glucose (1M)

50x TAE (1l)	242 g Tris-Base
(Tris/Acetic/EDTA)	57.1 ml Acetic acid
	100 ml EDTA (0.5 M, pH 8.0)

3.1.3 Oligos and primers

Primers were purchased from MWG-Biotech AG and had the following sequences:

PNA oligos

oligo1   5'-AATTGGATCCGAGAAGAAAA-3'

oligo2   5'-AATTTTTTCTTCTCGGATCC-3'

Primers for sequencing

T3 (pK2)   5'-ATTAACCCTCACTAAAGGGA-3'

T7 (pMII)   5'-TAATACGACTCACTATAGGG-3'

pEGFP-C1 (pEPI 1)   5'-ACCACAACTAGAATGCAGTGA-3'

Primers for RT-PCR

Forward primer   5'-GTTCCACTGAGCGTCAGACC-3'

Reverse primer   5'-CTCAAGTCAGAGGTGGCGAA-3'

3.1.4 Vectors

Table 3.1: List of used vectors

Name	Origin	Characteristics
pMII	laboratory's collection	human MII SAR-DNA in pBluescript SK+
pK2	laboratory's collection	complete non-expressing cDNA of SAF-A in pBluescript SK+
pEPI-1	gift of Dr. H.J. Lipps (University of Witten-Herdecke, Germany)	human interferonβ SAR-DNA in pEGFP-C1, functional promoter, episomally replicating
pHrP-C-T1T2 (rDNA)	gift of Dr. U. Scheer (University of Wuerzburg, Germany)	rDNA in pUC9 derivated vector
pBluescript SK+	laboratory's collection	Invitrogen
pRSET-A	laboratory's collection	bacterial expression vector (Invitrogen)
pSAF-A	laboratory's collection	cDNA of SAF-A cloned in pEGFP-C1
hFibrillarin	gift of Dr. U. Scheer (University of Wuerzburg, Germany)	fused with GFP
PML	gift of Dr. T. Hoffmann (HPI, Hamburg, Germany)	fused with GFP
Lamin-B1	gift of Dr. J. Ellenberg (EMBL, Heidelberg, Germany)	fused with GFP
pHM 838 (βGal)	laboratory's collection	β-Gal-NLS fused with GFP
pSV2-dhfr-8.32 (lacOp)	gift of Prof. A.S. Belmont (University of Illinois, Urbana, USA)	256 copies of lac operator sequence, dhrf gene for selection
p3'SS-EGFP-dimer-lacrep (lacI-GFP)	gift of Prof. A.S. Belmont (University of Illinois, Urbana, USA)	fused with GFP

3.2 Methods

3.2.1 General methods

The listed methods were taken from Sambrook and Russel (2001) and will not
be further described here.

- Determination of DNA concentration

- DNA gel electrophoresis

- DNA purification by CsCl density gradient centrifugation

3.2.2 Cloning a binding site for PNA

Plasmids were cut at the unique EcoRI restriction site with 10 U of the enzyme
for 3 h at 37°C. To remove the enzyme, products of digestion were precipitated
with 1:10 of 3 M NaAcetate and 2.5 volumes of 100 % cold ethanol, 1 h at
-20°C. Samples were then centrifuged 10 min at full speed, supernatant was
removed with a pump and pellets dried at 37°C. At the same time, 500 pmol
of complementary PNA oligos (see section 3.1.3) were annealed 5 min at 75°C
and cooled down at room temperature. Pellets of digested plasmids were
resuspended with the annealed oligos and ligated over night at 18°C with 1 U/μl
of T4 ligase in the appropriate buffer. To inactivate the ligase, products of
ligation were heated to 65°C for 15 min. To eliminate re-ligated plasmids
without insert, samples were digested again with EcoRI (10 U, 3 h at 37°C).
After purification through a GFX-column (Pharmacia) and ethanol precipitation,
the plasmids were used to electroporate competent XL-1 bacteria.

3.2.3 DNA sequencing

DNA sequencing was carried out by the dideoxy- or chain termination method
of Sanger *et al.* (1977), using the BigDye-kit from Applied Biosystems.

Reaction: 1 μg DNA template

10 pmol specific primer

3 μl Big-Dye (Terminator-Cycle-Sequencing-MIX)

5 μl 2.5x buffer

add dist. H_2O to 20 μl.

The specific primer used are listed in section 3.1.3.

PCR program:	25 cycles
Denaturation:	96°C 30 s
Annealing:	50°C 5 s
Elongation:	60°C 4 min

Amplified DNA was precipitated with ice cold ethanol (100 %) and pellets were air dried. The analysis of the sequences was performed at the Institute of Cell Biochemistry and Clinical Neurology of the University of Hamburg.

3.2.4 Labeling of plasmid DNA by PNA

Rhodamine-labeled PNA with the sequence:

$$\text{Rh-O-KK-JTJTTJTTTT-(O)}_3\text{-TTTTCTTCTC-K-NH}_2$$
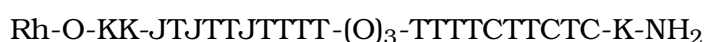
was synthesized and purified in the laboratory of Prof. P.E. Nielsen (Department of Medical Biochemistry and Genetics, The Panum Institute, University of Copenhagen, Denmark) as described in Christensen *et al.* (1995). PNA were dissolved in distilled water to a concentration of 100 pmol/µl. Small aliquots were stored light protected at -20°C. For hybridization, 375 pmol PNA were added to 30 µg of plasmid DNA (molar ratio of 50:1 (PNA:DNA)) in 120 µl TE and incubated for 3 h at 37°C in the dark.

3.2.4.1 Purification and concentration of PNA/DNA complexes

To quantitatively remove the excess of unbound PNA, samples were diluted into 2 ml sterile-filtered TE ($\varnothing$ 0.2 µm) and centrifuged (10 min at 5 000 g, 4°C) in Centricon ultrafiltration devices with 30 kDa cut-off. This washing step was repeated twice, then the labeled DNA was recovered by inverting the device and spinning for 2 min at 1 000 g, 4°C. The obtained PNA/DNA complexes had a final concentration of 0.5-1 µg/µl and were stored light protected at -20°C in small aliquots.

3.2.5 Electrophoretic mobility shift assay

Plasmid DNA (0.75 pmol) was incubated with increasing amounts of PNA in 20 µl TE for 3 h at 37°C in the dark. After incubation, PNA/DNA complexes were

digested with restriction enzymes to produce fragments of suitable dimension for mobility shift assays. pMII plasmid was digested with 10 U of XbaI and KpnI for 3 h at 37°C, while pK2 plasmid with 10 U of SmaI at 25°C. Products of digestion were analyzed in 1.5 % agarose gel to reveal the possible shift of the fragment containing the PNA target sequence.

3.2.6 Cell culture

COS 7 cells (African green monkey, kidney) were cultivated as a monolayer on plastic dishes ($\varnothing$ 10 cm) in Dulbecco's modified Eagle's medium (DMEM) with 10 % FCS, at 37°C in a humidified atmosphere containing 5 % CO_2. The medium was supplemented with 10 U/ml penicillinG and 100 µg/ml streptomycin. The cells were split every 2-3 days by detaching them from the plate with a short incubation in trypsin-solution and diluting them 1:5 or 1:10 in fresh medium.

CHO/dhfr- (Chinese hamster ovary cells with double deletion for dihydrofolate reductase gene) were purchased from ECAA (#94060607) and were cultivated in IDMEM or, later, in DMEM medium supplemented with 10 % FCS, 10 U/ml penicillinG, 100 µg/ml streptomycin, 2 mM L-glutamine, 0.1 mM hypoxanthine and 0.01 mM thymidine. Cells were adapted to DMEM medium by cultivation in IDMEM/DMEM mixtures with stepwise reduction of IDMEM every second or third day. Culture conditions were the same as described for COS 7 cells.

3.2.7 Transfection of eukaryotic cells

3.2.7.1 Transfection with polyethylenimine (PEI)

One day before transfection, cells were split 1:5. Serum-free medium (50 µl) was added to 10 µg DNA and the DNA mixed with PEI-working solution (300 µl serum-free medium and 4.5 µl 0.5 % PEI solution). This solution was incubated for 30 min at room temperature. During this time, the medium in the dishes was exchanged with 3 ml of fresh DMEM. The transfection solution was given to the cells drop by drop and mixed carefully. After 4 h the medium was replaced by DMEM medium and the cells further cultivated until analysis.

3.2.7.2 Transfection by electroporation

One day before transfection, cells were split 1:5. The cells were detached from the plate with a short incubation in trypsin-solution, resuspended in 10 ml of complete medium and transferred to a sterile tube. After short centrifugation (3 min, 200 g, 4°C) and removal of the supernatant, the cell pellet was resuspended in 800 μl complete medium containing 10 μg of vector DNA. The electroporation was carried out in 4 mm cuvettes at 325 V, 950 μF and ∞ Ω. After the pulse, cells were immediately resuspended in prewarmed medium, transferred to a plastic dish ($\varnothing$ 10 cm) and incubated under normal condition until analysis.

3.2.8 Microinjection of COS 7

One day before microinjection, cells were seeded onto 175 μm CELLocate coverslips (Eppendorf), or on glass bottom dishes, depending on further analysis. The PNA/DNA complexes were thawed at room temperature and centrifuged 15 min at 10 000 g at 4°C to avoid capillary clogging. Femtotip II capillaries were loaded from the rear with 1.5 μl of sample using microloaders. Table 3.2 shows the concentration of used probes. Filled capillaries were inserted into the holder and the holder mounted on the Micromanipulator 5170 (Eppendorf). The microinjection was performed in CO_2-independent medium using the Microinjector 5242 (Eppendorf). Cells were first focused at low magnification (10x objective), the capillary positioned roughly by eye in the middle of the plate and carefully moved down into the medium. Then the femtotip was focused and lowered carefully until the cells were almost in focus again; at that point the objective was changed to one with higher magnification (32x). For nuclear microinjection, the tip was positioned above a selected nucleus and moved down

Table 3.2: Concentration of samples used for microinjection.

Sample	Concentration
PNA/DNA complexes	0.5–1 μg/μl
Free PNA	2 pmol/μl
FITC-dextran	1 μg/μl
Expression vectors	0.5–1 ng/μl

until a white spot appeared on the cell surface and both cell and capillary were in focus. The tip was then carefully moved down a little bit more and this level set as the limit for the automatic injection. The injection pressure was set to 100 hPa for 0.5 s. Under these conditions, ∼0.3 pl of sample was injected per cell. The injection pressure was released by use of a foot switch and appears as a wave going through the whole nucleus. In each experiment, at least 50 cells were microinjected. At the end, the cells were washed twice with 1x PBS, and further cultivated in complete medium.

3.2.9 Sequential extraction of cells

Cells grown on glass coverslips coated with 0.1 % alcian blue and microinjected as described above (section 3.2.8) were processed 20 h after injection. Cells were washed briefly in 1x PBS and incubated with 100 µl CSK buffer (10 mM PIPES pH 6.8, 100 mM NaCl, 300 mM sucrose, 3 mM $MgCl_2$ and 0.5 % Triton X-100) for 10 min at room temperature. To stabilize the structures, sodium tetrathionate (2 mM) was added to the buffer. After washing in 1x PBS, cells on some coverslips were fixed 10 min at room temperature with 3.5 % paraformaldehyde and mounted in 40 % glycerol in 1x PBS on a slide, the rest was further treated with 100 µl extraction buffer (10 mM PIPES pH 6.8, 250 mM ammonium sulfate, 300 mM sucrose, 3 mM $MgCl_2$ and 0.5 % Triton X-100) for 10 min at room temperature, washed again in 1x PBS and finally incubated for 10 min at room temperature with 100 µl of 2 M NaCl in the same buffer. Before fixation with paraformaldehyde as described above, DNA was stained with TO-PRO-3 iodide (1 nM in 1x PBS) for 10 min at room temperature.

3.2.10 Hirt extraction

COS 7 cells were transfected by electroporation with 10 µg of unlabeled plasmid DNA, as described in section 3.2.7.2. Two days after transfection, the medium was removed and the plates were thoroughly washed with 1x PBS. Cells were then permeabilized by incubation with 3 ml of CSK buffer (see section 3.2.9) for 10 min at room temperature. After two washes in 1x PBS, half of the dishes were treated with 2 M NaCl in 10 mM PIPES pH 6.8, 300 mM sucrose, 3 mM $MgCl_2$ and 0.5 % Triton X-100 for 10 min at room temperature. Plates were washed again in 1x PBS, and cells on all plates were lysed with 3 ml of lysis buffer

(0.6 % SDS, 10 mM Tris-HCl, 10 mM EDTA) for 5 min at room temperature. The lysate was transferred to a tube, gently mixed with the same volume of 2 M NaCl in TE and stored at 4°C over night. The next day, plasmid DNA was separated from precipitated material (containing genomic DNA) by centrifugation at 10 000 g for 20 min in the cold, and further purified by phenol:chloroform extraction and isopropanol precipitation. The DNA pellet was washed in 70 % ethanol, air dried and resuspended in 50 µl of water. To quantify recovered plasmid DNA, XL-1 bacteria were transformed by electroporation with 1 µl of each DNA. Transformed bacteria were then plated on LB agar plates containing the appropriate antibiotic and incubated over night at 37°C. The next morning, resulting colonies were counted.

3.2.11 Real-time PCR (RT PCR)

Real-time PCR was carried out in a LightCycler (Roche) using the Light Cycler FastStart DNA Master SYBR Green I kit with 3 mM $MgCl_2$. Specific primers (listed in section 3.1.3) were designed in order to recognize both pBluescript SK+ and pEGFP-C1 plasmids.

Experimental protocol   preincubation 95°C 10 min

40 cycles:

Denaturation: 95°C 10 s

Annealing: 55°C 10 s

Elongation: 72°C 20 s

Melting curve analysis

Plasmid DNA, obtained by Hirt extraction, were diluted 1:40 in distilled water and 4 µl were used as template. Each sample was analyzed in duplicate, together with five standards and water as a negative control. The second derivative maximum method of the LightCycler Software was used for quantification analysis.

3.2.12 Establishment of stable cell lines

CHO/dhfr- cells were transfected with PEI with 10 µg of pSV2-dhfr-8.32 (lacOp). Two days after transfection, transformants were selected in DMEM without

hypoxanthine and thymidine, supplemented with antibiotics and 10 % dialyzed FCS. Under these conditions, only cells with integrated lacOp plasmid are able to grow. Many clones were visible after 10 days of selection and were further cultivated in DMEM medium with 10 % FCS. Aliquots were frozen in complete medium with 10 % DMSO and stored in liquid nitrogen.

In a second step, lacOp-stable cells were transfected with 10 μg of p3'SS-EGFP-dimer-lacrep (lacI-GFP). After two days of transfection, cells were selected in normal complete medium containing 200 μg/ml of hygromycin B, for 4 weeks. Again, aliquots of cells were frozen in complete medium with 10 % DMSO and stored in liquid nitrogen.

To obtain transfected clones which are derived from a single parental cell, stable CHO lacOp/lacI-GFP cells were detached from the dish by incubation in trypsin-solution and counted in a Neubauer chamber. The concentration of the cells was then progressively diluted to have 0.5 cell/100 μl medium, and 100 μl were plated into several 96-wells plates, paying attention to mix the suspension gently and repeatedly to keep the cells separated. In this way, statistically, one cell should be found in every second well. The next day, each well was screened for presence of one single cell and marked. Only well proliferating clones were further passaged to 24-wells, to 6-wells plate and finally to 10 cm dishes. In the first passage to 24-wells plates, 73 growing clones were also seeded onto coverslips to verify the expression's level and localization of lacI-GFP at the confocal microscope. Most of them were cultivated further, and later frozen in DMEM with 10 % DMSO and stored in liquid nitrogen.

3.2.13 Fixation and staining of cells for FACS analysis

One day before collection, stable CHO lacOp/lacI-GFP cell lines (subclones 2G10 and 3C4) were split 1:5. Cells were washed with cold 1x PBS/0.1 % EDTA (w/v) and detached from the plate by a short incubation in trypsin-solution. The cells were resuspended in 10 ml of cold 1x PBS/0.1 % EDTA (w/v) and centrifuged 5 min at 310 g in the cold. The supernatant was removed, the test tube was flicked and the pellet carefully resuspended in 0.7 ml 1x PBS/0.1 % EDTA (w/v). The well-resuspended cellular suspension was mixed with 10 ml of ice-cold methanol in a conical tube, gently inverted twice and incubated for at

least 20 min on ice, before storing at -20°C over night. The next day, samples were warmed to room temperature and centrifuged for 6 min at 310 g at 16°C. The supernatant was removed, and the pellet was resuspended in 5 ml of 1x PBS/0.1 % EDTA (w/v) (at room temperature) by inverting the tube twice. After 10 min at room temperature, the cells were collected by centrifugation as described above and resuspended in 0.5 ml PI solution (1x PBS with 1:15 RNaseA [10 mg/ml] and 1:30 PI [0.5 mg/ml]). The cells were incubated for 30 min at 37°C, and then cooled down over night in the dark. The next day, samples were further diluted in PI solution and analyzed for DNA content with a Coulter EPICS XL system. The FACS analysis was kindly performed by Dr. Daniel Speidel.

3.2.14 Preparation of fixed specimens for confocal microscopy

For analysis by laser confocal microscopy, cells were grown on coverslips. COS 7 cells were first microinjected, while CHO lacOp/lacI-GFP could be immediately prepared. Coverslips were briefly washed in 1x PBS and fixed for 15 min with 3.5 % paraformaldehyde in PBS. After washing in 1x PBS, coverslips were treated for 10 min at room temperature with 0.5 % Triton X-100 in 1x PBS, washed again and incubated with the DNA stain TO-PRO-3 iodide (1:1000 in 1x PBS) for 10 min at room temperature. After a final wash in 1x PBS, coverslips were mounted on slides with 1.5-2 µl of mounting medium, dried for a few minutes and sealed with transparent nail polish.

Different mounting medium were used:

conventional:	40 % glycerol in 1x PBS
DABCO:	100 mM Tris HCl pH 7.5, 90 % glycerol, 10 % DABCO
PPD:	100 mM Tris HCl pH 9, 40 % glycerol, 1 mg/ml PPD

DABCO (Sigma) and PPD (Sigma) are antifade reagents used to prevent bleaching of GFP-fusion proteins and stained DNA. Since DNA stained with TO-PRO-3 iodide is not visible at the microscope, mounting media were added with 3 µg/ml of Hoechst 33258.

3.2.14.1 Analysis of fixed cells

Coverslips prepared as described in section 3.2.14 were briefly and carefully washed with distilled water to remove any rest of salts and mounted with a drop of immersion oil (Zeiss) on the microscope. In Table 3.3 the used settings are shown. Zoom factor was adjusted between 2 (panorama) and 20 (details) depending on the target of analysis, and its dimension is indicated in every picture as a scale bar. Images were further processed with the program ImageJ, version 1.32j (http://rsb.info.nih.gov/ij), and Adobe Photoshop™ 6.0.

Table 3.3: Settings for taking images of fixed specimens.

Parameters	Settings
Laser	Argon/2: 458, 477, 488, 514 nm (GFP) HeNe 1: 543 nm (rhodamine) HeNe 2: 633 nm (TO PRO 3)
Laser output (Argon/2)	30 %
Filter	BP 505-530 (GFP) LP 560 (rhodamine) LP 650 (TO-PRO-3)
Wavelength for excitation	488 nm 10 % 543 nm 80 % 633 nm 3 %
Image size	512×512
Scan speed	9
Scan average	16
Zoom	2 to 20
Pinhole	1 airy unit
Objective	Plan-Apochromat 63x/1.4 Oil
Data depth	8 bit

3.2.14.2 Fluorescence Recovery After Photobleaching (FRAP)

FRAP is a live cell imaging technique used to examine dynamics of fluorescent molecules such as proteins or DNA. In a FRAP experiment, a pulse of high-intensity light from a laser is used to irreversibly photobleach a population of fluorophores in a region of interest (ROI). The recovery of fluorescence from surrounding areas is monitored over time and enables to determine the mobile

fraction of the population (indirectly also the immobile fraction) and the diffusion coefficient.

Experimental conditions

COS 7 cells were split 1:10 on glass bottom dishes two days before FRAP experiments. The next day cells were microinjected with suitable probes (see Table 3.2) and incubated over night in normal conditions. CHO lacOp/lacI-GFP cells were plated 1:5 one day before analysis on glass bottom dishes precoated with 0.1 % alcian blue. At the day of examination, medium was exchanged with prewarmed CO_2-independent medium and dishes were placed onto a heated stage to keep temperature at 37°C. A cell of interest was focused, and a region of interest in the nucleus was selected to be bleached as a narrow strip. Table 3.4 shows the settings used for FRAP experiments with rhodamine-PNA labeled DNA and GFP-fusion proteins.

Data analysis

Collected data were evaluated with help of the freeware program ImageJ. The image stacks were opened with the plug-in 'LSM reader' (kindly provided by Jerome Mutterer, Imaging & Microscopy, Istitut de Biologie moleculaire des plantes du CNRS, Strasbourg France) and identical regions of interest were defined in the bleached and unbleached area (small rectangles in Fig. 3.1). In these regions, the software can measure the mean fluorescence intensity for all

Fluorescence recovery over time

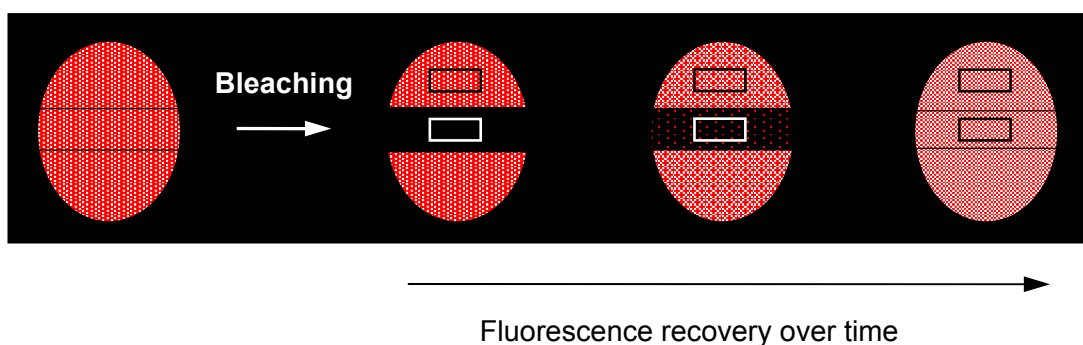**Figure 3.1: Fluorescence Recovery After Photobleaching (FRAP).** Schematic drawing representing a nucleus with homogeneously distributed fluorescent molecules. After photobleaching, the redistribution of fluorescent molecules in the bleached and unbleached areas is monitored over time. For quantitative analysis, ROI (small rectangles) are drawn in the bleached as well as in the unbleached area.

Table 3.4: Settings for FRAP experiments.

Parameters	Settings
Laser	Argon/2: 458, 477, 488, 514 nm (GFP)
	HeNe 1: 543 nm (rhodamine)
Laser output (Argon/2)	85 % (GFP)
	60 % (rhodamine)
Filter	BP 505-530 (GFP)
	LP 560 (rhodamine)
Wavelength for bleaching	458, 477, 488, 514 nm transmission: 100 % (GFP)
	488, 514, 543 nm transmission: 100 % (rhodamine)
Wavelength for excitation	488 nm 1 %
	543 nm 5 %
Image size	128×128
Number of images	400
Cycle delay	0.0 msec (GFP)
	1.0 s (rhodamine)
Number of images before bleaching	3
Iterations	30 (GFP)
	1500 (rhodamine)
ROI	X: variable; Y: 15 pixels
Scan speed	12 (max.)
Zoom	5
Pinhole	maximum
Objective	Plan-Apochromat 63x/1.4 Oil
Data depth	8 bit

images in the stack and export results as a text file; in addition, time stamps for all stack images were given as a text file by the same plug-in. Data were imported into MS Excel and further processed. For quantitative analysis, the loss of fluorescence in a non-bleached reference area of the analyzed nucleus (resulting from a dilution of the fluorescent molecules as they redistribute) was determined, and recovered fluorescence in the bleached area was normalized to the sum of mean intensities in the bleached and unbleached areas. This normalized fluorescence intensity was plotted as a function of time (Fig. 3.2).
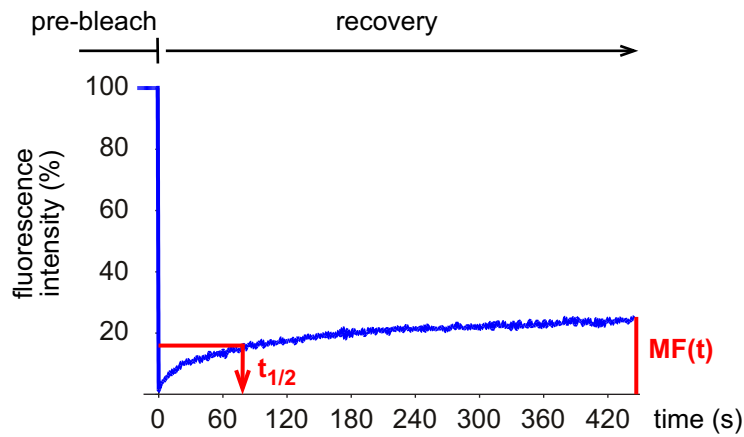
Figure 3.2: Plot of normalized FRAP data. The recovery of fluorescence in the bleached area is normalized to the mean of the total fluorescence. The obtained fluorescence intensity, average of all nuclei analyzed, is plotted against time. MF(*t*) indicates the mobile fraction at the last time point *t* of the recovery, $t_{1/2}$ is the diffusion time at which half of the fluorescent molecules have recovered.

The curve gives information about the diffusion time of the molecules under study and the percent of mobile fraction.

The high photostability of rhodamine fluorochrome leads to incomplete bleaching of rhodamine-labeled molecules in the ROI. To eliminate this component from the fluorescence recovery curves, new values, I_{new}, were calculated as follows:

$$I_{new} = (I_{t_{end}} - I_{t_0}) \cdot \frac{100}{100 - I_{t_0}}$$

with $I_{t_{end}}$ being the fluorescence intensity at the last time point and I_{t_0} the fluorescence intensity at $t = 0$.

3.2.14.3 4D life cell imaging

The LSM 510 confocal microscope can produce optical sections of an object in the Z-direction by mean of a Z-motor which moves the focus plane. This gives a stack of images which can be used to create three dimensional reconstructions of the focused object. Optical sectioning in the Z-direction can also be repeated after defined time intervals ('four dimensional' imaging).

Experimental conditions

CHO lacOp/lacI-GFP cells were plated 1:5 one day before analysis on glass bottom dishes precoated with 0.1 % alcian blue. The next day, medium was exchanged with prewarmed CO_2-independent medium and dishes were placed

Table 3.5: Settings for 4D imaging experiments.

Parameters	Settings
Laser	Argon/2: 458, 477, 488, 514 nm (GFP)
	HeNe 2: 633 nm (TO-PRO-3)
Laser output (Argon/2)	30 % (GFP)
Filter	BP 505-530 (GFP)
	LP 650 (TO-PRO-3)
Wavelength for excitation	488 nm 1 %
	633 nm 3 %
Image size	256×256
Number of images	15–40
Cycle delay	0.0 msec–1 min (GFP)
Scan speed	10
Zoom	5
Pinhole	2 airy units
Objective	Plan-Apochromat 63x/1.4 Oil
Number of slices/Z-stack	5-20
Data depth	8 bit

onto a heated stage at 37°C. Cells with one or two spots were examined. In Table 3.5 the settings used during the data collection are listed. The same conditions were also applied after treatment of the cells with 60 μM of the transcriptional inhibitor DRB for 2 h. The number of images and the interval between them were varied as described in the results part of this thesis.

Data analysis

Collected data from 4D imaging experiments were analyzed with help of the programs LSM 5 Image Browser and ImageJ.

Mobility of chromatin loci from measurement on one single spot:

Four dimensional live imaging was performed as fast as possible without delay between two subsequent Z-stacks. Each stack consisted of only 5 slices, with a total of 40 images. In order to reduce the time needed to scan, the images were taken at low resolution and with a scan average of 1. The total time needed for

the scanning was between 3 and 4 minutes for each nucleus depending on the thickness of the specimen on the z-axis. With the tool 3D View/ Projection of the Zeiss software, the series of images were projected onto the z-axis to yield a stack composed of 40 images taken over time. These stacks were further processed with the software ImageJ. A ROI of 6x6 pixels was drawn around the spot and the xy-coordinates of its center of mass were determined in every projected image. The measurements were saved as a text file and imported into MS Excel. In order to visualize the trajectories of the spots on a x-y diagram, the measured coordinates were re-calculated so that the position of the spots at $t = 0$ was at zero (0; 0). To find out how frequent the spots in a defined distance from the origin are, the distance, D, of each point from the origin was calculated as:

$$D = \sqrt{x^2 + y^2}$$

The distribution of D was automatically calculated by MS Excel using the 'frequency' function with a chosen range of distance.

The measured coordinates were also used to determine the distance, d, covered by the spot in Δt with the formula:

$$d = \sqrt{(x_2 - x_1)^2 + (y_2 - y_1)^2}$$

The results were given in a histogram as mean of all recorded nuclei.

Mobility of chromatin loci from measurement of distances between two spots:

As a control that drift and rotation are not contributing to the measured chromatin mobility, experiments were done in cells with two spots in the same nucleus. Z-stacks with more than 10 slices (optical sections) were recorded with a cycle delay of 1 min between each stack. The image stacks were opened with LSM 5 Image Browser and the stack for each time point saved as a distinct subset in a new .lsm file. The Z-stacks for every time point were then open with the plug-in 'LSM reader' of ImageJ. The tool 'Sync Measure 3D' allows measuring the 3D distance between two points in a Z-stack. The same stack was opened twice; a ROI (6x6 pixels, centered to the fluorescence's maximum intensity of the spot) was drawn around one spot in one stack and another ROI of same dimensions was drawn around the second spot. Resulting measurements

were saved as a text file and imported in MS Excel. These raw data were processed as follows. First, it was necessary to calculate the maximum range of fluctuation for one single spot during the collecting time. This parameter is given as the maximal amplitude of the oscillation, divided per number of spots in the nucleus. Then the mean distance between two spots was calculated adding to the maximum range of fluctuation the minimum of the oscillation. At the end, the fluctuation around the mean distance was obtained substracting the calculated mean distance from each measured distance in the collecting time. The values of fluctuation calculated for all analyzed nuclei were averaged and shown in a diagram as a function of time, together with the standard deviation for each time point.

Mean square change in distance ($\langle \Delta d^2 \rangle$) analysis:

If $d(t)$ is the measured 2D or 3D distance between two points at time t, the change in distance Δd in an interval time Δt is given by:

$$\Delta d = d(t_0 + \Delta t) - d(t_0)$$

The mean square change in distance $\langle \Delta d^2 \rangle$ was calculated as the average of all Δd^2 for each time point. Plotting $\langle \Delta d^2 \rangle$ against Δt the curve presents a linear increase later followed by a plateau. The slope of the linear part represents the diffusion coefficient of the analyzed locus, and the square root of the plateau represents the radius of its confinement.

4 Results

4.1 Labeling of plasmid DNA by peptide nucleic acid (PNA)

Peptide nucleic acids (PNA) were used to attach a fluorescent label, such as the rhodamine fluorochrome, to a plasmid DNA. This allows tracing its localization and mobility in the nuclei of living mammalian cells for the first time. To compare localization and mobility of different plasmids, a 10 bp purine rich sequence (5'-GAGAAGAAAA-3') was cloned into the unique EcoRI site of many different vectors and a rhodamine-labeled PNA was synthesized in collaboration with Prof. P.E. Nielsen (Copenhagen) to hybridize to that sequence. Figure 4.1 shows a simplified representation of used PNA bound to target DNA. To increase the stability of PNA/DNA complexes *in vivo*, the PNA sequence contained pseudoisocytosine in the half of the molecule which interacts with the DNA via Hoogstein hydrogen bonds, to confer pH independence, and three lysine residues to increase DNA binding efficiency due to their positive charges.

Conditions of optimal, stoichiometric and specific binding were determined by titration with increasing molar excess of PNA over DNA. After labeling, plasmid DNA was digested with restriction enzymes to produce fragments of suitable size for mobility shift assays in agarose gel. As shown in Figure 4.2, an excess of 50-fold PNA over DNA is sufficient to give a quantitative and complete binding as demonstrated by the complete and exclusive shift of the 175 bp fragment
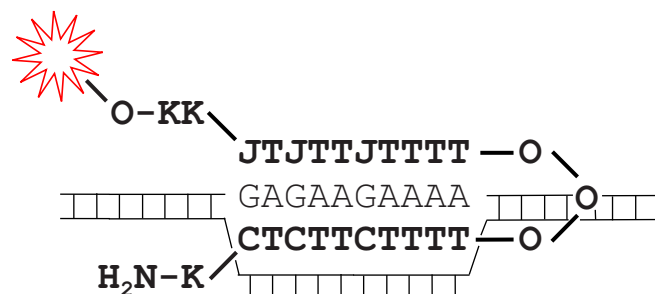

Figure 4.1: Schematic representation of PNA/DNA complex. PNA sequence is drawn in bold with a red star representing the rhodamine label. (O: ethylene-glycol linker; K: lysine; J: pseudoisocytosine). DNA is represented as a ladder.
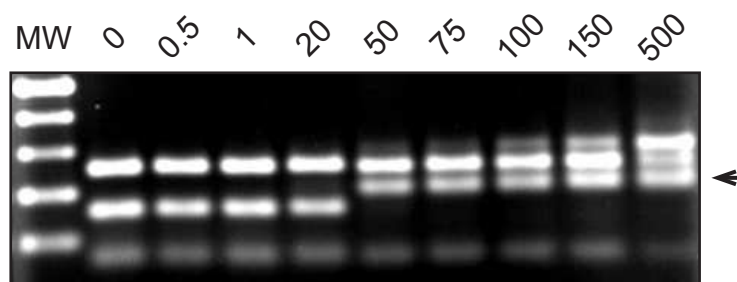
Figure 4.2: Determination of optimal PNA:DNA molar ratio for complex formation. pMII plasmid was incubated with increasing amount (0-500 molar excess) of PNA. After labeling, PNA/DNA complexes were digested with XbaI and XhoI which give small fragments well separable in a 1.5 % agarose gel, together with big fragments (not shown here). The arrow indicates the fragment of 175 bp shifted by the specific binding of PNA. MW: 100 bp DNA molecular weight.

containing the PNA binding site (arrow). Only with very high excess of PNA also other fragments were shifted. A PNA:DNA molar ratio of 50:1 was therefore chosen for all subsequent experiments.

4.1.1 Purification and concentration of PNA/DNA complexes

After labeling of plasmid DNA with 50-fold molar excess of PNA, the excess of unbound PNA was removed by filtration with Centricon ultrafiltration devices, simultaneously resulting in a concentration of PNA/DNA complexes to final concentration between 0.5 and 1 µg/µl. Once the complexes were purified from unbound PNA and concentrated, electrophoretic mobility shift assays with digested DNA were repeated to verify that the PNA molecules stayed attached to the target DNA during the whole procedure. As shown in Figure 4.3 the shift of the fragments containing the PNA binding site is still clearly visible, confirming the persistence of the PNA label on the DNA after purification. This is in line with previous reports describing that labeling of DNA by PNA is extremely stable. Interestingly, using the 100 kDa cut-off ultrafiltration devices almost two-thirds of the DNA were lost, while all DNA was retained with 30 kDa filters. It can be then roughly estimated that the dimension of labeled DNA in solution is comparable to that of a globular protein between 30 and 100 kDa, consistent with the size of a supercoiled plasmid (Zelphati *et al.*, 1999).
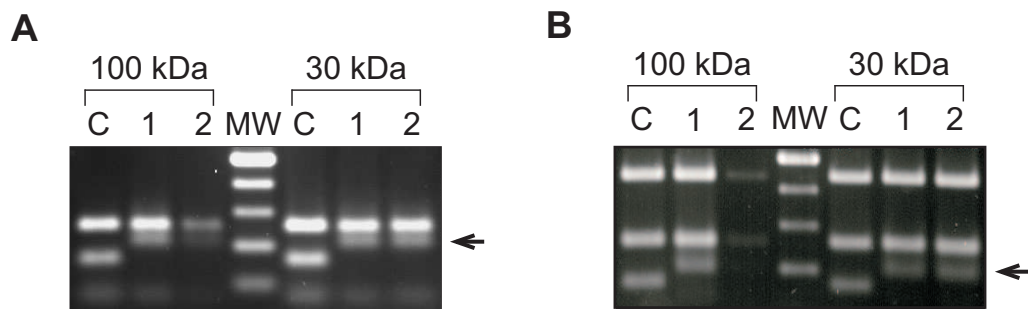
Figure 4.3: Purification of PNA/DNA complexes. After labeling and purification, mobility shift assays were performed to verify the persistence of the label on the specific fragment. Centricon ultrafiltration devices, with 100 and 30 kDa cut-off, were used to remove unbound PNA. pMII plasmid digested with XbaI/XhoI and pK2 plasmid digested with SmaI are shown in (A) and (B), respectively. The loss of pK2 through 100 kDa devices is even more evident than for pMII. MW: 100 bp DNA molecular weight; C: control DNA with unbound PNA; 1: after labeling; 2: after purification.

4.2 How to get PNA/DNA complexes into nuclei?

Preliminary experiments were performed to establish the best method to introduce labeled plasmids into living cells. Electroporation or chemical transfection of COS 7 cells did not introduce enough PNA/DNA complexes to be detected. Microinjection turned out to be the better solution. After a cytoplasmatic microinjection of COS 7 cells, the cytoplasm was stained by the PNA/DNA complexes and only weak nuclear signals could be observed (data not shown). To study the localization and mobility of plasmid DNA in live nuclei, microinjection directly into the nucleus gave better results.

4.3 Microinjection is not toxic for the cells

COS 7 cells were grown on CELLocate coverslips, which allow an easy identification of microinjected cells. From concentration of samples and microinjected volume, the number of microinjected plasmids was estimated to be around 1 500 copies. Even though this amount of singly labeled plasmid molecules was enough for microscopic detection, a 10-fold increase in copy number was used in the following experiments to have a more reproducible signal (Fig. 4.4).

Microinjection conditions were carefully optimized with respect to rate of cellular survival after the injection. One of the main factors involved is the pressure of injection. A too high pressure caused morphological alteration

~1 500 copies   ~15 000 copies
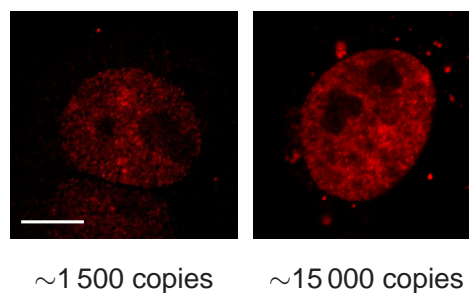
Figure 4.4: Comparison of amount of microinjected plasmid. The left panel shows a nucleus where ~1 500 plasmid copies were microinjected, the right panel a nucleus with 10-fold more of labeled plasmid. The two images were taken with the same settings at the confocal microscope. Scale bar: 10 μm.

LaminB1   PNA/DNA   merge
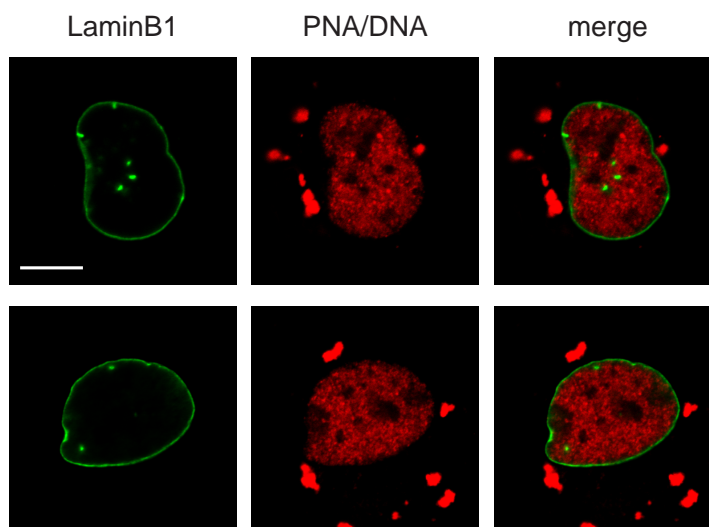
Figure 4.5: Cell viability after microinjection. COS 7 cells grown on CELLocate were co-microinjected directly into the nucleus with a mixture of PNA/DNA complexes and an expression vector for GFP-LaminB1. After fixation, cells were examined by confocal microscopy. LaminB1 was expressed and localized as a ring around the nucleus (the nuclear lamina). Injected PNA/DNA complexes remained entirely nuclear (a possible explanation of extranuclear signals is provided in section 4.5). Scale bar: 10 μm.
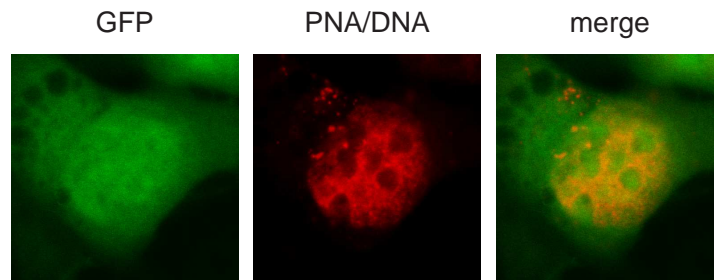
Figure 4.6: GFP expression from PNA-labeled plasmid. Labeling of pEPI-1 with PNA did not interfere with the expression of the GFP gene contained in the plasmid sequence.

of the cells shortly after injection, and after longer incubation the cells could not be found anymore, because they died and detached from coverslips. Only using a pressure of around 100 hPa cell survival was higher than 80 %. Cell viability was tested with a nuclear co-microinjection of PNA/DNA complexes with an expression vector encoding GFP-LaminB1 (Fig. 4.5). After 18 h, the presence of the fluorescent LaminB1 was examined by confocal microscopy. The transcription, translation and correct localization of the protein indicated that vital functions of the cells were not affected by the injection. In addition, microinjection of rhodamine PNA-tagged pEPI-1, a plasmid encoding the green fluorescent protein, resulted in green fluorescent cells, indicating that the expression of a gene contained in the injected plasmid was not affected by labeling with PNA (Fig. 4.6).

4.4 Nuclear localization is due to plasmid component of PNA/DNA complexes

To verify that the nuclear localization of complexes was due to the DNA and not to the PNA component, free rhodamine-labeled PNA was microinjected into nuclei of COS 7 cells together with FITC-dextran of high molecular weight (Fig. 4.7). Interestingly, very soon after the injection, the mixture divided into its two components: FITC-dextran remained trapped in the nuclei because of its high molecular weight, while free PNA relocated into the cytoplasm and formed granular aggregates. These findings were in agreement with recent experiments which demonstrate a strict requirement of a functional nuclear localization signal (NLS) attached to PNA molecules to achieve their nuclear localization
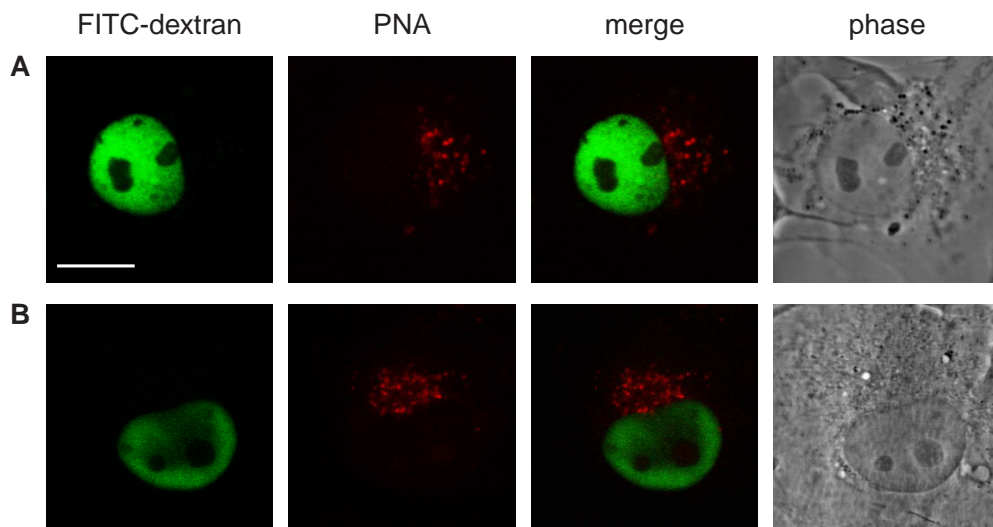
Figure 4.7: Microinjection of free PNA with FITC-dextran. COS 7 cells, grown on CELLocate, were nuclearly microinjected with a mixture of free PNA (in the same amount as used for the labeling of plasmid DNA) and FITC-dextran 250 kDa (1 µg/µl). Coverslips were fixed after 1 h (A) and over night (B) from microinjection. The two components of the mixture split up with PNA relocating to the cytoplasm where they were still visible after 18 h of incubation. The FITC-dextran, which cannot cross the nuclear membrane for its size, stayed in the nucleus and started to be degraded at the longer incubation. Scale bar: 10 µm.

(Braun *et al.*, 2002).

4.5 The final localization of an injected plasmid is reached after hours

Our first experiments focused on the question how long it takes until the injected DNA reaches its steady state. In a time course experiment, plasmid DNA labeled with rhodamine-PNA were microinjected into nuclei of COS 7 cells and coverslips fixed after 1 h, 6 h and over night from the microinjection. As shown in Figure 4.8, 1 h after microinjection the point of injection is still clearly visible as a bright accumulation of fluorescence. The labeled plasmids move slowly (6 h) to their final localization and once they have reached it, they do not change their localization significantly. The complexes stayed in the nuclei throughout all experiments and were localized identically even after long incubation up to 72 h (Fig. 4.9). In some cases, after long incubation times, it was possible to detect some fluorescent aggregate outside the nucleus. Probably these extranuclear
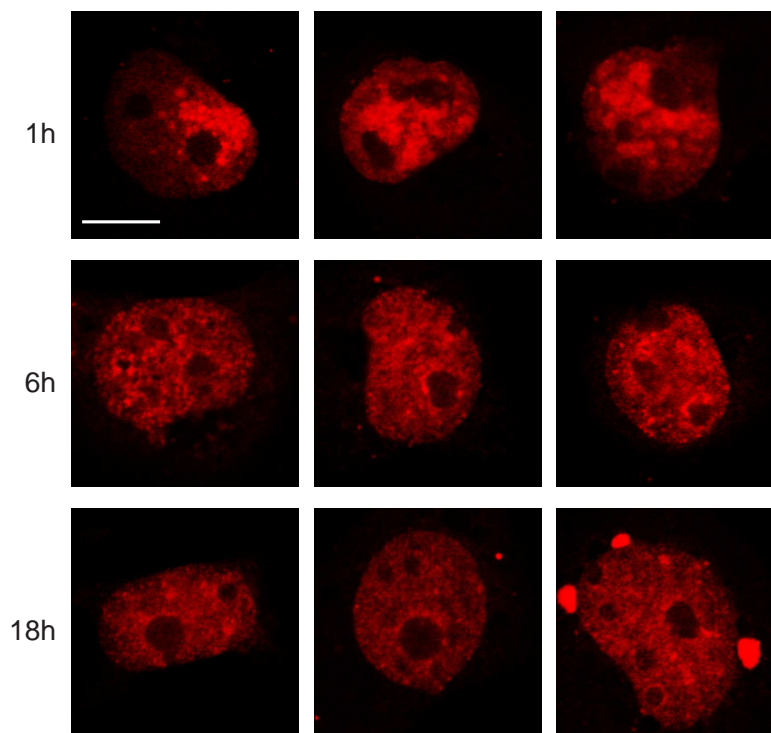
Figure 4.8: Time course. pMII plasmid labeled with rhodamine PNA was microinjected in COS 7 cells. Coverslips were fixed with 3.5 % paraformaldehyde and analyzed by confocal microscopy. The point of injection is still visible after 1 h as an accumulation of fluorescence. After 6 h the final location is reached and does not change with longer incubation (18 h). Scale bar: 10 μm.
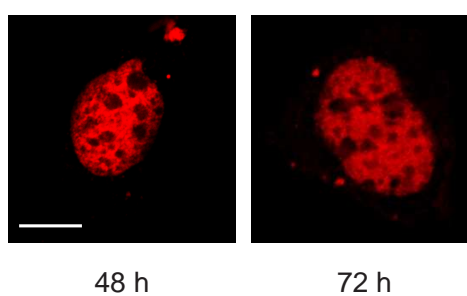
Figure 4.9: Stability of PNA/DNA complexes localization. pEPI-1 plasmid was microinjected in nuclei of COS 7 cells grown on CELLocate coverslips. Fixation after 2 and 3 days showed a high stability of the complexes since they are still clearly visible with their usual localization. Scale bar: 10 μm.

signals were constituted by PNA molecules that had detached from the plasmid and relocate outside the nucleus.

4.6 Nuclear localization of plasmid DNA

The nuclear localization of plasmid DNA labeled with PNA was examined by confocal microscopy in microinjected COS 7 cells after fixation as well as in live cells. Many different plasmids were analyzed and even though the localization of the plasmids was quite variable in individual cells, there was no detectable difference between different plasmids. In all cases, the distribution was not homogeneous but sponge-like with big areas and smaller numerous areas lacking detectable amount of labeled plasmids (Fig. 4.10 and Fig. 4.11). The localization of plasmid DNA in fixed cells was the same as for living cells, suggesting that the fixation with paraformaldehyde faithfully preserves the *in vivo* localization. In addition, the original vector pBlueScript and a prokaryotic expression vector, pRSET-A, were analyzed for plasmid localization and gave the same pattern of distribution (Fig. 4.12). Interestingly, plasmid containing a SAR, or a non-SAR, DNA element did not reveal any significant difference in the nuclear localization (Fig. 4.13). Thus it seems that the intranuclear distribution
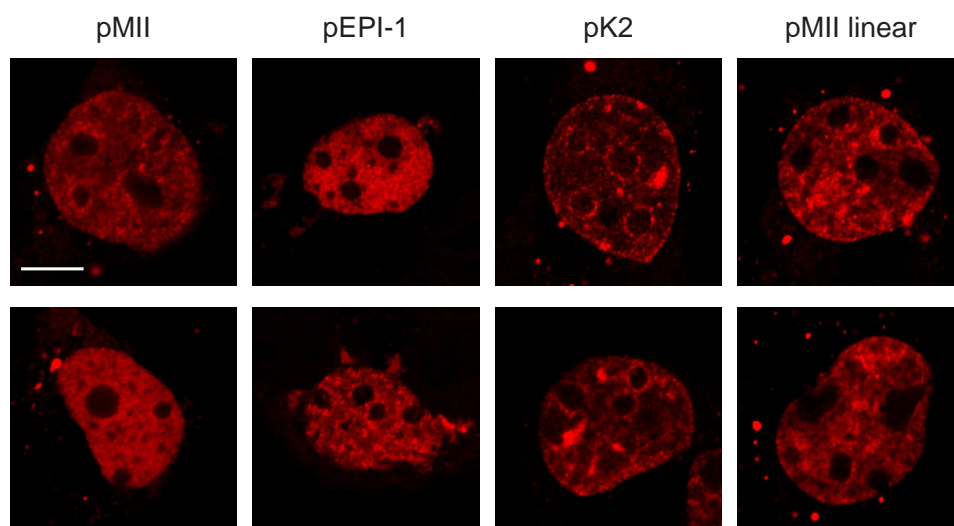
Figure 4.10: Nuclear localization of plasmid DNA in live cells. COS 7 cells grown on glass bottom dishes were microinjected and analyzed 18 h after microinjection by confocal microscopy on a heated stage. The intranuclear localization does not differ from the one in fixed cells. Scale bar: 10 μm.
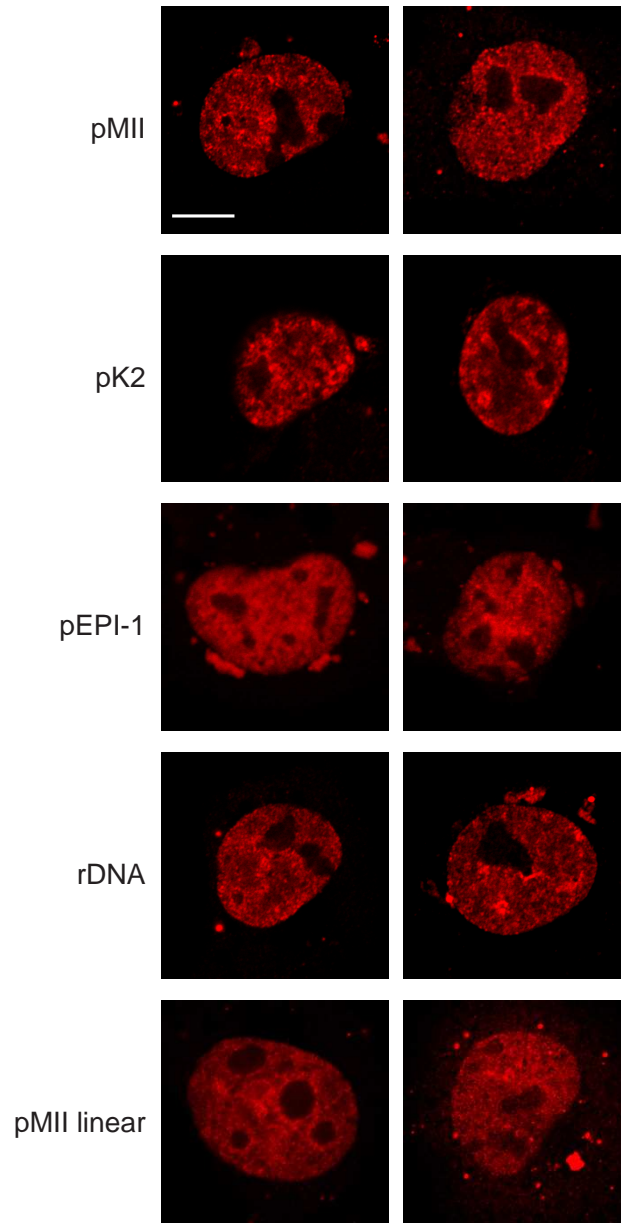
Figure 4.11: Nuclear localization of plasmid DNA in fixed cells. COS 7 cells grown on CELLocate coverslips were microinjected and fixed with 3.5 % paraformaldehyde 18 h after microinjection. Settings for microinjection and analysis by confocal microscopy, as described in Table 3.3, were the same for all used plasmids. Two typical nuclei are shown for each plasmid. Scale bar: 10 μm.
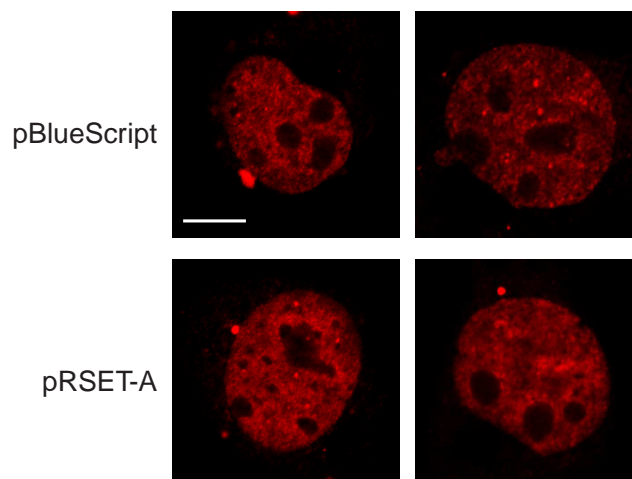
Figure 4.12: Localization of control plasmids. COS 7 cells grown on CELLocate were microinjected and fixed with 3.5 % paraformaldehyde 18 h later. As for the other plasmids, the localization was sponge-like. Scale bar: 10 μm.
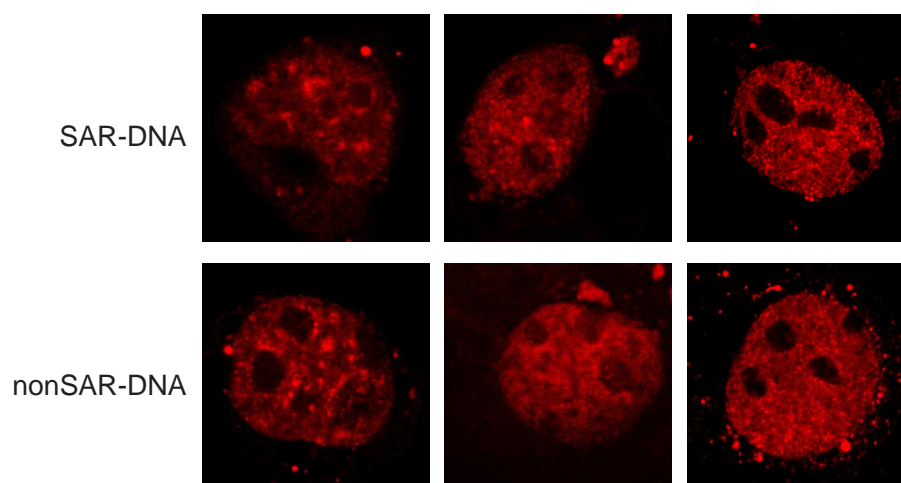
Figure 4.13: Localization of plasmid DNA is independent of its sequence. COS 7 cells grown on CELLocate were microinjected with pMII (SAR insert) and pK2 (nonSAR insert) plasmid and fixed with 3.5 % paraformaldehyde after 18 h from microinjection. The nuclear distribution of the two plasmids does not show significant differences.

of plasmid DNA is independent from its sequence.

4.7 Subnuclear localization of PNA/DNA complexes

To gain better knowledge about the localization of plasmid DNA, PNA/DNA complexes were co-microinjected with expression vectors coding for nuclear proteins fused to the green fluorescent protein (GFP). The co-microinjection of the complexes with the expression vector for the hFibrillarin-GFP demonstrated that the big areas avoid of plasmids are nucleoli (Fig. 4.14). The co-microinjection with the vector encoding PML protein highlighted some of the smaller numerous areas not containing detectable amount of plasmid (Fig. 4.15). However, several small regions contained neither PML protein nor PNA/DNA complexes, and probably represent other nuclear bodies such as Cajal bodies. The sponge-like distribution of the labeled plasmids reminded us of the distribution of scaffold attachment factor A (SAF-A), a well-known protein of the nuclear scaffold (Romig *et al.*, 1992). Experiments of co-microinjection with the expression vector encoding SAF-A tagged with GFP showed that there is a very similar distribution (Fig. 4.16).

Figure 4.14: Co-microinjection of PNA/DNA complexes with expression vector for hFibrillarin protein. COS 7 cells were co-microinjected with labeled plasmid DNA and an expression vector encoding hFibrillarin-GFP, and were fixed and analyzed 18 h later. The big regions avoid of plasmid DNA are filled in with the hFibrillarin which shows a globular pattern. Scale bar: 10 μm.

Figure 4.15: Co-microinjection of PNA/DNA complexes with expression vector for PML protein. COS 7 cells were co-microinjected with plasmid DNA and an expression vector encodin PML-GFP, and were fixed and analyzed 18 h later. There is a mutually exclusive localization of the plasmid DNA and the PML protein. Interestingly, in phase contrast, the overexpression of the protein highlighted the PML bodies with the typical doughnut-like morphology. Scale bar: 10 μm.

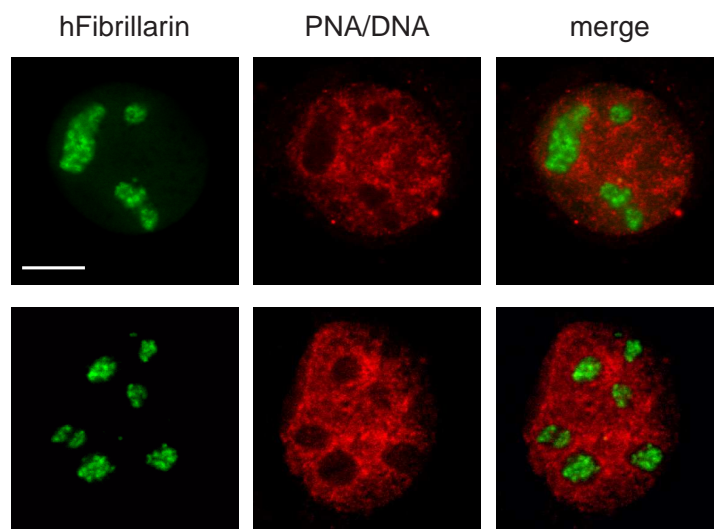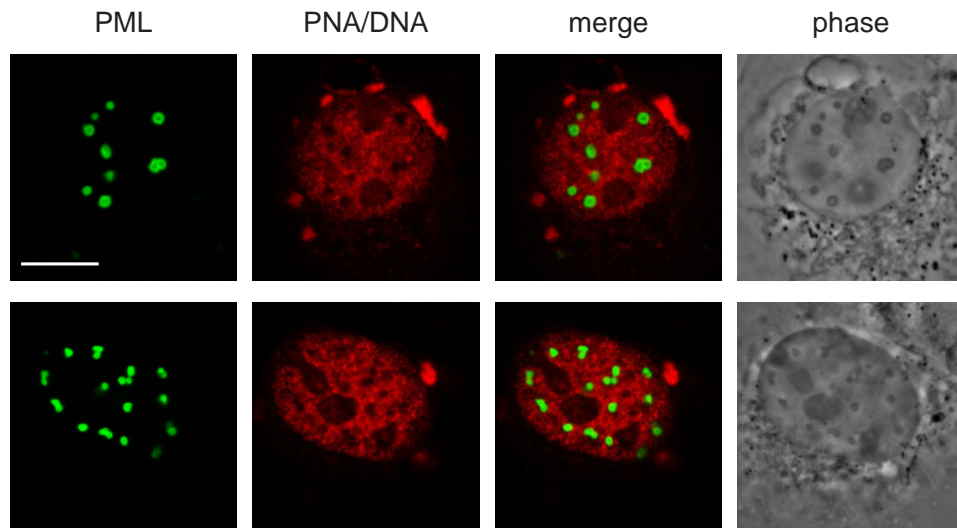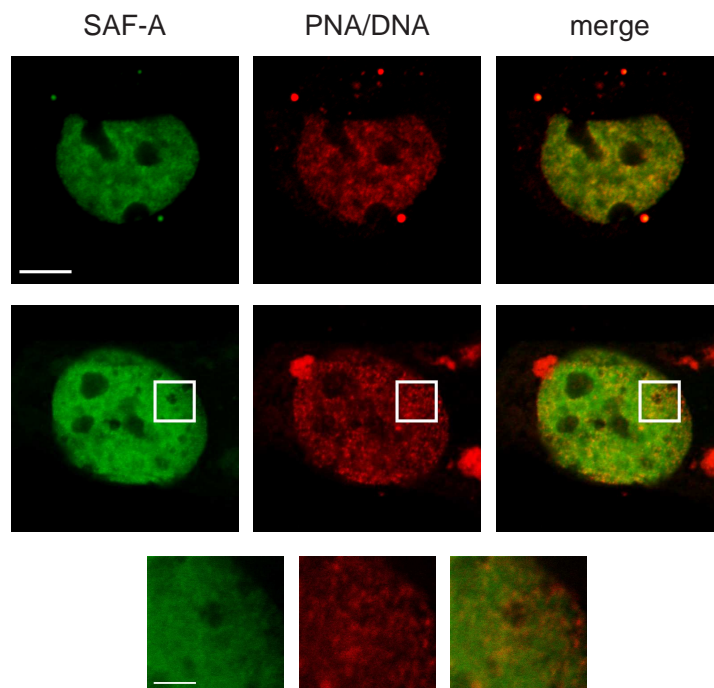**Figure 4.16: Co-microinjection of PNA/DNA complexes with expression vector for SAF-A.** COS 7 cells were co-microinjected with labeled plasmid DNA and an expression vector encoding SAF-A tagged with GFP, and were fixed and analyzed 18 h later. The fluorescent fusion protein and the DNA were not completely overlapping as shown in the inset (bottom panel, scale bar: 2 μm). Scale bar: 10 μm.

4.8 Plasmid DNA is resistant toward detergent and high salt extraction

The SAF-A-like intranuclear localization of the PNA/DNA complexes and the long time they need to reach their final location, induced us to investigate whether or not the plasmids were bound to the nuclear scaffold. To answer this question, COS 7 grown on CELLocate were microinjected and processed as described in section 3.2.9, before fixation with 3.5 % paraformaldehyde. Coverslips were then analyzed by confocal microscopy. As shown in Figure 4.17 (upper panel), when the nuclear membrane was dissolved by treatment with 0.5 % Triton X-100 and all soluble nuclear components were released, no big change in the intensity of fluorescence and localization was detectable. However the further incubation in 2 M NaCl resulted in a redistribution of the plasmid DNA to granular clusters in the nuclear interior as well as at the nuclear periphery (Fig. 4.17, lower panel). The staining of genomic DNA after high salt extraction, which removes histones and other soluble proteins, showed a typical halo with a core region surrounded by loops of DNA (Fig. 4.18).
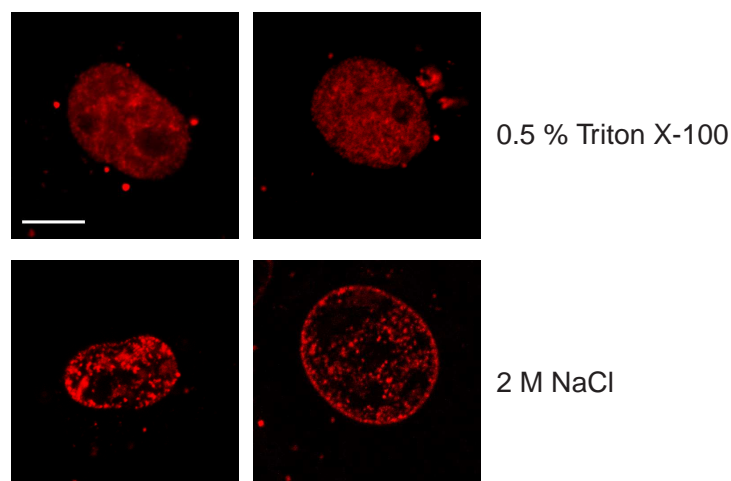
Figure 4.17: Sequential extraction of COS 7 cells. After treatment with 0.5 % Triton X-100 neither loss of fluorescence or relocation are visible. When a high salt extraction follows the permeabilization step, a loss of fluorescence and redistribution of remaining complexes are clearly visible. Scale bar: 10 μm.
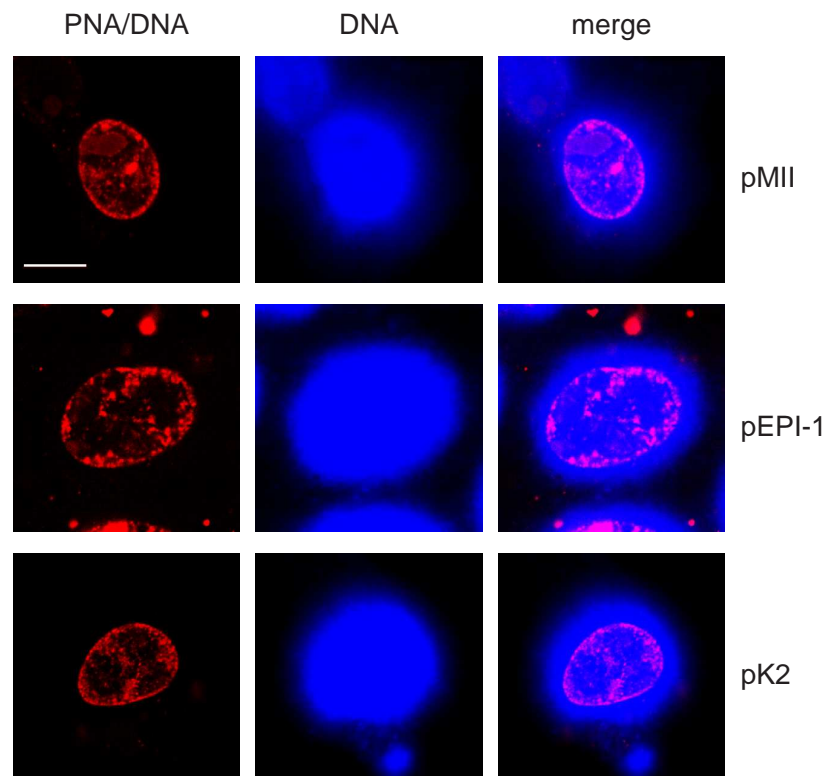
Figure 4.18: DNA loops and anchored plasmid DNA after high salt extraction. COS 7 cells were microinjected and processed as described in section 3.2.9. Genomic DNA was stained with TO-PRO-3 diluted 1:1000 in 1x PBS. To visualize the DNA loops protruding from the nucleus, the images were taken with high excitation of the HeNe 2 laser (633 nm) which produces an overexposed halo core. Scale bar: 10 μm.

4.8.1 Quantification of plasmid DNA bound to nuclear scaffold

In a next step, we quantified the amount of plasmid DNA that remains bound to the nuclear scaffold after sequential extraction. COS 7 cells were transfected by electroporation with different unlabeled plasmids (pMII, pEPI-1 and pK2 plasmids). After over night incubation, cells were sequentially extracted and plasmids separated from genomic DNA by Hirt extraction. Purified plasmids were quantified by transformation of competent XL-1 Blue bacteria counting the number of colonies on the plates and by real-time PCR. Both quantification methods show that around 50 % of the plasmid resist high salt extraction, independently of the sequence and of the presence of a promoter. Figure 4.19 represents the mean of at least three independent experiments, quantified in duplicate each; normalization to the amount of DNA recovered from untreated cells in the same experiment was performed before calculating the mean to

A

B
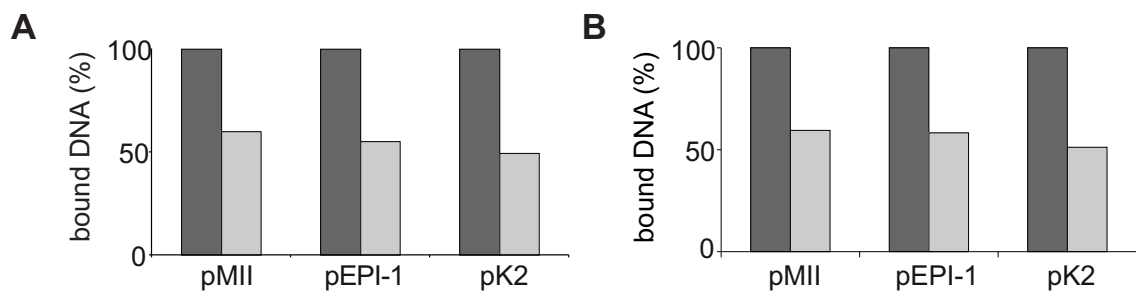
Figure 4.19: Resistance of transfected plasmid toward high salt extraction. COS 7 cells were electroporated with unlabeled pMII, pEPI-1 and pK2. After 20 h, cells were extracted with 0.5 % Triton X-100 and 2 M NaCl, and plasmid DNA recovered by Hirt extraction. The quantification counting the number of clones (A) and by real-time PCR (B) shows that approximately half of the plasmid remains bound to the nuclear scaffold after extraction with high salt (light-gray bars) in comparison to untreated cells (dark-gray bars).

compensate for differences in the absolute amount of recovered DNA.

4.9 Dynamics of plasmid DNA *in vivo*

As suggested by the extraction experiments described above, plasmid DNA is quite stably attached to the nuclear scaffold independently of its sequence. To further confirm this attachment, fluorescence recovery after photobleaching (FRAP) experiments were performed on living cells.

COS 7 cells were microinjected with PNA/DNA complexes and with expression vector encoding fluorescent proteins of known mobility as a control. After an over night incubation, fluorescent cells were examined by FRAP. The settings of the parameters for FRAP experiments with PNA/DNA complexes and GFP-tagged control proteins are described in Table 3.4. For each analyzed plasmid DNA and control protein, a gallery of images before the bleaching pulse, right after it and during the fluorescence recovery are shown together with processed data (panel A and B, respectively, for Fig. 4.20, Fig. 4.21, Fig. 4.22 and Fig. 4.23). The curve represents the mean of the curves obtained from 10 different bleached nuclei per plasmid. The fluorescence recovered homogeneously in the bleached area, without indication of nuclear subcompartments with higher plasmid mobility. It should be noted that bleaching of the rhodamine tag required a much higher number of bleaching pulses (1500 iterations) than normally employed for GFP-tagged proteins (30 iterations). To eliminate the
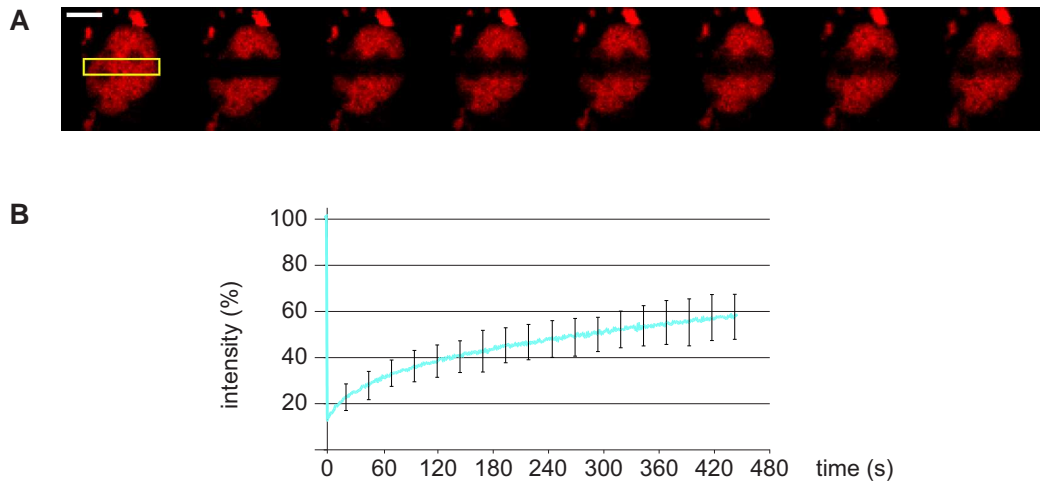
Figure 4.20: FRAP experiment with pMII plasmid. COS 7 cells, grown on glass bottom dishes, were microinjected with pMII labeled with rhodamine-PNA and analyzed on a heated stage after 18 h. (A) The yellow rectangle represents the region of interest undergoing photobleaching. The gallery shows the nucleus before and right after the bleaching together with the recovery over time. Images shown are each 75 s. Scale bar: 10 µm. (B) The recovery of fluorescence in the bleached region is plotted in function of time. The curve is the mean of 10 analyzed nuclei. The error bars represent the standard deviation.
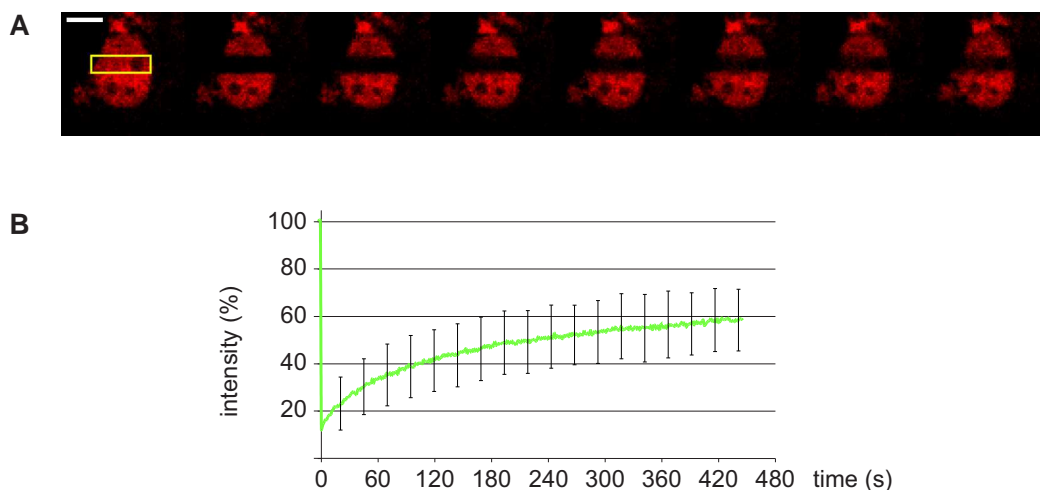
Figure 4.21: FRAP experiment with pEPI-1 plasmid. For the legend refer to Figure 4.20.
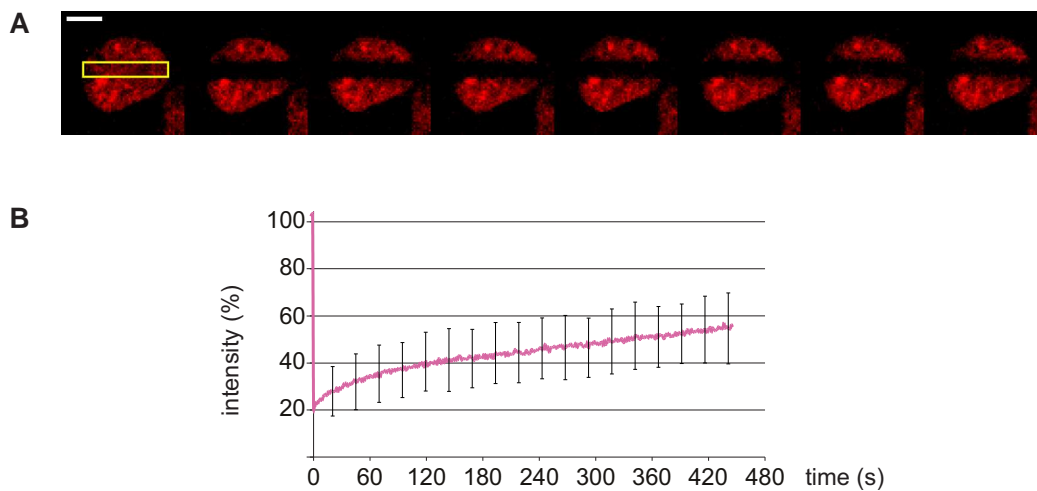
Figure 4.22: FRAP experiment with pK2 plasmid. For the legend refer to Figure 4.20.
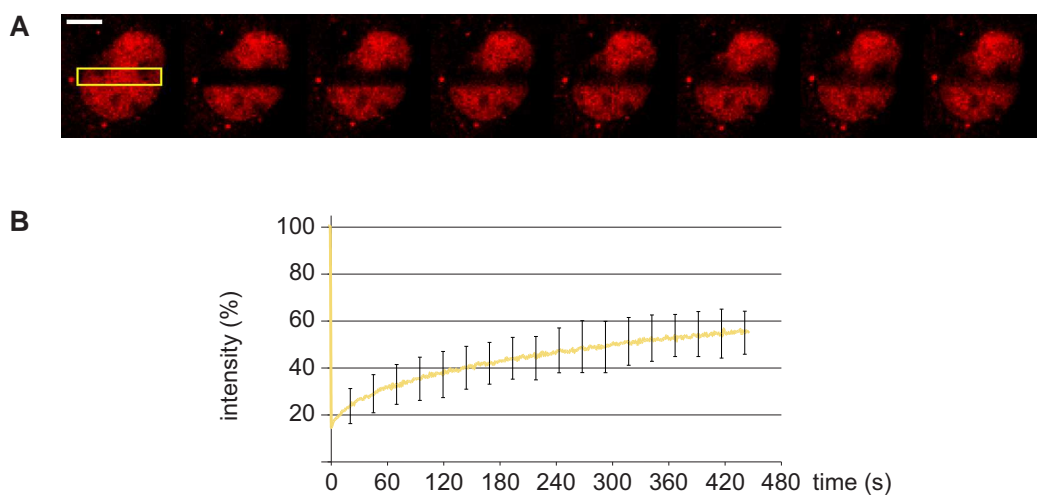
Figure 4.23: FRAP experiment with pMll linear plasmid. For the legend refer to Figure 4.20.
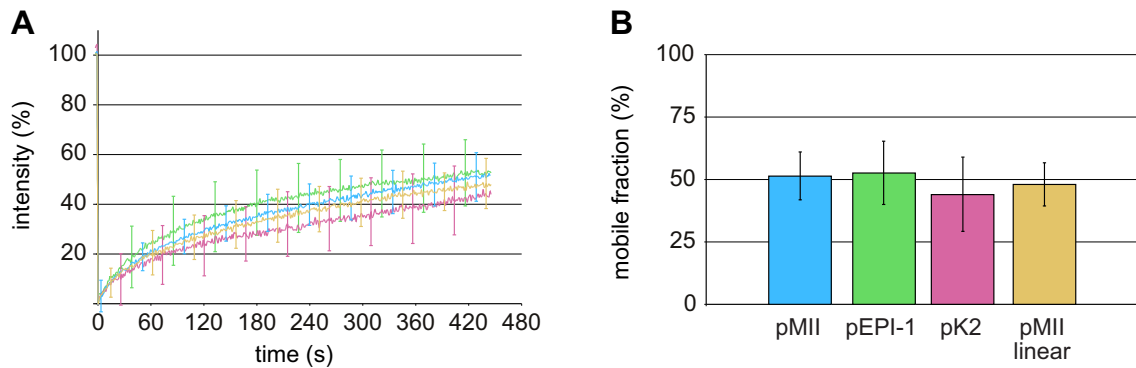
Figure 4.24: Re-elaborated curves and mobile fractions. (A) The FRAP data shown in Figure 4.20, Figure 4.21, Figure 4.22 and Figure 4.23 were re-elaborated in order to get rid of the PNA/DNA complexes not affected by bleaching while calculating the mobile fractions and diffusion times. The fluorescence intensity is plotted against time. pMII (blue curve): SAR+, promoter-; pEPI-1 (green curve): SAR+, promoter +; pK2 (dark-rosa curve): SAR-, promoter-; pMII linear (light-brown curve): as pMII but linearized. There is no significant difference in the mobile fraction of all tested plasmids. (B) Mobile fractions of analyzed plasmids at the last time point (445.37 s) of the recovery.

contribution of non bleached fluorochrome, which was around 10-20 % in the case of rhodamine-tagged plasmids, a new value of fluorescence intensity was calculated as described in section 3.2.14.2. Figure 4.24 shows the new curves all starting at zero (A), and the mobile fraction for each analyzed plasmids (B). There is no significant difference in the mobile fraction of the different plasmids, irrespective of the presence or absence of a SAR DNA sequence or of a functional eukaryotic promoter. From these curves, it is possible to calculate the diffusion time ($t_{1/2}$) as the time needed for half of the plasmid to come back into the bleached region (Table 4.1).

Table 4.1: Diffusion time ($t_{1/2}$) for microinjected DNA plasmid.

	pMII	pEPI-1	pK2	pMII linear
$t_{1/2}$ (s)	88.85	71.98	98.97	87.72

FRAP experiments were also done for nuclear proteins with known mobility, fused to GFP, such as β-Gal-NLS and LaminB1. As shown in Figure 4.25, LaminB1 has a very small mobile fraction (less than 10 %), and is almost immobile for hours, while β-Gal-NLS is a highly mobile protein which fully recovers within 15 s. Comparing the curves in Figure 4.24 and Figure 4.25,
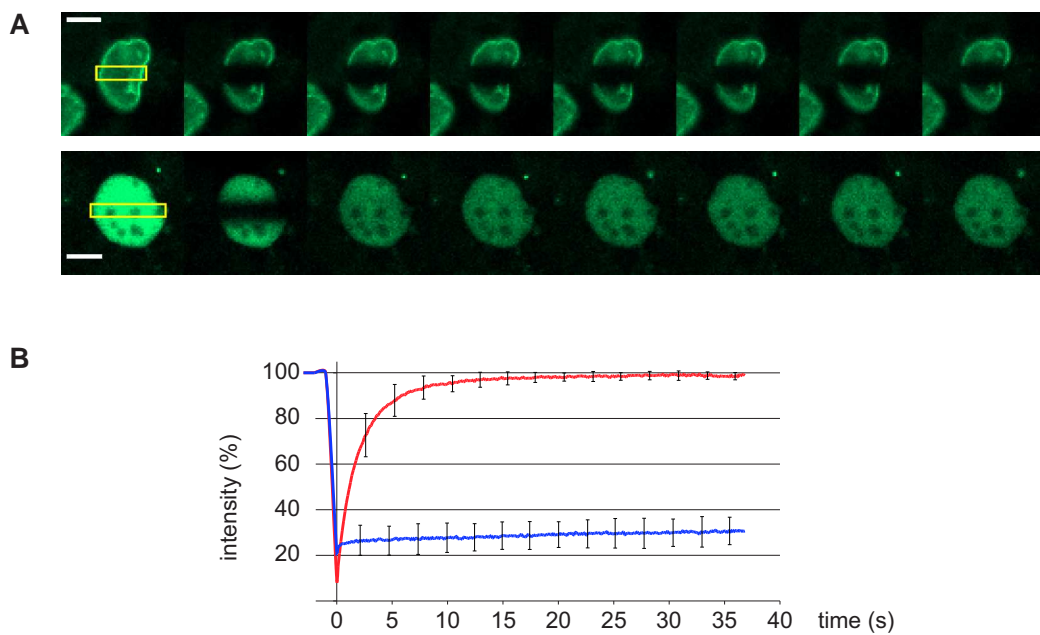
Figure 4.25: FRAP experiments for β-Gal-NLS and LaminB1. COS 7 cells grown on glass bottom dishes were microinjected and analyzed by confocal microscopy on a heated stage, 18 h later. (A) The region of interest (yellow rectangle) was photobleached with a short pulse of extremely intense light. The images were taken before photobleaching, immediately after and over time during the fluorescence recovery with an interval of 6 s between each shown image. The upper panel shows a typical cell expressing LaminB1, the lower a cell expressing the artificial soluble nuclear protein β-Gal-NLS. Scale bar: 10 µm. (B) Recovery curves for β-Gal-NLS (red) and for LaminB1 (blue): comparison of a fully mobile protein with one almost completely immobile.

it is evident that the plasmid DNA is 100-fold slower than the soluble protein of similar size. This difference is also evident comparing the diffusion coefficient of the mobile fraction (4.3×10^{-10} cm^2/s for plasmid DNA and 2.4×10^{-8} cm^2/s for β-Gal-NLS). Thus, the *in vivo* mobility of plasmid DNA is several orders of magnitude lower than known for free diffusion, consistent with a strong, but not complete, attachment to the nuclear scaffold.

4.10 Establishment of CHO lacOp/lacI-GFP stable cell line

In a second part of this work, we investigated the mobility of endogenous chromatin in living cells. The sequence specific visualization of genomic DNA was achieved using the *lac* operator/repressor system, based on binding of sequence-specific DNA-binding proteins. For this purpose, chinese hamster (*Cricetulus Griseus*) ovary cells (CHO) with a double deletion of the gene for the dihydrofolate reductase (dhfr) were used. These epithelial cells were chemically transfected with the lacOp vector (see Table 3.1) containing 256 copies of the *lac* operator sequence and the dhfr gene for selection. Transfected cells were grown in selection medium without any addition of nucleosides and with 10 % dialyzed FCS, so that only the few cells which had incorporated the plasmid could survive. After 10 days of selection, these cells were once again chemically transfected with a vector encoding the *lac* repressor (lacI) fused to GFP (Chen and Matthews, 1992). Cells were then grown for the first week in selective medium still containing dialyzed FCS to keep selection for lacOp transfectants, but with addition of hygromycin B (200 μg/ml) for selection of positive transfectants to lacI-GFP. In this way, only cells which have also integrated the second plasmid can grow further.

Since the integration of lacOp is random, it was necessary to subclone CHO lacOp/lacI-GFP stable cell line by serial dilution. Of 73 individual subclones, only 9 clones were negative for lacI-GFP, while all others displayed spot-like signals at the point of the lacOp integration site. To define where the spot localizes inside the nucleus, complete optical sections (Z-stacks) with a small zoom (factor 2) were taken and analyzed as a 3D projection of the brightest point on the y-axis. Rotation of the three dimensional projection indicated that, in almost all subclones, the spot was preferentially located in the interior of the nucleus. However a few subclones, which interestingly were growing a bit slower, showed a peripheral location of the spot. Figure 4.26 shows three different subclones with typical location of the spots. For further experiments subclones were chosen where the spot was localized either at the nuclear periphery or in the nuclear interior.

2G10   3C4   3F9
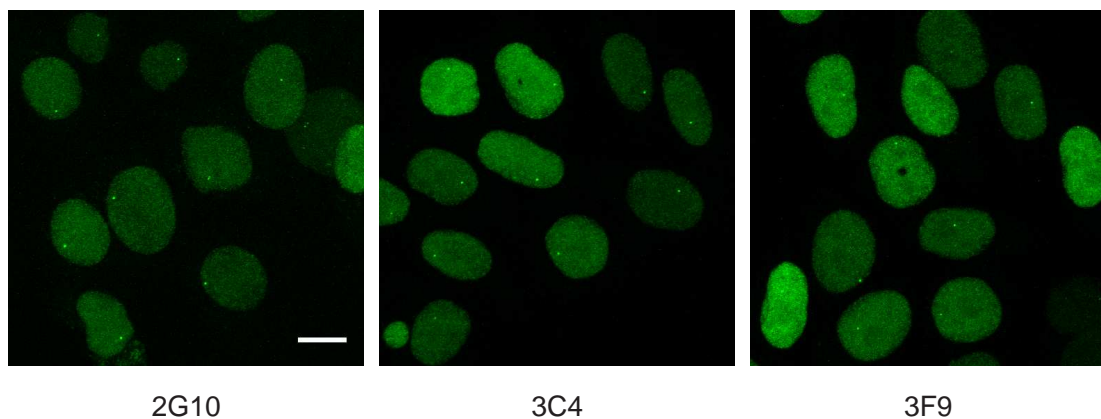
Figure 4.26: Stable lacOp/lacI-GFP cell clones. Subclones of CHO lacOp/lacI-GFP were grown on coverslips coated with 0.1 % alcian blue, fixed 10 min with 3.5 % paraformaldehyde and analyzed by confocal microscopy. Shown here are subclones 2G10, 3C4 and 3F9, three of the 73 analyzed subclones. All cells express lacI-GFP and all have at least one bright spot. These images are Z-projection of the maximal fluorescence intensity of a Z-stack (Z-stacks were processed with ImageJ). In this way, spots that in different cells lie in different Z-optical sections are visible at the same time. In 3D projections, it is clear that the spot localizes in the nuclear interior for subclones 2G10 and 3C4, while more at the periphery for subclone 3F9. Note that not all expressed protein is able to bind to the *lac* operator array producing a nucleoplasmic background. Scale bar: 10 μm.

4.11 The integration site of *lac* operator

The integration site of the *lac* operator array was determined by visual inspection of mitotic cells. Cells from different subclones were grown on coverslips and enriched for mitotic cells by incubation with nocodazole (40 ng/ml) for two hours prior to fixation with paraformaldehyde and staining of DNA with TO-PRO-3. Images were collected as simultaneous Z-stack in the green and far-red channels for GFP and TO-PRO-3, respectively, and the 3D projection carefully analyzed to individuate the chromosomes with integrated *lac* operator arrays as the one anchoring fluorescent *lac* repressor in a bright doublet. This approach did not allow determining the specific chromosome on which the lacOp array had integrated, but the detection with lacI-GFP revealed a bright spot on a long arm, not far away from the centrosome, of chromosomes with medium tending to big size. Figure 4.27 shows the localization of doublets for subclones 2G10 and 3C4.
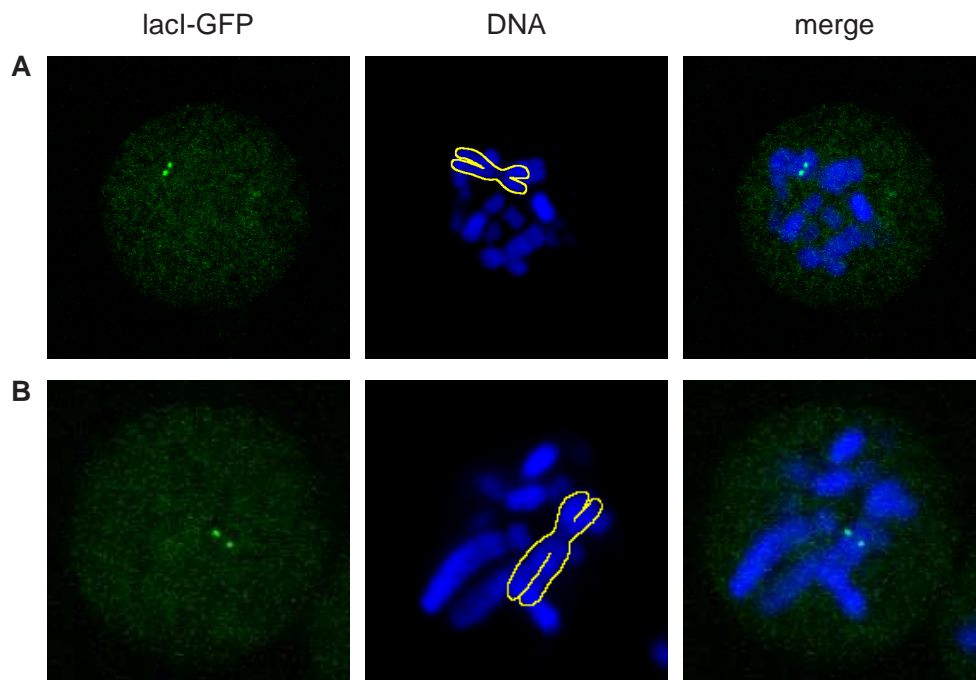
Figure 4.27: Doublets on chromosomes. After incubation with nocodazole, cells grown on coverslips were fixed and analyzed by confocal microscopy. DNA was stained with TO-PRO-3 (1:1000 in 1x PBS). Z-stacks were processed with ImageJ and projected on the z-axis as maximal fluorescence intensity. To better discriminate the chromosome with the integration site, only a few slices of the Z-stacks were projected and combined in the merge. The yellow line traces the boundaries of the affected chromosomes. (A) and (B) are metaphases of the subclones 2G10 and 3C4, respectively.

4.12 FACS analysis

The microscopic analysis of some monoclonal subclones revealed a low number of cells with two spots, in addition to the vast majority of cells with a single spot. These two spots were preferentially located far away from each other. To investigate the nature of the 'two spots' phenotype, cells were analyzed for DNA content by flow cytometry. Cells from two different subclones (2G10 and 3C4) showed a distribution of the cells in G1, S and G2 phases, typical of well proliferating cells. In addition, though, a small fraction of cells (4–7 %) with a double content of DNA was detectable (Fig. 4.28). Thus, the cells having two spots most likely represent tetraploid cells. Interestingly, cells harboring two bright spots were often found in clusters obviously stemming from a single original cell, suggesting that polyploidy does not interfere with proliferation.
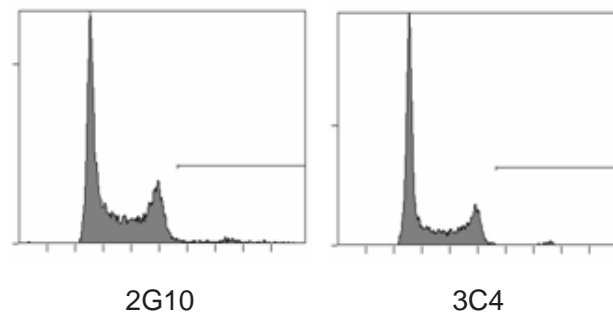
Figure 4.28: Flow cytometry histograms of CHO lacOp/lacI-GFP subclones. Cells were fixed in cold methanol, stained with propidium iodide and 10 000 cells were analyzed for the DNA content by FACS. The bar in the histograms represents the small fraction of tetraploid cells (6–7 % for 2G10; 4–5 % for 3C4). The number of analyzed events (y-axis) is plotted against the DNA content (x-axis).

4.13 *Lac* repressor remains bound to its target sequence throughout mitosis

The progression of CHO lacOp/lacI-GFP cells through mitosis was investigated by confocal microscopy with cells grown on coverslip. Figure 4.29 shows cells of subclone 3C4 in different phases of the mitotic process. The labeling of chromatin loci with lacI-GFP allows following the cell division in all its phases. At the interphase one single spot is visible in the nucleus. At the prophase the spot appears as a closely spaced doublet, since the DNA has replicated and sister chromatids condense into chromosomes. Once the chromosomes have fully condensed, they migrate to the metaphase plate, being attached at the microtubules via their kinetochores. During this movement, the doublet is still clearly visible. At the anaphase the sister chromatids are separated and move towards the poles of the spindle. At that point the doublet returns to be a single spot, one on each chromatid. During telophase, chromatids which have reached two opposite poles, decondense and form two new daughter cells, each of them still having the labeled chromatin locus as the mother cell. This demonstrates that the binding of *lac* repressor to the *lac* operator sequence is stable throughout mitosis and does not interfere with such a fundamental process.
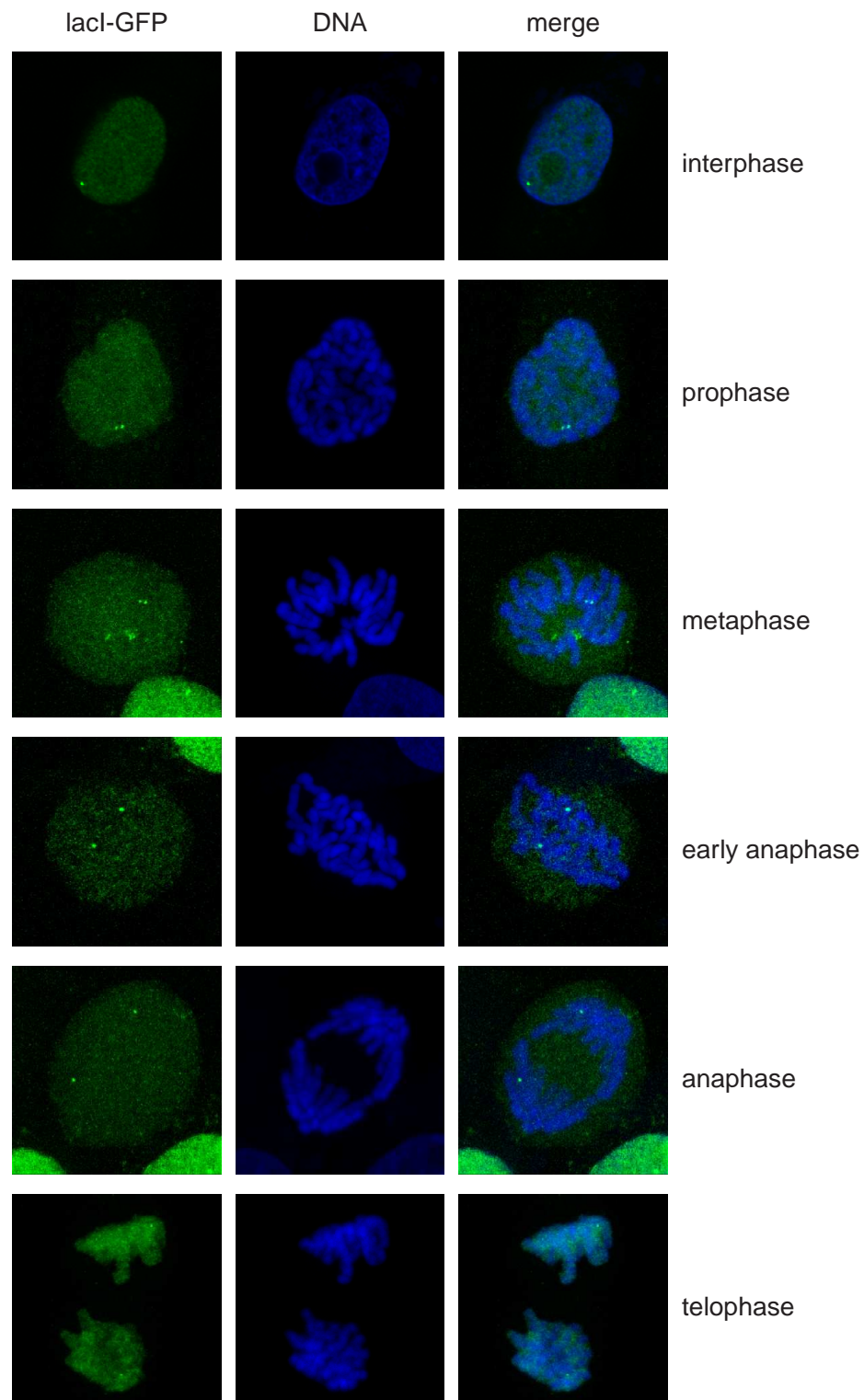
Figure 4.29: Persistance of lacI-GFP DNA-bindig during mitosis. 3C4 cells grown on coverslips were fixed, stained with TO-PRO-3 and analyzed by confocal microscopy. Cells in progressive phases of mitosis are shown. All panels are Z-projection of the maximal fluorescence intensity of a Z-stack taken in multitrack for GFP and TO-PRO-3 with an average scan of 4 (the interphase panel is a single optical section collected with an average scan of 16).

4.14 Mobility of chromatin loci *in vivo*

The *lac* operator/repressor system allows not only the *in vivo* visualization of chromatin loci, but also studies on their dynamics.

To gain insights into short-range chromatin motion we used subclones which differ in the nuclear localization of the spot: subclone 3C4 with the spot at the nuclear interior and subclone 3F9 with the spot close to the nuclear periphery. The same experiments were repeated with subclone 2G10 (spot at the nuclear interior) with comparable results as for subclone 3C4 (data not shown). Four dimensional live cell imaging was performed as described in Table 3.5 and data further analyzed as described in section 3.2.14.3. First the measured coordinates of the spots were re-calculated so that the initial position of the spot, at $t = 0$, were set to zero (0;0) for all analyzed nuclei. The path of the spot over time was represented in a x-y diagram made with help of MS Excel. Figure 4.31 shows the trajectories of 22 individual spots from 3C4 cell line, and demonstrates that labeled chromatin loci move in a 'random walk' within a highly constrained volume of the nucleus. It is evident that the most points (coordinates of the spot at each time point) are located within a circle with radius of 0.5 μm, much fewer points in a ring between 0.5 μm and 1 μm from the origin; only sporadic points can also be found at a distance more than 1 μm from the origin. The same information can be given with a frequency histogram or 'density plot' (Fig. 4.31, right panels) as distribution of the points' distances from the origin in defined intervals. The distribution of these calculated distances presents most of the values in 0.4 μm from the origin with the rest distributed as a tail skewed to the right. The shape of the distribution for 3C4 cells treated
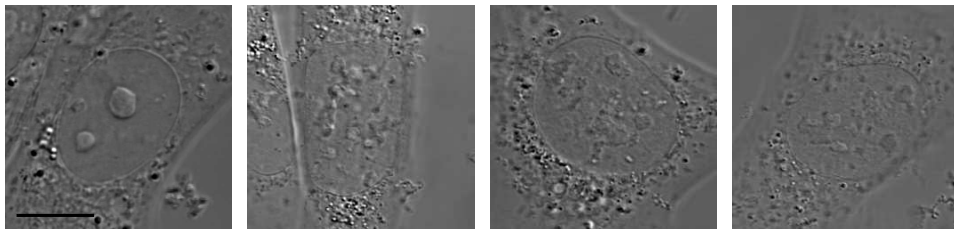
Figure 4.30: DRB treatment is effective. Differential interference contrast (DIC) images of CHO lacOp/lacI-GFP cells before (first image on the left) and after incubation with DRB. It is evident the loss of nucleolar structure induced by this sinthetic inhibitor of transcription. Scale bar: 10 μm.
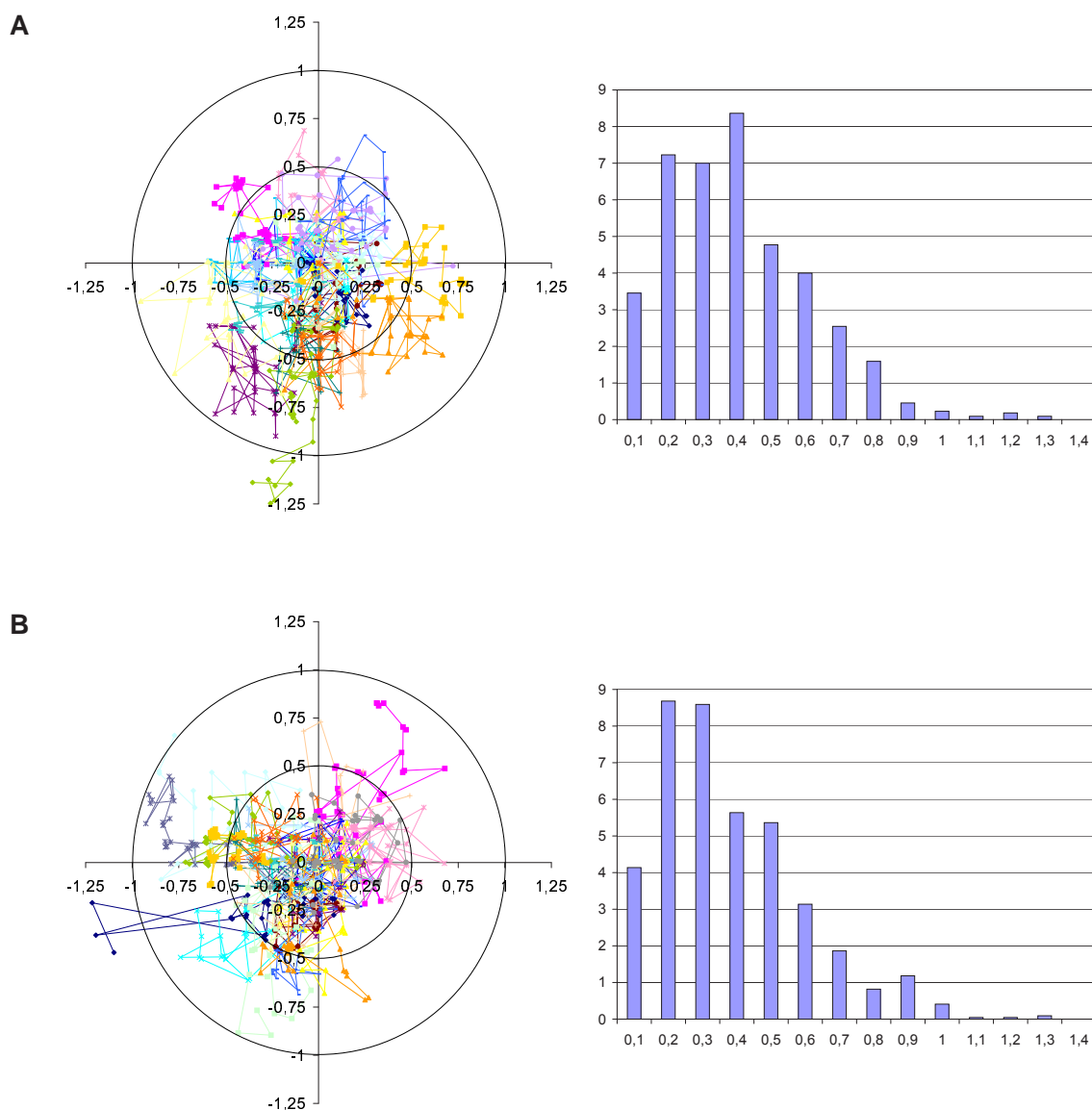
Figure 4.31: Paths and frequency histograms for spots in the nuclear interior. Four dimensional imaging was performed with subclone 3C4 grown on glass bottom dishes. Left panels display the random walks of the 22 recorded spots in a x-y diagram. Right panels are density plots of the distances from the initial position of each spots at each time point. Represented is the mean distribution of all values with an interval of 0.1 μm. (A) and (B) show, respectively, the results with and without active transcription.
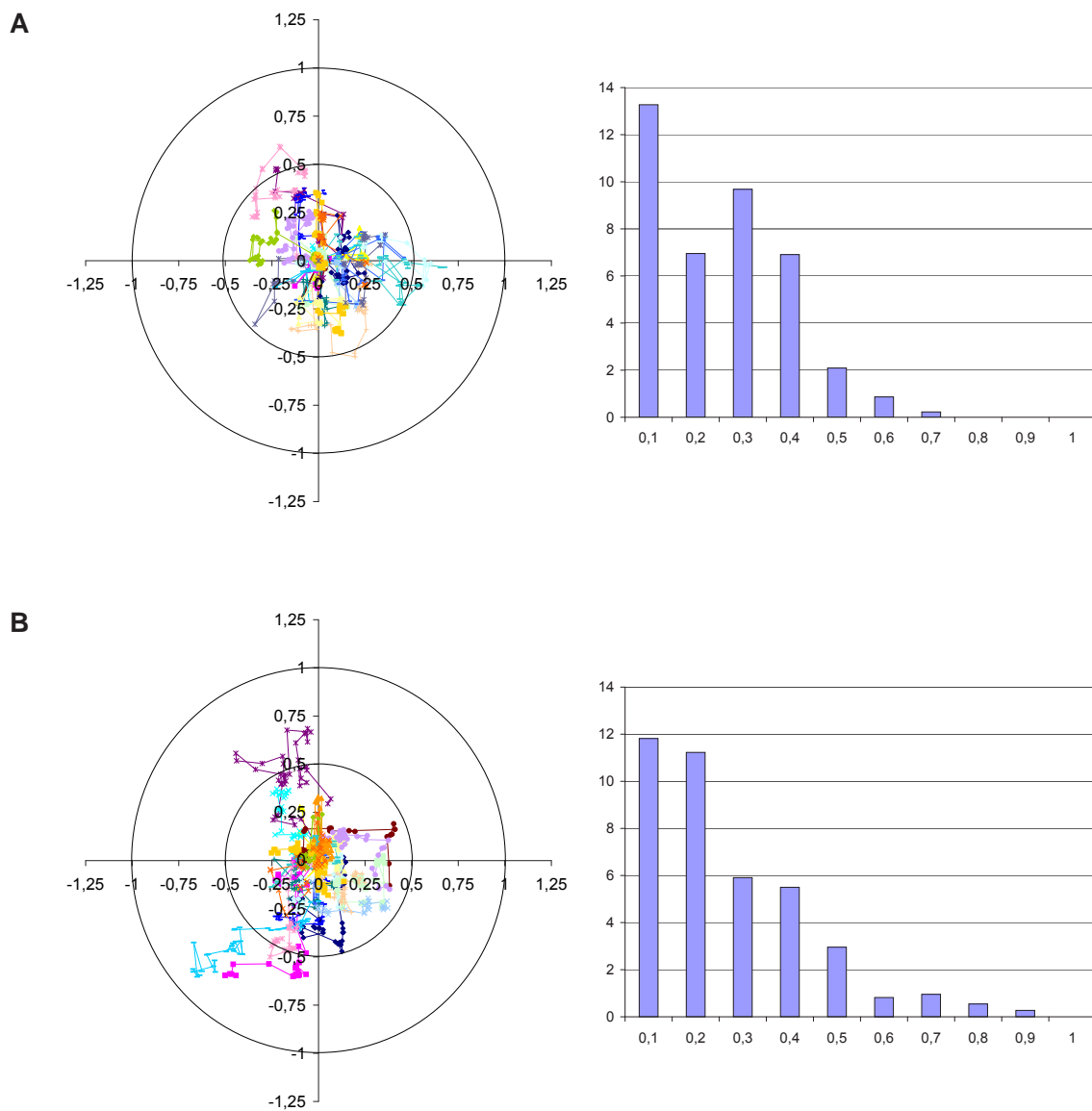
Figure 4.32: Paths and frequency histograms for spots at the nuclear periphery. Four dimensional imaging was performed with subclone 3F9 grown on glass bottom dishes. For the legend refer to Figure 4.31.

with the transcriptional inhibitor DRB is very similar, but the curve starts earlier to skew to the right. It seems that chromatin mobility is more constrained than under normal conditions when the transcription is inhibited. The effectiveness of DRB was verified by visual inspection of the nucleoli, which are known to be disrupted by DRB and form nucleolar necklaces (Fig. 4.30). Importantly, in subclone 3F9, which has a much more peripheral spot, the range of movement is even more constrained (Fig. 4.32). Note the accumulation of the points very close to the origin and how a circle with radius of 0.5 µm includes almost all of them. As expected from the trajectories, the distribution of distances (Fig. 4.32, right panels) presents the most values in the smallest intervals, with a distribution strongly skewed to the right.

The raw data were also processed to investigate the movement of chromatin
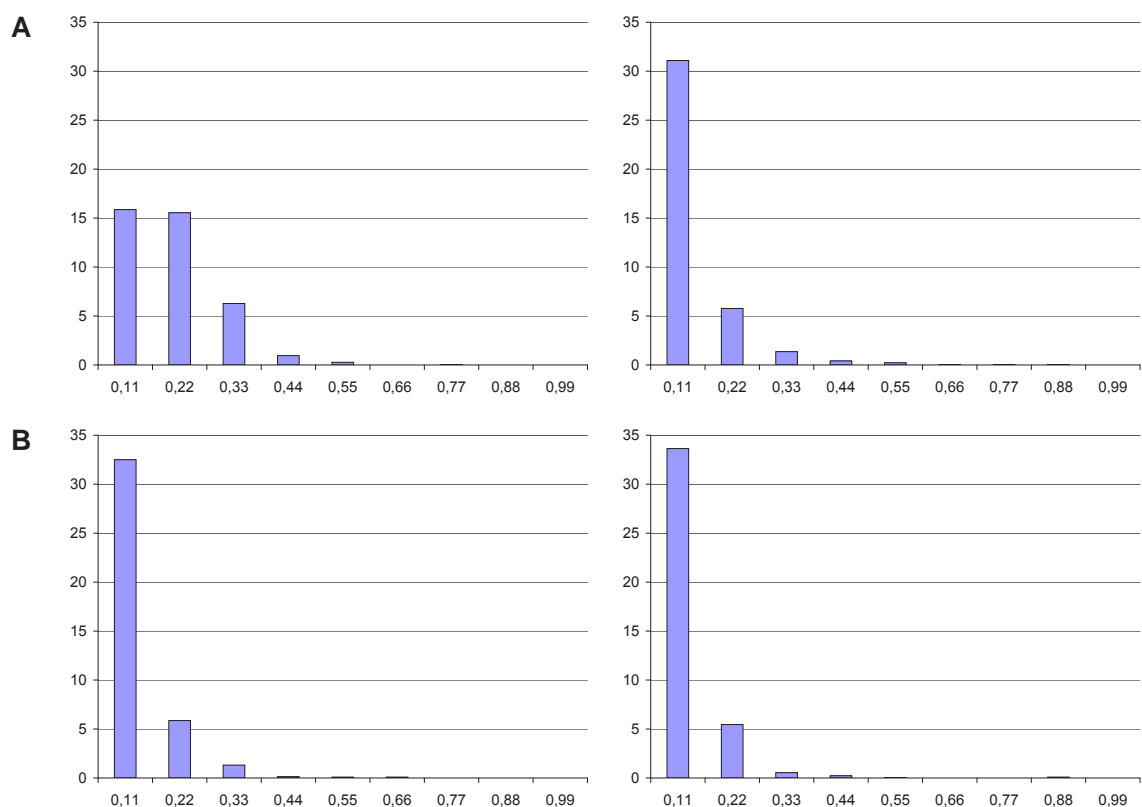
Figure 4.33: Density plots of distances between two time frames. Calculated distances between two successive time points for all analyzed nuclei (22 nuclei for both subclones) were averaged and distributed on intervals corresponding to 1 pixel (0.11 µm). Panels on the left show the distribution of distances in normal condition, while panels on the right after inhibition of transcription with DRB. (A) and (B) are density plots for subclones 3C4 and 3F9, respectively.

loci between two subsequent time points. The results are shown as frequency diagrams in Figure 4.33. The distribution of calculated distances was analyzed in intervals with the size of one pixel (0.11 μm) since a smaller interval would have no relevance. In subclone 3C4 (Fig. 4.33, panel A), DRB treatment results in very small movements after inhibition of transcription. In contrast, the distribution of distances for subclone 3F9 (Fig. 4.33, panel B) has already a peak in the first interval when transcription is active. Thus, the vicinity of the spot to the nuclear lamina seems to constrain its movement independent of the transcriptional status of the cell.

The difference in mobility of internal or peripheral loci is also evident in a mean square change in distance ($\langle \Delta d^2 \rangle$) analysis (Fig. 4.34). For short analysis times, the plot of $\langle \Delta d^2 \rangle$ against time shows linearity, indicating diffusive motion. The slope of the calculated trendlines is the diffusion coefficient of the analyzed chromatin loci. Table 4.2 shows the diffusion coefficients of subclones 3C4 and 3F9, respectively. The diffusion coefficients for the two subclones are significantly different, but the inhibition of transcription with DRB produces only a slight difference in the diffusion coefficient of each locus.
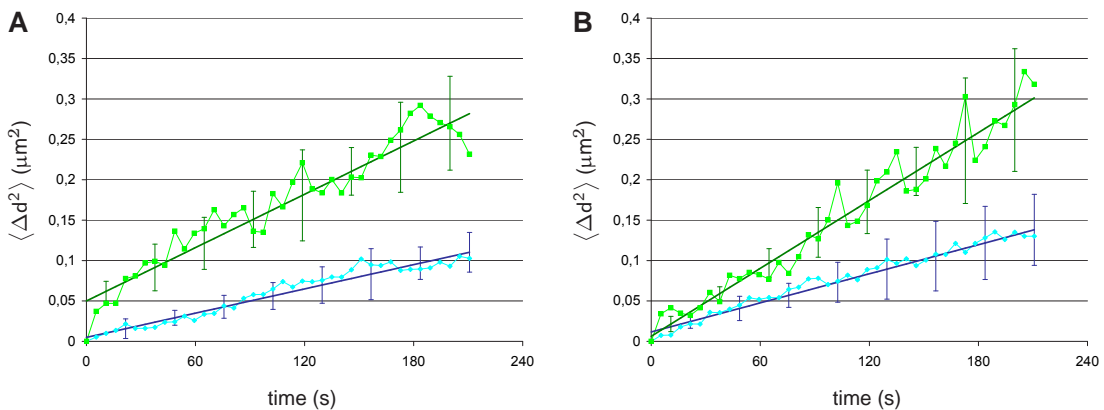
Figure 4.34: Mean square change in distance $\langle \Delta d^2 \rangle$. The same raw data used to determine the path and mobility of subclones 3C4 and 3F9 are used here to calculate the mean square change in distance $\langle \Delta d^2 \rangle$ (μm^2) which is plotted in function of time interval Δt (s). (A) and (B) represent, respectively, the measurements in active or inactive transcriptional status of the cells. The light-green curves are the mean square change in distance for subclone 3C4, the light-blue curves for subclone 3F9. In dark-green and dark-blue are the calculated trendlines for subclones 3C4 and 3F9, respectively. The slope of the trendline is the diffusion coefficient (see Table 4.2). The error bars represent the standard deviation. There is a clear difference in the mobility of the two subclones.

Table 4.2: Diffusion coefficients (cm^2/s) for subclones 3C4 and 3F9.

	– DRB	+ DRB
subclone 3C4	11×10^{-12}	14×10^{-12}
subclone 3F9	5×10^{-12}	6×10^{-12}

4.14.1 Chromatin mobility in tetraploid cells

The chromatin mobility shown in the previous section is measured in two dimensions, but drift or rotation of the nucleus might also contribute to it with apparent motion. To avoid this, and at the same time verify the obtained data, we measured the change in distance between two spots in the same nucleus over time. To do that, subclone 3C4 was used which has a small amount of tetraploid cells (4-5 %), and therefore two spots. Thus one spot was used as reference point and the distance was measured in three dimensions with 'Sync Measure 3D', a tool of the freeware ImageJ. The data were collected and processed as described in section 3.2.14.3. The averaged fluctuation around the mean distance is plotted against time in Figure 4.35.

The same raw data were also used in a mean square change in distance ($\langle \Delta d^2 \rangle$) analysis. As shown in Figure 4.36 the curve is composed at first by a linear increment (free diffusion) followed by a plateau (constrained movement). However, after treatment with DRB (Fig. 4.36, B) the spots reach the plateau
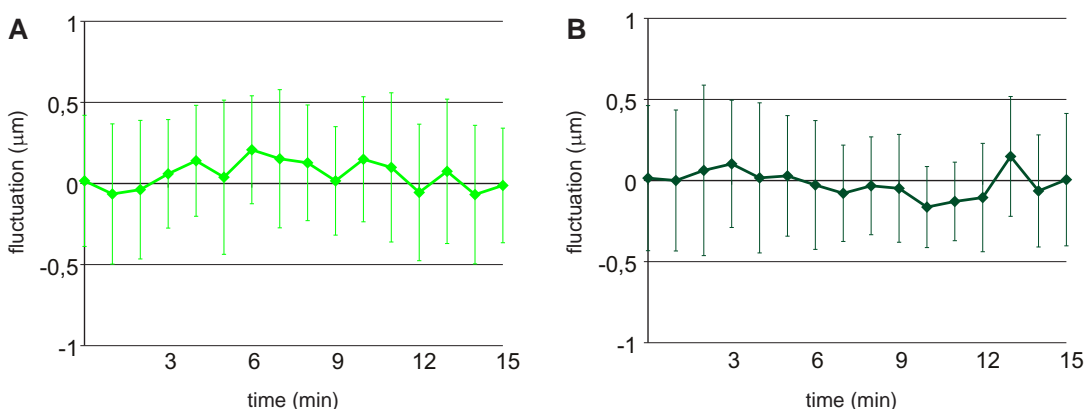
Figure 4.35: Fluctuation in distances between two spots. 3C4 cells were grown on glass bottom dishes and analyzed by confocal microscopy. The curves represent the mean fluctuation for 15 analyzed nuclei before (A) and after (B) incubation with DRB. The error bars represent the standard deviation at each time point.
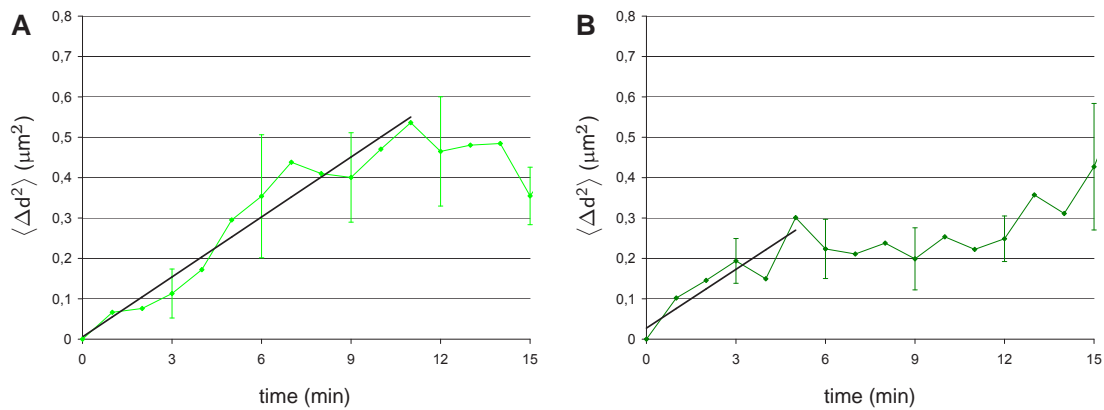
Figure 4.36: Mean square change in distance $\left\langle \Delta d^2 \right\rangle$ between two spots. The $\left\langle \Delta d^2 \right\rangle$ (μm^2) is plotted against Δt (min). The curves are the average of 15 analyzed nuclei before (A) and after (B) inhibition of transcription. In (B) the plateu is reached earlier, indicating a more constrained mobility of the spot. The error bars represent the standard deviation.

earlier, being more constrained than in transcriptional active cells. This reflects also a different radius of confinement which can be estimated from the square root of the plateau. For untreated cells the radius is $\sim$0.7 μm whereas for inhibited cells is $\sim$0.5 μm, values fully in line with data obtained from measurments in two dimensions (see Fig. 4.31). The diffusion coefficients, estimated from the slopes of the linears, are very similar to values shown in Table 4.2.

4.15 FRAP analysis for lacI-GFP

In addition to mobility assay of labeled chromatin loci, the dynamics of the *lac* repressor fused to GFP was investigated.

First, FRAP analysis was done to investigate whether an inhibition of transcription alters intranuclear viscosity. The experiments were performed as described in section 3.2.14.2, in a narrow strip across the nucleus. The recovery of lacI-GFP in the bleached area was very fast, indicating that the protein is able to diffuse freely in the nucleus. Figure 4.37 shows typical results for subclone 2G10. The experiments were also performed with subclone 3C4 with identical results (data not shown). It is evident that the lack of transcription does not affect the viscosity of the nucleus since the normalized curves, before and after DRB treatment, are not significantly different.

In a second set of experiments a circular area ($\varnothing$ 10 pixels) comprising the
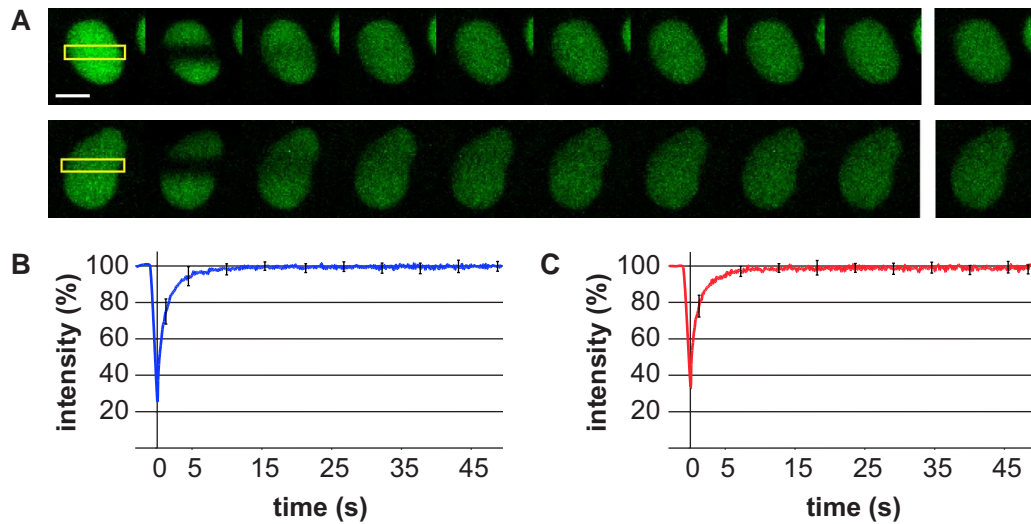
Figure 4.37: FRAP of nucleoplasmic lacI-GFP. 2G10 cells were grown on glass bottom dishes and analyzed on a heated stage. (A) The yellow rectangle represents the region of interest undergoing photobleaching. The gallery shows the nucleus before and right after the bleaching together with the recovery over time. Between the individual images there are 2 s; the last image shows the last time point (49.26 s). A nucleus before and after treatment with DRB is represented in the upper and lower panel, respectively. Scale bar: 10 μm. (B) The fluorescence recovery is plotted against time. The curve is the mean of 15 analyzed nuclei. The error bars represent the standard deviation. (C) Same curve as in (B) for cells treated 2 h with DRB.
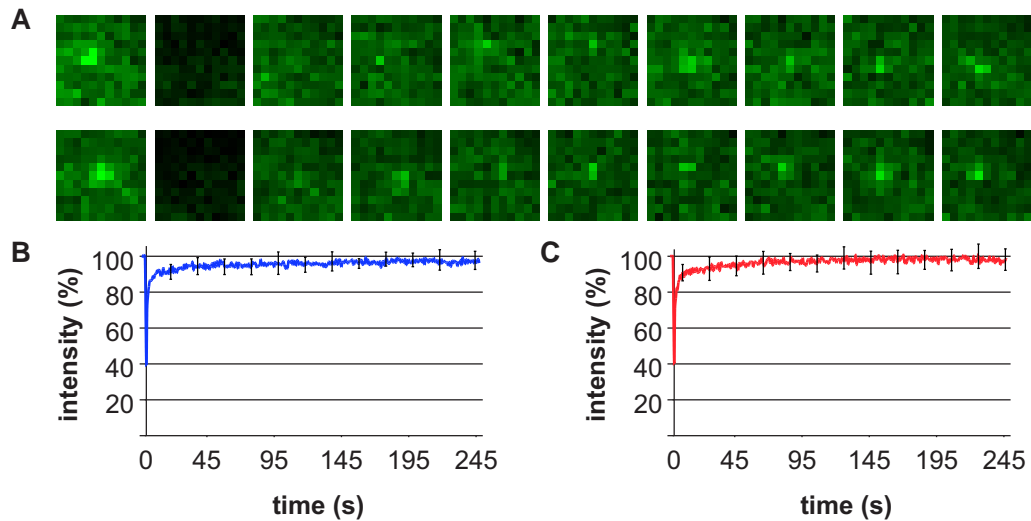
Figure 4.38: FRAP of lacI-GFP at the spot. Fluorescence recovery for lacI-GFP bound to the operator in 2G10 cells, imaged every 0.5 s for a total of approx. 4 min. (A) The gallery shows the spot before, right after the bleaching and during the recovery. The interval time between each image is of 25 s and each of them has a side of 2.5 μm. The upper and lower panel represent, respectively, a spot before and after inhibition of transcription. (B) Fluorescence recovery is plotted against time. The curve is the mean of 15 analyzed nuclei. The error bars represent the standard deviation. In (C) same representation as in (B) for cells treated with DRB. Note that the two curves are almost overlapping.

bright spot was bleached at the lacOp integration site, and the recovery of fluorescence monitored over time. As shown in Figure 4.38 the recovery of the mean fluorescence intensity in the bleached region is as fast as for the nucleoplasmic fraction of the protein seen in Figure 4.37. However, a bright pixel, that indicates detectable exchange between bleached and unbleached *lac* repressor bound to its target site, is not evident before approximately 50 s from the bleaching. This result correlates well with the known strong binding of the repressor to the DNA binding sequence.

5 Discussion

The interphase cell nucleus is a highly organized and dynamic organelle. Several fundamental processes such as transcription, replication, RNA processing and DNA repair take place in specific nuclear subcompartments (Lamond and Earnshaw, 1998; Dundr and Misteli, 2001) and there is growing evidence for relations between the functional complexity and the high degree of nuclear organization (Misteli, 2000).

The major component of the interphase nucleus, the chromatin, is organized in a way that each chromosome occupies a distinct, non overlapping territory (Cremer and Cremer, 2001). The chromosomes themselves are build up by subchromosomal foci, that can be visualized by labeling DNA with fluorescent nucleotide analogs (Zink *et al.*, 1998b). The space between different chromosomes is called interchromatin domain (ICD) compartment and hosts several nuclear subdomains which lack chromatin. The interconnection between chromosome territories (architecture) and gene expression (function) is achieved by gene organization. In fact, chromatin is folded in a way that active gene are often located at the surface of the territory which is in direct contact with the interchromatin space (Verschure *et al.*, 1999; Mahy *et al.*, 2002a). Owing to this arrangement, the newly synthesized RNA can be directly released in this compartment.

A lot of effort is put into understanding the molecular basis for nuclear compartmentalization. It is likely that an extended network exists in the nucleus which provides a platform for the organization of nuclear subdomains and for supporting their functionality. This network, composed of proteins and RNA, can be isolated by removing loosely bound proteins and chromatin, and was called nuclear matrix or scaffold (Berezney and Coffey, 1974). The association of chromosome territories with the nuclear matrix was investigated by Ma *et al.* (1999). In this study, the extraction of the nuclear matrix with RNase and 2 M NaCl leads to the disruption of chromosomes territories. These finding are fully in line with the 'loop' organization model for the chromatin. Specific sequences

on the DNA, called S/MAR (see section 1.2), attach the chromatin fibers to the matrix, to create topologically independent loop domains. Interestingly, many virus genomes have also been shown to bind to the nuclear matrix directly, carrying their own SAR (Pommier *et al.*, 1990; Mearini *et al.*, 2003), or indirectly, encoding a protein that acts as a bridge between the genome and the nuclear matrix (Krithivas *et al.*, 2002) or preferentially integrating in proximity of S/MAR DNA elements (D'Ugo *et al.*, 1998). In addition to structural function, S/MAR elements are also involved in the regulation of gene expression and DNA replication. However, genes in experimentally transfected plasmids or viral genomes not containing S/MAR elements are also efficiently transcribed. It therefore appeared desirable to investigate the fate of these small foreign DNA molecules in the nucleus of living cells. The finding of a reduced mobility for plasmid DNA, even in presence of an active promoter, lead us to label distinct loci on genomic DNA to investigate their dynamics in relation to different specific localization and trascriptional status of the cell.

5.1 Localization of small circular DNA

Several plasmids were specifically labeled using a rhodamine-tagged peptide nucleic acid (PNA) clamp to study their localization and dynamics in nuclei of living cells. The PNA clamp seemed to be a promising approach to address the question, since a similar method, a fluorescein-conjugated PNA, was previously used to study nuclear import of plasmids in permeabilized cells (Wilson *et al.*, 1999). This direct labeling technique allows tracking plasmid DNA in transient assays which was not possible with other established *in vivo* DNA visualization methods, such as the *lac* operator/repressor system (Robinett *et al.*, 1996) used in this work to label specific loci of endogenous DNA. To be effective, the latter system requires the integration of direct repeats of the binding sites at one or few sites in the DNA under study and expression of the protein for indirect detection. However such long repeats are intrinsically unstable and prone to recombination, so that they can hardly be used for small DNA molecules in a transient state.

To allow studies in living cells, it was necessary to find a method for

nuclear introduction of PNA-tagged plasmid DNA which preserves morphology and functionality of the cells. Pilot experiments showed that this is best accomplished by microinjection directly into the nucleus. Particular attention was paid to find out the amount of labeled plasmid which was detectable and at the same time not saturating the system. The amount of microinjected plasmid was varied between 0.1 and 1 % of the genomic DNA content of the host nucleus, and control experiments verified that this amount was not interfering with vital nuclear processes such as transcription and translation (Fig. 4.5). Moreover, PNA/DNA complexes show a very high stability in *in vivo* condition, since it was impossible to detect nuclear export of fluorescence as seen for free unbound PNA (Fig. 4.7). After microinjection into the nucleus, the localization of several plasmids DNA was examined in living and fixed cells (Fig. 4.10 and Fig. 4.11). Interestingly, although variable in the individual nuclei, the pattern of distribution of labeled plasmid in both conditions was the same, indicating that the fixation with paraformaldehyde preserves the *in vivo* localization. In all analyzed nuclei, labeled plasmids are not homogeneously distributed, but many areas of different dimensions are lacking fluorescence. This sponge-like localization is also typical for a linearized plasmid, which has lost the supercoiled topology. Interestingly, a plasmid containing rRNA genes is not preferentially targeted to nucleoli. In addition, the same heterogeneous distribution is seen also with plasmid of entirely prokaryotic sequence, thus suggesting an independence of the localization from the plasmid sequence (Fig. 4.12).

To identify the nuclear regions free of labeled plasmid, co-microinjection experiments were performed with expression vectors encoding GFP-tagged proteins markers of some nuclear subcompartments. In this way, nucleoli and PML nuclear bodies could be identified as regions without detectable amount of PNA/DNA complexes (Fig. 4.14 and Fig. 4.15). This heterogeneous distribution is comparable with the localization of labeled plasmids seen by Wilson *et al.* (1999) and with the localization of SV40 in fixed cells, which also excludes nucleoli (Dean, 1997). Although Dean (1997) found an association of SV40 with splicing speckles, such a localization was not evident in the experiments performed in this work.

The sponge-like localization of plasmid DNA reminded us of the distribution

of SAF-A, a nuclear matrix and S/MAR binding protein (Romig *et al.*, 1992; Herrmann *et al.*, 2004). To verify a possible colocalization of plasmid DNA with the protein, co-microinjection experiments were performed again. We found that there is a significant, but not complete overlapping between SAF-A and the labeled plasmid (Fig. 4.16).

The similar distribution to a nuclear matrix protein prompted us to investigate the possibility of a binding with the nuclear matrix. Using a modified protocol for matrix extraction, it was seen that after removal of loosely bound proteins with detergent, no change in the distribution or fluorescence intensity was detectable. However, additional incubation with 2 M NaCl, which extracts tightly bound proteins, produced a consistent loss of fluorescence and a redistribution into a more granular pattern, with a preference for the nuclear periphery. An involvement of the nuclear matrix in the localization and resistance toward detergent and high salt of plasmid DNA, is compatible with the finding in earlier studies of the presence of between 20 000 and 60 000 binding site for DNA per nucleus in matrix preparation, which is significantly higher than the number of plasmid copies microinjected here (Luderus *et al.*, 1992; Kay and Bode, 1994).

Binding of genomic DNA to the nuclear matrix occurs via specific DNA sequences, called S/MAR (see section 1.2), which organize the chromatin in topologically independent loops. Is the presence of such a sequence necessary for anchoring plasmids to the matrix? Surprisingly, there was no difference using plasmids containing a SAR DNA, such as pMII and pEPI-1, or a plasmid of comparable size, but without SAR DNA, such as pK2. In confocal slices all the plasmids showed the same granular distribution and loss of fluorescence as a result of high salt extraction (Fig. 4.18). In addition, two different quantification methods demonstrate that around 50 % of plasmids was retained after 'matrix' extraction, independently of the presence of a SAR element on the plasmid (Fig. 4.19). The attachment to the nuclear matrix is also independent of the presence in the plasmid of an active promoter, as in pEPI-1. This would have been plausible, because it has been speculated that DNA could be tethered to the nuclear matrix or to the transcription factories by interaction between the active promoter and the matrix-bound RNA polymerase II (Jackson and

Cook, 1993; Iborra *et al.*, 1996).

Nothing is known yet about the nuclear proteins which provide DNA binding sites, but it is very likely that a variety of proteins, such as matrix-associated transcription factors are involved (van Wijnen *et al.*, 1993). It was found earlier that different subsets of proteins are responsible of binding of supercoiled DNA or single strand DNA to the matrix (Kay and Bode, 1994). One of these subsets specifically interacts with DNA with superhelical density below 0.04 and had a topoisomerization activity. Topoisomerase II, a well-known component of isolated nuclear matrix, could then be involved in the attachment of circular DNA to the matrix. However, in a recent study, it was shown that topoisomerase II freely diffuse in the nucleus of living cells (Christensen *et al.*, 2002), arguing against its involvement in attaching plasmid DNA to the matrix.

Since the binding of plasmid DNA to the nuclear matrix is independent of the presence of a SAR sequence, S/MAR binding proteins such as SAF-A (Romig *et al.*, 1992; Kipp *et al.*, 2000) or SAF-B (Renz and Fackelmayer, 1996; Nayler *et al.*, 1998) are unlikely to be responsible for immobilization of plasmid DNA. This is particular remarkable because it was recently demonstrated *in vivo* that pEPI-1 is bound to SAF-A after many generations of episomal replication (Piechaczek *et al.*, 1999; Baiker *et al.*, 2000; Jenke *et al.*, 2002; Jenke *et al.*, 2004). In these reports, the SAR DNA element inserted in the vector and the interaction with SAF-A, were essential for episomal replication and to prevent its integration into the genome.

Future experiments will address the nature of the proteins that affect the localization and mobility of plasmid DNA. Tagged PNA clamps will be a valuable tool for interaction screening of nuclear proteins, and will allow specific enrichment for the involved factors than can then be identified by mass spectrometry. Understanding the molecular mechanism that tethers plasmids to the nuclear matrix, and thereby creates a permissive environment for expression of enclosed genes, might allow the rational design of compounds to block this interaction. Possibly this will later enable inhibition of the expression of some viral genes and attenuate viral infections.

5.2 Dynamics of plasmid DNA

The most striking result in the present work is that plasmid DNA is not present in soluble, freely diffusible form in the nucleus.

Fluorescence recovery after photobleaching (FRAP) experiments were performed to investigate the nuclear mobility of several different plasmids tagged with rhodamine-PNA, after their microinjection in the nucleus. In this live imaging method, fluorescent molecules are irreversibly photobleached in a small nuclear area with a high-intensity laser beam and the recovery of fluorescence from neighborhood molecules, which are still fluorescent, in the bleached region is measured over time (Houtsmuller and Vermeulen, 2001). For all analyzed plasmids, the normalized fluorescence recovery curve shows a slow and incomplete recovery (Fig. 4.20, Fig. 4.21, Fig. 4.22 and Fig. 4.23). The diffusion time ($t_{1/2}$) of the different plasmids, calculated as the time needed by half of the measured recovered plasmid to recover in the bleached region, ranges between 72 and 99 s, indicating a very slow dynamics if compared with the soluble control protein β-Gal-NLS fused to GFP, which shows a complete recovery within 15 s and has a $t_{1/2}$ of 1.14 s (Fig. 4.25).

Another parameter which can be calculated from recovery curves is the diffusion coefficient. A diffusion coefficient of 4.3 x 10^{-10} cm^2/s can be estimated for plasmid DNA. This diffusion coefficient is two orders of magnitude lower than the one measured for β-Gal-NLS (2.4 x 10^{-8} cm^2/s), compatible with a strong, but not complete, attachment to the nuclear matrix.

During the time of recovery experiment, the fluorescence in the bleached area does not reach a plateau, indicating that fluorescent and photobleached PNA/DNA complexes are not yet in equilibrium, but still exchanging. The measured recovery curves are best described as the superposition of a typical first-order recovery curve, such as the one obtained for β-Gal-NLS (Fig. 4.25, red curve), and a linear increase over time (Fig. 5.1). Most probably, the curve reflects the presence of two distinct populations of plasmids which differ in their mobility: a 'mobile' fraction (comprising 25-33 % of the plasmid) and a larger fraction (67-75 %) which is transiently 'immobilized' on a structure and dissociate from there at a constant net rate of ~5 %/min. Figure
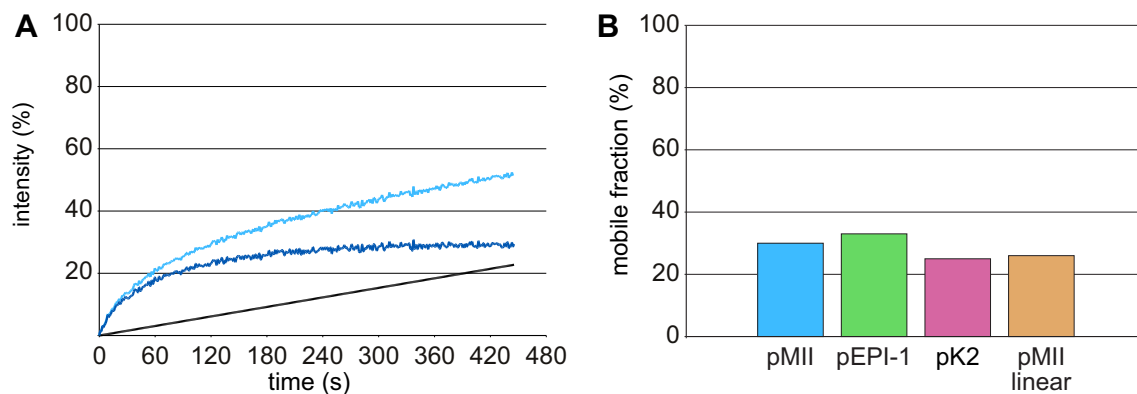
Figure 5.1: Interpretation of fluorescence recovery curve and mobile fractions. (A) The normalized recovery curve (light-blue) for pMII plasmid is composed of a linear component (black line) and a typical first-order recovery curve (dark-blue). The linear component indicates a transient immobilization of plasmid DNA. This interpretation of the recovery curve can be applied to all examined plasmids. (B) Mobile fractions calculated without the linear component. There is no significant difference between the analyzed plasmids.

5.1 (B) represents the mobile fractions for all analyzed plasmids without the contribution of the linear component. Interestingly the same model can be applied to SAF-A, a protein of the nuclear matrix which is relatively immobile. As for the plasmid, FRAP analysis over long time revealed for SAF-A the presence of a subpopulation which is only transiently bound to the nuclear matrix and is released from there at a constant net rate, contributing to the fluorescence recovery curve as a linear component (Schwander, 2004).

The slow dynamics of plasmid DNA is fully in line with other results obtained in this work, such as the long time needed by the plasmids to acquire their final localization. It is not possible to formally rule out an involvement of bound PNA to the localization and the low mobility of the plasmid. However, this seems not likely for two reasons. On one hand, PNA/DNA complexes behave as a soluble entity of expected size during ultrafiltration, excluding formation of aggregates which could limit their mobility. On the other hand, quantification of DNA after detergent and high salt extraction was performed with unlabeled as well as labeled plasmid (Fig. 4.17 and Fig. 4.19) yielding identical results. This excludes the possibility of PNA interference with the behavior of plasmid under study. Furthermore PNA binding to pEPI-1 plasmid was also not interfering with the expression of the GFP protein (Fig. 4.6).

This was the first time that mobility of supercoiled plasmids was investigated,

so the results can only be compared with the dynamics of other macromolecules such as proteins or dextrans of similar size. From the experiments of ultrafiltration, it can be inferred that the supercoiled plasmids have the dimension of a globular protein with size between 30 and 100 kDa. Proteins with this size are able to freely diffuse in the nucleus, if they are not constrained by specific interaction with other nuclear components (Calapez *et al.*, 2002; Stenoien *et al.*, 2001). Recently FITC-conjugated dextrans of different sizes were microinjected into the nucleus and their diffusional properties analyzed. Molecules with a size smaller than 500 kDa freely diffuse in the nucleus, while only dextrans of significant bigger size have a reduced nuclear mobility. Thus, at comparable size, the mobility of plasmid DNA is significantly lower than that of dextrans. The slow dynamics of plasmid DNA is not a direct consequence of its topological conformation. In fact, FRAP experiments with relaxed molecules (linaerized pMII plasmid) gave the same result. This finding is fully in line with the observations of Lukacs and coworkers who examined the mobility of fluorescein-tagged dsDNA fragments of variable sizes in the cytoplasm and in the nucleus (Lukacs *et al.*, 2000).

5.3 Dynamics of chromatin loci *in vivo*

To track and analyze the movement of endogenous chromatin in living cells, we used the *lac* operator/repressor system developed by Belmont and coworkers (Robinett *et al.*, 1996). To address this question, chinese hamster ovary cells (CHO) were used to establish stable cell lines containing randomly integrated operator repeats and at the same time constitutively expressing the *lac* repressor fused to GFP for direct visualization in living cells. CHO lacOp/lacI stable cell lines were subcloned by serial dilution and the obtained subclones analyzed at the confocal microscope for the presence of a single bright spot in the nucleus, indicating the binding of the fluorescent fusion protein to its target sequence. In the first reports describing the *lac* operator/repressor system as a specific label for chromatin, the integration of *lac* repeats was followed by gene amplification using the expression of dihydrofolate reductase, present on the integrated vector, and methotrexate selection. The amplification produced

a homogeneously staining regions (HSR) of ~90 Mbp which behaved as an independent chromosomal band (Robinett *et al.*, 1996; Li *et al.*, 1998). In the present work we did not use any gene amplification, since the detection with lacI-GFP of the integrated vector(s), in fixed specimens analyzed by confocal microscopy, already produced a clearly detectable spot. In addition, in this way, the possible interference of the inserted sequence with cellular processes was reduced to minimal levels.

Confocal analysis revealed different nuclear localizations of the spots of distinct subclones. As shown by three dimensional reconstructions of Z-stacks, in some subclones the spot was localized at the nuclear interior, while in others it was more at the periphery (Fig. 4.26). To address the question whether the localization of the labeled chromatin affects its mobility, short-term mobility of individual spots was analyzed in subclones 3C4 and 3F9 which significantly differ for the spot localization in the nucleus. The spot in 3C4 cells localizes at the nuclear interior, while in 3F9 cells localizes close to the periphery. Drawing the trajectories of each spot in a x-y diagram, it was evident that the spots of both clones move with a random walk. However, the movement of the spot at the nuclear periphery (subclone 3F9) is more constrained and results in a high concentration of points in a smaller area (Fig. 4.32). This aspect is even clearer in a density plot representing the distances of the spot from the origin at each time point (right panels in Fig. 4.31 and Fig. 4.32). The histograms reveal that in 3F9 cells 92 % of the spots are distributed over 4 intervals, for a total distance of 0.4 μm. In comparison, in 3C4 subclone, considerable less spots can be found in the same intervals (65 %). In addition, the distributions do not significantly change for both subclones, when the mobility of the spot is measured in transcriptionally inhibited cells. The difference in behavior of the two subclones can also be seen in density plots representing the distance covered by the spot in two subsequent time points. As shown in Figure 4.33, movements in the 100 nm range (the size of one pixel) are typical for spots of 3F9 cells independently of the transcriptional status of the cells (81.2 % and 84.4 % of spots before and after treatment with DRB, respectively), whereas in 3C4 cells the movement is almost equally distributed in two pixels (39 % in both intervals) in actively transcribing cells, but is constrained to only one pixel after inhibition

with DRB (77.7 % in the first pixel and 14 % in the second pixel).

The dynamic short-range chromatin mobility in subclones 3F9 and 3C4 was measured calculating xy-coordinates and distances from the origin in two dimensions. Even though particular attention was paid at choosing only nuclei which did not move during the recording time, an influence on the measured mobility from rotation or translation of the nucleus cannot be excluded. To verify the reliability of our data, we measured change in distance between two spots in tetraploid cells over time. Thus one of the spots was taken as reference point and the three dimensional distances between the two spots for each time frame were calculated using the tool 'Sync Measure 3D' of the freeware ImageJ. In this way, possible drift or rotation of the nucleus which might lead to apparent motion were excluded. The measurements were done in subclone 3C4, with the spot at the nuclear interior. The spots move towards and away from each other producing a change in distance which is plotted against time (Fig. 4.35). A radius of confinement for the spot can be calculated from the mean square change in distance ($\langle \Delta d^2 \rangle$) analysis of the data. In cells actively transcribing, the locus can move in a defined nuclear volume with a radius of $\sim$0.7 μm, whereas after inhibition of transcription with DRB it is constrained to a radius of $\sim$0.5 μm. These values are fully in line with the measurements of mobility in 3C4 cells harboring only one spot (Fig. 4.31). This range of movement correlates well also with values found in previous studies on the mobility of interphase chromatin of other organisms such as *S. cerevisiae*, *D. melanogaster* and humans (Abney *et al.*, 1997; Vazquez *et al.*, 2001; Heun *et al.*, 2001). Noteworthy, there is a significantly difference in nuclear diameter, and thus in nuclear volume, in mammalian cells, *Drosophila* spermatocytes and budding yeast. In fact, mammalian nuclei and fly spermatocytes in mid G2 have a diameter of $\sim$10 μm, while the nuclear diameter in yeast is only $\sim$2 μm. This difference in nuclear volumes substantially limits the range of environments accessible for a chromatin locus in mammalian cells and *Drosophila* spermatocytes, whereas in yeast a locus can access a larger proportion of the nuclear volume (Gasser, 2002; Chubb and Bickmore, 2003).

The inhibition of transcription seems not to affect the mobility of a nuclear peripheral spot, such as in subclone 3F9, while it slightly reduces the mobility

of nucleoplasmic spots, such as in subclone 3C4, suggesting the involvement of the nuclear organization in limiting chromatin movement. This observed constrained movement of spots could arise from the interaction of the chromatin with structural compartments of the nucleus such as the nuclear lamina or the nuclear matrix. Even though the existence of a nuclear matrix is highly debated (Hancock, 2000; Pederson, 2000b), it could play a role in anchoring the chromatin and thereby limit its mobility. One of the most abundant proteins of the nuclear matrix is SAF-A, a protein able to bind DNA and RNA. FRAP experiments in living 293 cells constitutively expressing SAF-A fused to the green fluorescence protein showed an increased amount of the mobile fraction of the protein after inhibition of transcription with DRB. A more accurate analysis with mutants of SAF-A lacking respectively the DNA binding domain (ΔN45), the RNA binding domain (ΔRGG) or both ($\Delta\Delta$), revealed that the increase in the mobile fraction is due to the release from the matrix of the fraction bound to RNA (Reuschlein, 2004). However the fraction of SAF-A that remains immobile ($\sim$40 %) might be still enough to keep the chromatin anchored after treatment with DRB.

The mobility of nuclear proteins in living cells was extensively investigated in the last years using FRAP experiments with the surprising result that many proteins are highly mobile. Here, FRAP analysis were done for the unbound nucleoplasmic fraction of lacI-GFP and for the fluorescent repressor bound to the cognate sequence. The unbound fraction freely diffuses in the nucleus (Fig. 4.37) and has a diffusion coefficient of 9.6 x 10^{-7} cm^2/s, approximately 2.5 times greater than the diffusion coefficient of β-Gal-NLS (2.4 x 10^{-8} cm^2/s), a soluble, freely diffusing nuclear protein. Interestingly, after inhibition of transcription the diffusion coefficient and $t_{1/2}$ of the *lac* repressor did not change significantly, suggesting that there is no alteration in the intranuclear viscosity. When a small circular region comprising the spot was photobleached at the lacOp integration site (Fig. 4.38), the recovery of the mean fluorescence intensity was fast for unbound fraction, as already seen with a strip across the nucleus. However, only after $\sim$50 s it was possible to see again a bright spot indicating the exchange between bound photobleached molecules and unbound fluorescent molecules. This result is not surprising considering the strong binding of the *lac* repressor

to its DNA target sequence.

The influence of the association of specific chromatin loci to nuclear subcompartments was also investigated by Bickmore and coworkers. They found that in human cells the association of chromatin loci with the nuclear lamina or nucleoli constrains their movement, suggesting a role for such subcompartments in maintaining the three dimensional organization of the chromatin in the human nucleus (Chubb *et al.*, 2002). Importantly, the lack of transcription caused by DRB influences nuclear compartmentalization inducing dispersal of nucleoli (Fig. 4.30).

The specific site of integration of *lac* operator repeats in the subclones used in this work is not yet determined. However it is reasonable that the environment affects the condensation status of the inserted sequences. Thus, the spot at the nuclear periphery could originate from insertion close to a highly condensed heterochromatic region, whereas a spot in the nuclear interior could origin from insertion near an actively transcribed region on a decondensed loop at the boundary of the chromosome territory or in a loop that extends into the interchromatin space (Mahy *et al.*, 2002b). The inhibition of transcription with DRB would then produce no detectable effect in the case of a transcriptionally silent heterochromatic locus, but would result in a condensation of the transcribed loop and therefore in a reduced mobility of the chromatin at that site (Chubb and Bickmore, 2003). In future experiments it will be interesting to measure the level of transcription of dhfr gene which is integrated at the same site with *lac* operator arrays and was used for selection of cells that had incorporated the lacOp repeats. On the basis of our present knowledge, we expect a reduced level of transcription in subclones with the spot close to the nuclear periphery compared to subclones with the spot at the nuclear interior. The lower level of transcription of dhfr, in cells deficient for dihydrofolate reductase, could be then the molecular reason for the slower growth of subclones as 3F9 with the spot at the nuclear periphery.

The relation between heterochromatin and constrained motion is the subject of a speculative model of Gasser (2002). The model predicts that the progressive differentiation within a multicellular organism cell will restrict both the expression profile and the dynamics of the interphase chromatin. Nonetheless

reactivation of gene expression and increased mobility of the chromatin could occur during meiosis or oncogenic transformation.

This work shows for the first time that the dynamics of incoming DNA, such as vector used for gene therapy or viral genomes, is strongly reduced. We show also that endogenous DNA is constrained in its movement and this reflects slight differences depending on the specific nuclear localization of analyzed chromatin loci and transcriptional status of the cells. It will be interesting to further investigate the nuclear factors which interact with foreign DNA, decreasing its mobility, in order to optimize gene therapy or prevent viral infection. More experiments are also needed to better understand if a 'cause-effect' relation between the nuclear organization and the functional status of the nucleus exists, and how it works.

6 Summary

In the first part of this work, the fate of plasmid DNA labeled with PNA was investigated in living cells. It was shown that foreign DNA rapidly undergoes interaction with intranuclear structural sites that strongly reduce its mobility and restrict the DNA to regions excluding nucleoli and nuclear bodies as PML bodies. The labeled plasmids partially colocalize with SAF-A, a well characterized marker of the nuclear matrix, and are resistant towards extraction by detergent and, in part, elevated salt concentration. Importantly the localization and low mobility are independent of plasmid sequence and do not require the presence of either a S/MAR DNA element or a functional promoter.

In the second part of this work, the attention was focused on chromatin mobility in living mammalian cells by using the *lac* operator/repressor system. The experiments show that the labeled chromatin loci are highly dynamic, moving around by random walk, but are locally constrained in a defined nuclear volume. Interestingly, the mobility of the analyzed loci depends on their location and partially on the transcriptional status of the cell.

Bibliography

Abney, J. R., Cutler, B., Fillbach, M. L., Axelrod, D. and Scalettar, B. A. (1997), 'Chromatin dynamics in interphase nuclei and its implications for nuclear structure', *J Cell Biol* **137**(7), 1459–68.

Adachi, Y., Kas, E. and Laemmli, U. K. (1989), 'Preferential, cooperative binding of DNA topoisomerase II to scaffold-associated regions', *Embo J* **8**(13), 3997–4006.

Baiker, A., Maercker, C., Piechaczek, C., Schmidt, S. B., Bode, J., Benham, C. and Lipps, H. J. (2000), 'Mitotic stability of an episomal vector containing a human scaffold/matrix-attached region is provided by association with nuclear matrix', *Nat Cell Biol* **2**(3), 182–4.

Belmont, A. (2003), 'Dynamics of chromatin, proteins, and bodies within the cell nucleus', *Curr Opin Cell Biol* **15**(3), 304–10.

Belmont, A. S. (2001), 'Visualizing chromosome dynamics with GFP', *Trends Cell Biol* **11**(6), 250–7.

Belmont, A. S. and Bruce, K. (1994), 'Visualization of G1 chromosomes: a folded, twisted, supercoiled chromonema model of interphase chromatid structure', *J Cell Biol* **127**(2), 287–302.

Belmont, A. S., Dietzel, S., Nye, A. C., Strukov, Y. G. and Tumbar, T. (1999b), 'Large-scale chromatin structure and function', *Curr Opin Cell Biol* **11**(3), 307–11.

Belmont, A. S., Li, G., Sudlow, G. and Robinett, C. (1999a), 'Visualization of large-scale chromatin structure and dynamics using the lac operator/lac repressor reporter system', *Methods Cell Biol* **58**, 203–22.

Belmont, A. S. and Straight, A. F. (1998), 'In vivo visualization of chromosomes using lac operator-repressor binding', *Trends Cell Biol* **8**(3), 121–4.

Bentin, T., Larsen, H. J. and Nielsen, P. E. (2003), 'Combined triplex/duplex invasion of double-stranded DNA by "tail-clamp" peptide nucleic acid', *Biochemistry* **42**(47), 13987–95.

Berezney, R. and Coffey, D. S. (1974), 'Identification of a nuclear protein matrix', *Biochem Biophys Res Commun* **60**(4), 1410–7.

Branden, L. J., Mohamed, A. J. and Smith, C. I. (1999), 'A peptide nucleic acid-nuclear localization signal fusion that mediates nuclear transport of DNA', *Nat Biotechnol* **17**(8), 784–7.

Braun, K., Peschke, P., Pipkorn, R., Lampel, S., Wachsmuth, M., Waldeck, W., Friedrich, E. and Debus, J. (2002), 'A biological transporter for the delivery of peptide nucleic acids (PNAs) to the nuclear compartment of living cells', *J Mol Biol* **318**(2), 237–43.

Bridger, J. M., Kill, I. R., O'Farrell, M. and Hutchison, C. J. (1993), 'Internal lamin structures within G1 nuclei of human dermal fibroblasts', *J Cell Sci* **104 (Pt 2)**, 297–306.

Broers, J. L., Machiels, B. M., van Eys, G. J., Kuijpers, H. J., Manders, E. M., van Driel, R. and Ramaekers, F. C. (1999), 'Dynamics of the nuclear lamina as monitored by GFP-tagged A-type lamins', *J Cell Sci* **112 (Pt 20)**, 3463–75.

Calapez, A., Pereira, H. M., Calado, A., Braga, J., Rino, J., Carvalho, C., Tavanez, J. P., Wahle, E., Rosa, A. C. and Carmo-Fonseca, M. (2002), 'The intranuclear mobility of messenger RNA binding proteins is ATP dependent and temperature sensitive', *J Cell Biol* **159**(5), 795–805.

Carmo-Fonseca, M., Mendes-Soares, L. and Campos, I. (2000), 'To be or not to be in the nucleolus', *Nat Cell Biol* **2**(6), E107–12.

Chao, M. V., Martinson, H. G. and Gralla, J. D. (1980), 'lac Operator nucleosomes. 2. lac Nucleosomes can change conformation to strengthen binding by lac repressor', *Biochemistry* **19**(14), 3260–9.

Chen, J. and Matthews, K. S. (1992), 'Deletion of lactose repressor carboxyl-terminal domain affects tetramer formation', *J Biol Chem* **267**(20), 13843–50.

Chodosh, L. A., Fire, A., Samuels, M. and Sharp, P. A. (1989), '5,6-Dichloro-1-beta-D-ribofuranosylbenzimidazole inhibits transcription elongation by RNA polymerase II in vitro', *J Biol Chem* **264**(4), 2250–7.

Christensen, L., Fitzpatrick, R., Gildea, B., Petersen, K. H., Hansen, H. F., Koch, T., Egholm, M., Buchardt, O., Nielsen, P. E., Coull, J. and et al. (1995), 'Solid-phase synthesis of peptide nucleic acids', *J Pept Sci* **1**(3), 175–83.

Christensen, M. O., Larsen, M. K., Barthelmes, H. U., Hock, R., Andersen, C. L., Kjeldsen, E., Knudsen, B. R., Westergaard, O., Boege, F. and Mielke, C. (2002), 'Dynamics of human DNA topoisomerases IIalpha and IIbeta in living cells', *J Cell Biol* **157**(1), 31–44.

Chubb, J. R. and Bickmore, W. A. (2003), 'Considering nuclear compartmentalization in the light of nuclear dynamics', *Cell* **112**(4), 403–6.

Chubb, J. R., Boyle, S., Perry, P. and Bickmore, W. A. (2002), 'Chromatin motion is constrained by association with nuclear compartments in human cells', *Curr Biol* **12**(6), 439–45.

Cremer, T. and Cremer, C. (2001), 'Chromosome territories, nuclear architecture and gene regulation in mammalian cells', *Nat Rev Genet* **2**(4), 292–301.

Croft, J. A., Bridger, J. M., Boyle, S., Perry, P., Teague, P. and Bickmore, W. A. (1999), 'Differences in the localization and morphology of chromosomes in the human nucleus', *J Cell Biol* **145**(6), 1119–31.

Cutrona, G., Carpaneto, E. M., Ulivi, M., Roncella, S., Landt, O., Ferrarini, M. and Boffa, L. C. (2000), 'Effects in live cells of a c-myc anti-gene PNA linked to a nuclear localization signal', *Nat Biotechnol* **18**(3), 300–3.

Dean, D. A. (1997), 'Import of plasmid DNA into the nucleus is sequence specific', *Exp Cell Res* **230**(2), 293–302.

Demidov, V. V., Potaman, V. N., Frank-Kamenetskii, M. D., Egholm, M., Buchard, O., Sonnichsen, S. H. and Nielsen, P. E. (1994), 'Stability of peptide nucleic acids in human serum and cellular extracts', *Biochem Pharmacol* **48**(6), 1310–3.

Dickinson, L. A., Joh, T., Kohwi, Y. and Kohwi-Shigematsu, T. (1992), 'A tissue-specific MAR/SAR DNA-binding protein with unusual binding site recognition', *Cell* **70**(4), 631–45.

Dickinson, L. A., Kohwi-Shigematsu, T., Joh, T. and Kohwi, Y. (1995), 'Nucleolin is a matrix attachment region DNA-binding protein that specifically recognizes a region with high base-unpairing potential A tissue-specific MAR/SAR DNA-binding protein with unusual binding site recognition', *Mol Cell Biol* **15**(1), 456–65.

D'Ugo, E., Bruni, R., Argentini, C., Giuseppetti, R. and Rapicetta, M. (1998), 'Identification of scaffold/matrix attachment region in recurrent site of woodchuck hepatitis virus integration', *DNA Cell Biol* **17**(6), 519–27.

Dundr, M. and Misteli, T. (2001), 'Functional architecture in the cell nucleus', *Biochem J* **356**(Pt 2), 297–310.

Egholm, M., Christensen, L., Dueholm, K. L., Buchardt, O., Coull, J. and Nielsen, P. E. (1995), 'Efficient pH-independent sequence-specific DNA binding by pseudoisocytosine-containing bis-PNA', *Nucleic Acids Res* **23**(2), 217–22.

Everett, R. D. (2001), 'DNA viruses and viral proteins that interact with PML nuclear bodies', *Oncogene* **20**(49), 7266–73.

Fackelmayer, F. O. (2000), 'Die Architektur des Zellkerns', *Biospektrum* **6**, 441–44.

Fackelmayer, F. O. (2004), 'Nuclear architecture and gene expression in the quest for novel therapeutics', *Curr Pharm Des* **10**(23), 2851–60.

Fey, E. G., Krochmalnic, G. and Penman, S. (1986), 'The nonchromatin substructures of the nucleus: the ribonucleoprotein (RNP)-containing and RNP-depleted matrices analyzed by sequential fractionation and resinless section electron microscopy', *J Cell Biol* **102**(5), 1654–65.

Fiandaca, M. J., Hyldig-Nielsen, J. J., Gildea, B. D. and Coull, J. M. (2001), 'Self-reporting PNA/DNA primers for PCR analysis', *Genome Res* **11**(4), 609–13.

Foisner, R. (2001), 'Inner nuclear membrane proteins and the nuclear lamina', *J Cell Sci* **114**(Pt 21), 3791–2.

Fraefel, C., Bittermann, A. G., Bueler, H., Heid, I., Bachi, T. and Ackermann, M. (2004), 'Spatial and temporal organization of adeno-associated virus DNA replication in live cells', *J Virol* **78**(1), 389–98.

Gasser, S. M. (2002), 'Visualizing chromatin dynamics in interphase nuclei', *Science* **296**(5572), 1412–6.

Hancock, R. (2000), 'A new look at the nuclear matrix', *Chromosoma* **109**(4), 219–25.

Harrer, M., Luhrs, H., Bustin, M., Scheer, U. and Hock, R. (2004), 'Dynamic interaction of HMGA1a proteins with chromatin', *J Cell Sci* **117**(Pt 16), 3459–71.

Hart, C. M. and Laemmli, U. K. (1998), 'Facilitation of chromatin dynamics by SARs', *Curr Opin Genet Dev* **8**(5), 519–25.

He, D. C., Nickerson, J. A. and Penman, S. (1990), 'Core filaments of the nuclear matrix', *J Cell Biol* **110**(3), 569–80.

Heng, H. H., Goetze, S., Ye, C. J., Liu, G., Stevens, J. B., Bremer, S. W., Wykes, S. M., Bode, J. and Krawetz, S. A. (2004), 'Chromatin loops are selectively anchored using scaffold/matrix-attachment regions', *J Cell Sci* **117**(Pt 7), 999–1008.

Herrmann, F. (2002), 'Untersuchungen zu funktionellen Weckselwirkungen des Kernproteins SAF-A', *Diplomarbeit, Universitaet Konstanz* .

Herrmann, F., Bossert, M., Schwander, A., Akgun, E. and Fackelmayer, F. O. (2004), 'Arginine methylation of scaffold attachment factor A (SAF-A) by hnRNP-particle associated PRMT1', *J Biol Chem* .

Heun, P., Laroche, T., Shimada, K., Furrer, P. and Gasser, S. M. (2001), 'Chromosome dynamics in the yeast interphase nucleus', *Science* **294**(5549), 2181–6.

Hiscox, J. A. (2002), 'The nucleolus–a gateway to viral infection?', *Arch Virol* **147**(6), 1077–89.

Hofmann, T. G. and Will, H. (2003), 'Body language: the function of PML nuclear bodies in apoptosis regulation', *Cell Death Differ* **10**(12), 1290–9.

Houtsmuller, A. B., Rademakers, S., Nigg, A. L., Hoogstraten, D., Hoeijmakers, J. H. and Vermeulen, W. (1999), 'Action of DNA repair endonuclease ERCC1/XPF in living cells', *Science* **284**(5416), 958–61.

Houtsmuller, A. B. and Vermeulen, W. (2001), 'Macromolecular dynamics in living cell nuclei revealed by fluorescence redistribution after photobleaching', *Histochem Cell Biol* **115**(1), 13–21.

Hu, M. C. and Davidson, N. (1987), 'The inducible lac operator-repressor system is functional in mammalian cells', *Cell* **48**(4), 555–66.

Iborra, F. J., Pombo, A., Jackson, D. A. and Cook, P. R. (1996), 'Active RNA polymerases are localized within discrete transcription "factories' in human nuclei', *J Cell Sci* **109 (Pt 6)**, 1427–36.

Izaurralde, E., Kas, E. and Laemmli, U. K. (1989), 'Highly preferential nucleation of histone H1 assembly on scaffold-associated regions', *J Mol Biol* **210**(3), 573–85.

Jackson, D. A. and Cook, P. R. (1993), 'Transcriptionally active minichromosomes are attached transiently in nuclei through transcription units', *J Cell Sci* **105 (Pt 4)**, 1143–50.

Jenke, A. C., Stehle, I. M., Herrmann, F., Eisenberger, T., Baiker, A., Bode, J., Fackelmayer, F. O. and Lipps, H. J. (2004), 'Nuclear scaffold/matrix attached region modules linked to a transcription unit are sufficient for replication and maintenance of a mammalian episome', *Proc Natl Acad Sci U S A* **101**(31), 11322–7.

Jenke, B. H., Fetzer, C. P., Stehle, I. M., Jonsson, F., Fackelmayer, F. O., Conradt, H., Bode, J. and Lipps, H. J. (2002), 'An episomally replicating vector binds to the nuclear matrix protein SAF-A in vivo', *EMBO Rep* **3**(4), 349–54.

Jenuwein, T., Forrester, W. C., Fernandez-Herrero, L. A., Laible, G., Dull, M. and Grosschedl, R. (1997), 'Extension of chromatin accessibility by nuclear matrix attachment regions', *Nature* **385**(6613), 269–72.

Kanda, T., Sullivan, K. F. and Wahl, G. M. (1998), 'Histone-GFP fusion protein enables sensitive analysis of chromosome dynamics in living mammalian cells', *Curr Biol* **8**(7), 377–85.

Kato, N. and Lam, E. (2001), 'Detection of chromosomes tagged with green fluorescent protein in live Arabidopsis thaliana plants', *Genome Biol* **2**(11), RESEARCH0045.

Kay, V. and Bode, J. (1994), 'Binding specificity of a nuclear scaffold: supercoiled, single-stranded, and scaffold-attached-region DNA', *Biochemistry* **33**(1), 367–74.

Kiledjian, M. and Dreyfuss, G. (1992), 'Primary structure and binding activity of the hnRNP U protein: binding RNA through RGG box', *Embo J* **11**(7), 2655–64.

Kipp, M., Gohring, F., Ostendorp, T., van Drunen, C. M., van Driel, R., Przybylski, M. and Fackelmayer, F. O. (2000), 'SAF-Box, a conserved protein domain that specifically recognizes scaffold attachment region DNA', *Mol Cell Biol* **20**(20), 7480–9.

Knudsen, H. and Nielsen, P. E. (1996), 'Antisense properties of duplex- and triplex-forming PNAs', *Nucleic Acids Res* **24**(3), 494–500.

Krithivas, A., Fujimuro, M., Weidner, M., Young, D. B. and Hayward, S. D. (2002), 'Protein interactions targeting the latency-associated nuclear antigen of Kaposi's sarcoma-associated herpesvirus to cell chromosomes', *J Virol* **76**(22), 11596–604.

Kruhlak, M. J., Lever, M. A., Fischle, W., Verdin, E., Bazett-Jones, D. P. and Hendzel, M. J. (2000), 'Reduced mobility of the alternate splicing factor (ASF) through the nucleoplasm and steady state speckle compartments', *J Cell Biol* **150**(1), 41–51.

Lamond, A. I. and Earnshaw, W. C. (1998), 'Structure and function in the nucleus', *Science* **280**(5363), 547–53.

Lever, M. A., Th'ng, J. P., Sun, X. and Hendzel, M. J. (2000), 'Rapid exchange of histone H1.1 on chromatin in living human cells', *Nature* **408**(6814), 873–6.

Li, G., Sudlow, G. and Belmont, A. S. (1998), 'Interphase cell cycle dynamics of a late-replicating, heterochromatic homogeneously staining region: precise choreography of condensation/decondensation and nuclear positioning', *J Cell Biol* **140**(5), 975–89.

Lichter, P., Cremer, T., Borden, J., Manuelidis, L. and Ward, D. C. (1988), 'Delineation of individual human chromosomes in metaphase and interphase cells by in situ suppression hybridization using recombinant DNA libraries', *Hum Genet* **80**(3), 224–34.

Lippincott-Schwartz, J. and Patterson, G. H. (2003), 'Development and use of fluorescent protein markers in living cells', *Science* **300**(5616), 87–91.

Lippincott-Schwartz, J., Snapp, E. and Kenworthy, A. (2001), 'Studying protein dynamics in living cells', *Nat Rev Mol Cell Biol* **2**(6), 444–56.

Liu, Y., Braasch, D. A., Nulf, C. J. and Corey, D. R. (2004), 'Efficient and isoform-selective inhibition of cellular gene expression by peptide nucleic acids', *Biochemistry* **43**(7), 1921–7.

Luderus, M. E., de Graaf, A., Mattia, E., den Blaauwen, J. L., Grande, M. A., de Jong, L. and van Driel, R. (1992), 'Binding of matrix attachment regions to lamin B1', *Cell* **70**(6), 949–59.

Lukacs, G. L., Haggie, P., Seksek, O., Lechardeur, D., Freedman, N. and Verkman, A. S. (2000), 'Size-dependent DNA mobility in cytoplasm and nucleus', *J Biol Chem* **275**(3), 1625–9.

Ma, H., Siegel, A. J. and Berezney, R. (1999), 'Association of chromosome territories with the nuclear matrix. Disruption of human chromosome territories correlates with the release of a subset of nuclear matrix proteins', *J Cell Biol* **146**(3), 531–42.

Mahy, N. L., Perry, P. E. and Bickmore, W. A. (2002b), 'Gene density and transcription influence the localization of chromatin outside of chromosome territories detectable by FISH', *J Cell Biol* **159**(5), 753–63.

Mahy, N. L., Perry, P. E., Gilchrist, S., Baldock, R. A. and Bickmore, W. A. (2002a), 'Spatial organization of active and inactive genes and noncoding DNA within chromosome territories', *J Cell Biol* **157**(4), 579–89.

Manders, E. M., Kimura, H. and Cook, P. R. (1999), 'Direct imaging of DNA in living cells reveals the dynamics of chromosome formation', *J Cell Biol* **144**(5), 813–21.

Marshall, W. F., Straight, A., Marko, J. F., Swedlow, J., Dernburg, A., Belmont, A., Murray, A. W., Agard, D. A. and Sedat, J. W. (1997), 'Interphase chromosomes undergo constrained diffusional motion in living cells', *Curr Biol* **7**(12), 930–9.

Martens, J. H., Verlaan, M., Kalkhoven, E., Dorsman, J. C. and Zantema, A. (2002), 'Scaffold/matrix attachment region elements interact with a p300-scaffold attachment factor A complex and are bound by acetylated nucleosomes', *Mol Cell Biol* **22**(8), 2598–606.

McNally, J. G., Muller, W. G., Walker, D., Wolford, R. and Hager, G. L. (2000), 'The glucocorticoid receptor: rapid exchange with regulatory sites in living cells', *Science* **287**(5456), 1262–5.

Mearini, G., Chichiarelli, S., Zampieri, M., Masciarelli, S., D'Erme, M., Ferraro, A. and Mattia, E. (2003), 'Interaction of EBV latent origin of replication with the nuclear matrix: identification of S/MAR sequences and protein components', *FEBS Lett* **547**(1-3), 119–24.

Misteli, T. (2000), 'Cell biology of transcription and pre-mRNA splicing: nuclear architecture meets nuclear function', *J Cell Sci* **113 (Pt 11)**, 1841–9.

Misteli, T. (2001), 'Protein dynamics: implications for nuclear architecture and gene expression', *Science* **291**(5505), 843–7.

Moir, R. D., Yoon, M., Khuon, S. and Goldman, R. D. (2000), 'Nuclear lamins A and B1: different pathways of assembly during nuclear envelope formation in living cells', *J Cell Biol* **151**(6), 1155–68.

Molenaar, C., Wiesmeijer, K., Verwoerd, N. P., Khazen, S., Eils, R., Tanke, H. J. and Dirks, R. W. (2003), 'Visualizing telomere dynamics in living mammalian cells using PNA probes', *Embo J* **22**(24), 6631–41.

Nayler, O., Stratling, W., Bourquin, J. P., Stagljar, I., Lindemann, L., Jasper, H., Hartmann, A. M., Fackelmayer, F. O., Ullrich, A. and Stamm, S. (1998), 'SAF-B protein couples transcription and pre-mRNA splicing to SAR/MAR elements', *Nucleic Acids Res* **26**(15), 3542–9.

Nickerson, J. A., Krochmalnic, G., Wan, K. M. and Penman, S. (1989), 'Chromatin architecture and nuclear RNA', *Proc Natl Acad Sci U S A* **86**(1), 177–81.

Nielsen, P. E. (2001), 'Peptide nucleic acid: a versatile tool in genetic diagnostics and molecular biology', *Curr Opin Biotechnol* **12**(1), 16–20.

Nielsen, P. E., Egholm, M., Berg, R. H. and Buchardt, O. (1991), 'Sequence-selective recognition of DNA by strand displacement with a thymine-substituted polyamide', *Science* **254**(5037), 1497–500.

Nielsen, P. E., Egholm, M. and Buchardt, O. (1994), 'Sequence-specific transcription arrest by peptide nucleic acid bound to the DNA template strand', *Gene* **149**(1), 139–45.

Paulasova, P., Andreo, B., Diblik, J., Macek, M. and Pellestor, F. (2004), 'The peptide nucleic acids as probes for chromosomal analysis: application to human oocytes, polar bodies and preimplantation embryos', *Mol Hum Reprod* **10**(6), 467–72.

Pederson, T. (1998), 'The plurifunctional nucleolus', *Nucleic Acids Res* **26**(17), 3871–6.

Pederson, T. (2000a), 'Diffusional protein transport within the nucleus: a message in the medium', *Nat Cell Biol* **2**(5), E73–4.

Pederson, T. (2000b), 'Half a century of "the nuclear matrix"', *Mol Biol Cell* **11**(3), 799–805.

Pellestor, F. and Paulasova, P. (2004), 'The peptide nucleic acids (PNAs), powerful tools for molecular genetics and cytogenetics', *Eur J Hum Genet* .

Phair, R. D. and Misteli, T. (2000), 'High mobility of proteins in the mammalian cell nucleus', *Nature* **404**(6778), 604–9.

Phair, R. D. and Misteli, T. (2001), 'Kinetic modelling approaches to in vivo imaging', *Nat Rev Mol Cell Biol* **2**(12), 898–907.

Piechaczek, C., Fetzer, C., Baiker, A., Bode, J. and Lipps, H. J. (1999), 'A vector based on the SV40 origin of replication and chromosomal S/MARs replicates episomally in CHO cells', *Nucleic Acids Res* **27**(2), 426–8.

Platani, M., Goldberg, I., Lamond, A. I. and Swedlow, J. R. (2002), 'Cajal body dynamics and association with chromatin are ATP-dependent', *Nat Cell Biol* **4**(7), 502–8.

Politz, J. C., Tuft, R. A., Pederson, T. and Singer, R. H. (1999), 'Movement of nuclear poly(A) RNA throughout the interchromatin space in living cells', *Curr Biol* **9**(6), 285–91.

Pommier, Y., Cockerill, P. N., Kohn, K. W. and Garrard, W. T. (1990), 'Identification within the simian virus 40 genome of a chromosomal loop attachment site that contains topoisomerase II cleavage sites', *J Virol* **64**(1), 419–23.

Ray, A. and Norden, B. (2000), 'Peptide nucleic acid (PNA): its medical and biotechnical applications and promise for the future', *Faseb J* **14**(9), 1041–60.

Renz, A. and Fackelmayer, F. O. (1996), 'Purification and molecular cloning of the scaffold attachment factor B (SAF-B), a novel human nuclear protein that specifically binds to S/MAR-DNA', *Nucleic Acids Res* **24**(5), 843–9.

Reuschlein, K. (2004), 'Untersuchungen zur Mobilitaet des Kernmatrixproteins SAF-A in lebenden Zellen', *Diplomarbeit, Hochschule fuer Angewandte Wissenschaften Hamburg* .

Robinett, C. C., Straight, A., Li, G., Willhelm, C., Sudlow, G., Murray, A. and Belmont, A. S. (1996), 'In vivo localization of DNA sequences and visualization of large-scale chromatin organization using lac operator/repressor recognition', *J Cell Biol* **135**(6 Pt 2), 1685–700.

Romig, H., Fackelmayer, F. O., Renz, A., Ramsperger, U. and Richter, A. (1992), 'Characterization of SAF-A, a novel nuclear DNA binding protein from HeLa cells with high affinity for nuclear matrix/scaffold attachment DNA elements', *Embo J* **11**(9), 3431–40.

Sambrook, J. and Russel, D. (2001), 'Molecular cloning'.

Sanger, F., Nicklen, S. and Coulson, A. R. (1977), 'DNA sequencing with chain-terminating inhibitors', *Proc Natl Acad Sci U S A* **74**(12), 5463–7.

Scheer, U. and Hock, R. (1999), 'Structure and function of the nucleolus', *Curr Opin Cell Biol* **11**(3), 385–90.

Scheer, U., Hugle, B., Hazan, R. and Rose, K. M. (1984), 'Drug-induced dispersal of transcribed rRNA genes and transcriptional products: immunolocalization and silver staining of different nucleolar components in rat cells treated with 5,6-dichloro-beta-D-ribofuranosylbenzimidazole', *J Cell Biol* **99**(2), 672–9.

Schubeler, D., Mielke, C., Maass, K. and Bode, J. (1996), 'Scaffold/matrix-attached regions act upon transcription in a context-dependent manner', *Biochemistry* **35**(34), 11160–9.

Schwander, A. (2004), 'Die funktionelle Domaenenstruktur des humanen Kernproteins Scaffold Attachment Factor A', *Dissertation, Universitaet Hamburg* .

Seksek, O., Biwersi, J. and Verkman, A. S. (1997), 'Translational diffusion of macromolecule-sized solutes in cytoplasm and nucleus', *J Cell Biol* **138**(1), 131–42.

Shav-Tal, Y., Darzacq, X., Shenoy, S. M., Fusco, D., Janicki, S. M., Spector, D. L. and Singer, R. H. (2004), 'Dynamics of single mRNPs in nuclei of living cells', *Science* **304**(5678), 1797–800.

Shelby, R. D., Hahn, K. M. and Sullivan, K. F. (1996), 'Dynamic elastic behavior of alpha-satellite DNA domains visualized in situ in living human cells', *J Cell Biol* **135**(3), 545–57.

Shiraishi, T. and Nielsen, P. E. (2004), 'Down-regulation of MDM2 and activation of p53 in human cancer cells by antisense 9-aminoacridine-PNA (peptide nucleic acid) conjugates', *Nucleic Acids Res* **32**(16), 4893–902.

Shopland, L. S. and Lawrence, J. B. (2000), 'Seeking common ground in nuclear complexity', *J Cell Biol* **150**(1), F1–4.

Stenoien, D. L., Patel, K., Mancini, M. G., Dutertre, M., Smith, C. L., O'Malley, B. W. and Mancini, M. A. (2001), 'FRAP reveals that mobility of oestrogen receptor-alpha is ligand- and proteasome-dependent', *Nat Cell Biol* **3**(1), 15–23.

Straight, A. F., Belmont, A. S., Robinett, C. C. and Murray, A. W. (1996), 'GFP tagging of budding yeast chromosomes reveals that protein-protein interactions can mediate sister chromatid cohesion', *Curr Biol* **6**(12), 1599–608.

Svahn, M. G., Lundin, K. E., Ge, R., Tornquist, E., Simonson, E. O., Oscarsson, S., Leijon, M., Branden, L. J. and Smith, C. I. (2004), 'Adding functional entities to plasmids', *J Gene Med* **6 Suppl 1**, S36–44.

Thomson, I., Gilchrist, S., Bickmore, W. A. and Chubb, J. R. (2004), 'The radial positioning of chromatin is not inherited through mitosis but is established de novo in early G1', *Curr Biol* **14**(2), 166–72.

Tsukamoto, T., Hashiguchi, N., Janicki, S. M., Tumbar, T., Belmont, A. S. and Spector, D. L. (2000), 'Visualization of gene activity in living cells', *Nat Cell Biol* **2**(12), 871–8.

van Drunen, C. M., Sewalt, R. G., Oosterling, R. W., Weisbeek, P. J., Smeekens, S. C. and van Driel, R. (1999), 'A bipartite sequence element associated with matrix/scaffold attachment regions', *Nucleic Acids Res* **27**(14), 2924–30.

van Roessel, P. and Brand, A. H. (2002), 'Imaging into the future: visualizing gene expression and protein interactions with fluorescent proteins', *Nat Cell Biol* **4**(1), E15–20.

van Wijnen, A. J., Bidwell, J. P., Fey, E. G., Penman, S., Lian, J. B., Stein, J. L. and Stein, G. S. (1993), 'Nuclear matrix association of multiple sequence-specific DNA binding activities related to SP-1, ATF, CCAAT, C/EBP, OCT-1, and AP-1', *Biochemistry* **32**(33), 8397–402.

Vazquez, J., Belmont, A. S. and Sedat, J. W. (2001), 'Multiple regimes of constrained chromosome motion are regulated in the interphase Drosophila nucleus', *Curr Biol* **11**(16), 1227–39.

Verschure, P. J., Van Der Kraan, I., Enserink, J. M., Mone, M. J., Manders, E. M. and Van Driel, R. (2002), 'Large-scale chromatin organization and the localization of proteins involved in gene expression in human cells', *J Histochem Cytochem* **50**(10), 1303–12.

Verschure, P. J., van Der Kraan, I., Manders, E. M. and van Driel, R. (1999), 'Spatial relationship between transcription sites and chromosome territories', *J Cell Biol* **147**(1), 13–24.

Visser, A. E., Jaunin, F., Fakan, S. and Aten, J. A. (2000), 'High resolution analysis of interphase chromosome domains', *J Cell Sci* **113 (Pt 14)**, 2585–93.

Wang, G., Xu, X., Pace, B., Dean, D. A., Glazer, P. M., Chan, P., Goodman, S. R. and Shokolenko, I. (1999), 'Peptide nucleic acid (PNA) binding-mediated induction of human gamma-globin gene expression', *Nucleic Acids Res* **27**(13), 2806–13.

Wang, G. and Xu, X. S. (2004), 'Peptide nucleic acid (PNA) binding-mediated gene regulation', *Cell Res* **14**(2), 111–6.

Webb, C. D., Teleman, A., Gordon, S., Straight, A., Belmont, A., Lin, D. C., Grossman, A. D., Wright, A. and Losick, R. (1997), 'Bipolar localization of the replication origin regions of chromosomes in vegetative and sporulating cells of B. subtilis', *Cell* **88**(5), 667–74.

Wilson, G. L., Dean, B. S., Wang, G. and Dean, D. A. (1999), 'Nuclear import of plasmid DNA in digitonin-permeabilized cells requires both cytoplasmic factors and specific DNA sequences', *J Biol Chem* **274**(31), 22025–32.

Yamaguchi, Y., Wada, T. and Handa, H. (1998), 'Interplay between positive and negative elongation factors: drawing a new view of DRB', *Genes Cells* **3**(1), 9–15.

Zbarskii, I. and Debov, S. (1948), 'On the protein of the cell nucleus', *Dokl. Akad. Nauk. SSSR* **63**, 795–98.

Zelphati, O., Liang, X., Hobart, P. and Felgner, P. L. (1999), 'Gene chemistry: functionally and conformationally intact fluorescent plasmid DNA', *Hum Gene Ther* **10**(1), 15–24.

Zhao, K., Kas, E., Gonzalez, E. and Laemmli, U. K. (1993), 'SAR-dependent mobilization of histone H1 by HMG-I/Y in vitro: HMG-I/Y is enriched in H1-depleted chromatin', *Embo J* **12**(8), 3237–47.

Zhong, S., Salomoni, P. and Pandolfi, P. P. (2000), 'The transcriptional role of PML and the nuclear body', *Nat Cell Biol* **2**(5), E85–90.

Zink, D. and Cremer, T. (1998a), 'Cell nucleus: chromosome dynamics in nuclei of living cells', *Curr Biol* **8**(9), R321–4.

Zink, D., Cremer, T., Saffrich, R., Fischer, R., Trendelenburg, M. F., Ansorge, W. and Stelzer, E. H. (1998b), 'Structure and dynamics of human interphase chromosome territories in vivo', *Hum Genet* **102**(2), 241–51.

Zink, D., Sadoni, N. and Stelzer, E. (2003), 'Visualizing chromatin and chromosomes in living cells', *Methods* **29**(1), 42–50.

Curriculum vitae

Name: Giulia Mearini
Date of birth: 28.01.1975
Place of birth: Livorno (Italy)
Nationality: Italian

Education

Jul. 1994	High school diploma (classical studies)
Sept. 1994 - Feb. 2000	Degree (with honor) in Biological Science at the University "La Sapienza" of Rome (Italy). Thesis title: "Interaction of Epstein-Barr origins of replication and nuclear matrix: characterization of the DNA sequences and proteins species involved in the binding".
Mar. 2000 - Sept. 2000	Internship at the Department of Genetic, University "La Sapienza" of Rome (Italy)
Oct. 2000 - Feb.2001	Internship at the Department of Microbiology, University "La Sapienza" of Rome (Italy)
Mar. 2001 - Dec. 2004	PhD student at the Heinrich-Pette-Institute for Experimental Virology and Immunology at the University of Hamburg (Germany), under the supervision of Dr. Frank O. Fackelmayer, head of the Department of molecular cell biology. Thesis title: "Sequence specific visualization of DNA in live mammalian cells".